Chiral matter-wave solitons in a density-dependent gauge theory

Robert James Dingwall

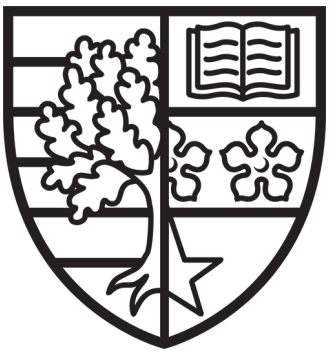

A thesis submitted for the degree of Doctor of Philosophy

Institute of Photonics and Quantum Sciences
Heriot-Watt University
Edinburgh, United Kingdom

April 2019

Abstract

In this thesis, we study the properties of one-dimensional chiral matter-wave solitons described by a density-dependent gauge theory. We begin, by first detailing the origin of the physical model, in which a synthetic density-dependent gauge potential is optically engineered in an ultracold bosonic gas. The resulting equation of motion for the condensate, which takes the form of a *'chiral nonlinear Schrödinger equation',* will then be the main focus of this work, as the prose of the thesis changes from the field of condensed matter physics to that of nonlinear dynamics. In particular, we will demonstrate how the introduction of the density-dependent gauge potential leads to the breakdown of integrability, Galilean invariance, and chiral symmetry in the model and show how these properties, in part, lead to the emergence of both dark and bright chiral soliton solutions. From this, we will derive the principle conservation laws of the model using variational techniques and illustrate the semi-classical behaviour of the solitons in the context of the density-dependent gauge theory. The majority and remainder of this thesis, will then be devoted to two of the traditional problems in nonlinear physics for the bright chiral soliton: the stability in response to a linear perturbation and the collision dynamics between pairs of solitons. Here, we will find that the gauge theory features *near*-integrable dynamics in the case of a single-soliton, but is dominated by *non*-integrable dynamics in the two-soliton case. This result demonstrates the role and importance of non-integrability in the description of nonlinear models, while potentially offering new possibilities for the coherent control of solitons in the ultracold setting.

Acknowledgements

It is hard to comprehend that nine years of work and study has culminated in this moment. Before I left for university, I did not know how to work a washing machine or cook a meal. Yet now, I stand here, albeit with a severely reduced hairline, ready to submit this thesis. This work was of course not accomplished alone, but together with many great people who I would like to express my thanks and gratitude to in the following words.

First and foremost, I thank my supervisor Patrik for all his support, guidance, and tutelage over the last five years for both my masters and doctoral studies. When lost in the sea of despair and frustration, a meeting with Patrik was always able to shed light on the issues and keep my spirits high.

Secondly, I thank Matthew, who in several ways has been an adoptive postdoc, but also someone that I have had the good fortune to also call a friend. Thank you for hosting me in the trips to Newcastle and Okinawa, as well as for the food and drink. As I learned a thing or two about cold atoms and solitons from you, I hope you also learned a thing or two from me.

I'd also like to extend a thank you to my friends at Heriot-Watt: Sharad, Alex, Ollie, Yvan, Ross, Susan, Artur, and of course Stuart, who has been a good friend to laugh, annoy, and talk to for the past nine years. Furthermore, I would also like to thank all the people that I had the opportunity to meet at the schools in Glasgow, Dunedin, and Okinawa, for making these trips memorable and fun. These experiences, mostly involving food, alcohol, and late nights, were some of my favourite moments in recent years and I am entirely grateful to be part of them.

Additionally, I'd like to thank Ian, Chris, Julie, and all the staff in the CM-CDT for providing me the opportunity and funding for my doctoral studies, as well as their support.

Last, but not least, I wholeheartedly thank my family both in Inverness and Edinburgh, particularly my mother and father, for all their loving support over the years. A special mention also goes to my aunt and late uncle in Edinburgh, who have also supported me in my studies for all these years.

Thank you everyone,

Robert

ACADEMIC REGISTRY

Research Thesis Submission

Please note this form should be bound into the submitted thesis.

Name*:*	Robert James Dingwall		
School:	Engineering and Physical Sciences		
Version: *(i.e. First, Resubmission, Final)*	Final	Degree Sought:	PhD, Physics

Declaration

In accordance with the appropriate regulations I hereby submit my thesis and I declare that:

1. The thesis embodies the results of my own work and has been composed by myself
2. Where appropriate, I have made acknowledgement of the work of others
3. Where the thesis contains published outputs under Regulation 6 (9.1.2) these are accompanied by a critical review which accurately describes my contribution to the research and, for multi-author outputs, a signed declaration indicating the contribution of each author (complete Inclusion of Published Works Form – see below)
4. The thesis is the correct version for submission and is the same version as any electronic versions submitted*.
5. My thesis for the award referred to, deposited in the Heriot-Watt University Library, should be made available for loan or photocopying and be available via the Institutional Repository, subject to such conditions as the Librarian may require
6. I understand that as a student of the University I am required to abide by the Regulations of the University and to conform to its discipline.
7. Inclusion of published outputs under Regulation 6 (9.1.2) shall not constitute plagiarism.
8. I confirm that the thesis has been verified against plagiarism via an approved plagiarism detection application e.g. Turnitin.

* *Please note that it is the responsibility of the candidate to ensure that the correct version of the thesis is submitted.*

Signature of Candidate*:*		Date:	

Submission

Submitted By *(name in capitals):*	
Signature of Individual Submitting:	
Date Submitted:	

For Completion in the Student Service Centre (SSC)

Received in the SSC by *(name in capitals):*			
Method of Submission *(Handed in to SSC; posted through internal/external mail):*			
*E-thesis Submitted (**mandatory for final theses**)*			
Signature:		Date:	

ACADEMIC REGISTRY

Inclusion of Published Works

Declaration

This thesis contains one or more multi-author published works. In accordance with Regulation 6 (9.1.2) I hereby declare that the contributions of each author to these publications is as follows:

Citation details	R.J. Dingwall and P. Ohberg, Phys. Rev. A Vol. 99, pg.023609, (2019)
Author 1	RJD performed the analytical and numerical calculations, as well as preparing the manuscript.
Author 2	PO supervised the work and provided insight on how to approach the problem, in addition to revisions of the manuscript
Signature:	
Date:	

Citation details	R. J. Dingwall, M. J. Edmonds, J. L. Helm, B. A. Malomed, P. Ohberg, New. J. Phys. Vol. 20, pg.043004, (2018).
Author 1	RJD performed the entirety of the numerical simulations and linear variational analysis, in addition to writing most of the manuscript and deriving the conservation laws.
Author 2	MJE performed the asymptotic variational analysis, in addition to writing some parts of the manuscript. MJE also performed some numerical simulations to verify results.
Author 3,4,5	JLM, BAM, and PO all supervised the work and provided insight on how to approach the problem. All three also revised certain parts of the manuscript.
Signature:	
Date:	

Contents

List of publications

The content of this thesis is based, in part, on the following two publications:

(i) R. J. Dingwall, and P. Öhberg
Stability of matter-wave solitons in a density-dependent gauge theory
Phys. Rev. A **99**, 023609 (2019)

Abstract: We consider the linear stability of chiral matter-wave solitons described by a density-dependent gauge theory. By studying the associated Bogoliubov-de Gennes equations both numerically and analytically, we find that the stability problem effectively reduces to that of the standard Gross-Pitaevskii equation, proving that the solitons are stable to linear perturbations. In addition, we formulate the stability problem in the framework of the Vakhitov-Kolokolov criterion and provide supplementary numerical simulations which illustrate the absence of instabilities when the soliton is initially perturbed. These results justify the production of chiral solitons in ultracold experiments and their potential application for practical transport dynamics in interferometry and atomtronics.

(ii) R. J. Dingwall, M. J. Edmonds, J. L. Helm, B. A. Malomed, and P. Öhberg
Non-integrable dynamics of matter-wave solitons in a density-dependent gauge theory
New. J. Phys. **20**, 043004 (2018)

Abstract: We study interactions between bright matter-wave solitons which acquire chiral transport dynamics due to an optically-induced density-dependent gauge potential. Through numerical simulations, we find that the collision dynamics feature several non-integrable phenomena, from inelastic collisions including population transfer and radiation losses to the formation of short-lived bound states and soliton fission. An effective quasi-particle model for the interaction between the solitons is derived by means of a variational approximation, which demonstrates that the inelastic nature of the collision arises from a coupling of the gauge field to velocities of the solitons. In addition, we derive a set of interaction potentials which show that the influence of the gauge field appears as a short-range potential, that can give rise to both attractive and repulsive interactions.

Chapter 1

Introduction

In the past half-century, the study of solitons has seen a massive resurgence in activity following the ground-breaking development of the Inverse Scattering Transform in the study of fully-integrable nonlinear partial differential equations [1–5]. These solitary waves, characterised by their permanent form while moving at a constant velocity, appear in a multitude of physical systems, branching together intricate topics in mathematics such as integrability and nonlinear phenomena, to the fields of hydrodynamics [6], biology [7, 8], nonlinear optics [9, 10], and condensed matter physics [11–15]. In particular, the prediction and experimental realisation of solitons in these systems, has been a major triumph for the description of nonlinear models in nature, and an important factor behind proposals for the application of solitons in long-distance optical communications [16–18].

At the forefront of soliton research, are low-temperature ensembles of bosonic and fermionic atoms, or more commonly referred to as ultracold quantum gases [14, 15, 19]. Since their first production in a series of independent experiments before the turn of the millennium [20–22], these systems have developed as a highly controllable environment to study not only soliton dynamics, but also various aspects of theoretical physics in the ultracold setting. For this purpose, they can be composed of a large variety of bosonic or fermionic elements and isotopes, including several of the alkali and alkaline-earth metals [20–24], and lanthanides [25, 26]. Additionally, they can be prepared in various trapping geometries, ranging from harmonic to periodic [27], as well as the possibility to realise arbitrary shapes using painted potentials and spatial light modulators [28, 29]. On top of this, the effective dimensionality of the system can be reduced by restricting the spatial extent of the trapping potentials [30], in analogy to the confinement of charge carriers in semiconductor physics [31]. Furthermore, the strength of the interactions between the condensate atoms can be controlled using Feshbach resonances [32], which was applied to great success in observing the crossover between a state of Cooper pairs and a condensate of diatomic molecules in a degenerate fermi gas [33].

The ability to prepare, control, and study these ultracold systems, is undoubtedly one of the greatest achievements of modern condensed matter physics and one of the primary reasons behind proposals for their application in quantum simulation. The general idea here, as originally proposed by Feynman [34, 35], is to simulate the dynamics of complicated quantum many-body models through analogue systems which are engineered to emulate the desired effects. In this way, one can obtain valuable insight into a given model while overcoming many of the difficulties encountered in classical computation, such as the scaling of the Hilbert space and the fermion sign problem in quantum Monte Carlo simulations. Furthermore, one could also test theories beyond the reach of experimental studies, like black hole evaporation in general relativity and the behaviour of strongly interacting matter in quantum chromodynamics [36, 37]. So far, these ideas have been successfully realised in ultracold gases, with notable works including the Mott-insulator to superfluid phase transition [38], the paramagnetic to anti-ferromagnetic phase transition under an applied magnetic field [39], atomic Zitterbewegung [40, 41], and the emulation of the Hofstadter Hamiltonian [42]. Quantum simulators are of course not only limited to ultracold systems, but have also been successfully realised in systems of trapped-ions [43], photonics [44], and superconducting circuits [45].

Although the primary purpose of a quantum simulator is to gain insight from the study of an analogue model, in many cases the techniques of engineering these simulators can often lead to new novel means for the control and manipulation of the host system. In particular, with the advent of synthetic gauge potentials in ultracold gases [46, 47], new possibilities are now available for the coherent control of the gas in the theme of nonlinear dynamics. It is for this reason that the following thesis is presented, as we set out to study how the dynamics of an ultracold bosonic gas is modified by the presence an optically-induced density-dependent gauge potential [48], with the ultimate goal centered on how emergent phenomena could be exploited in applications like interferometry and future atomtronic based technologies [49–51]. For this reason, we will study in this thesis, the topic of chiral solitons described by the density-dependent gauge theory and consider two of the important problems for the production of these solutions in future ultracold experiments; the stability of the soliton in response to a linear perturbation [52], and the collision dynamics between pairs of solitons [53].

Chapter 2

Synthetic gauge potentials in ultracold atomic gases

2.1 Introduction

For the construction of an analogue model to simulate various problems in condensed matter physics, such as the standard and fractional quantum Hall effect, we require the engineering of a system which describes the dynamics of a single or ensemble of charged particles in an applied potential. For the latter point, the availability of various trapping geometries in ultracold gases makes these system a promising candidate for this purpose. However as an ultracold gas is charge neutral, and therefore does not move under an applied electromagnetic field due to the Lorentz force, this immediately puts the proposition of realising a quantum simulator in these systems into question.[i]

The solution to this problem, is the engineering of *artificial* or *synthetic* gauge fields which arise from applied forces on the condensate which mimic the motion of a charged particle. Generally, this can be achieved using three methods:

(i) *The introduction of rotation, such as through asymmetric trapping potentials and laser spooning, with the vector potential related to the Coriolis force in the rotating frame* [55–58].

(ii) *Light-matter interactions, where a set of geometrical gauge potentials emerge from the adiabatic motion of an optical dressed state that is composed of multiple internal states of the atoms* [59, 60].

(iii) *Floquet engineering, where gauge potentials arise from modulating the trapping potential, such as by shaking or changing the on-site interaction energy of an optical lattice* [61, 62].

[i]Note, that an applied electromagnetic field will still affect the condensate atoms, such as through the Zeeman splitting of the fine and hyperfine structure [54], as well as controlling the scattering strength of the condensate through Feshbach resonances [32].

Using these techniques, researchers have been able to realise a comprehensive catalogue of artificial gauge theories in ultracold gases, including abelian gauge potentials in the spirit of electromagnetism, but also for non-abelian models which describe more complicated theories of particle interactions (see [46, 47] for reviews). This has principally lead to the generation of effective spin-orbit coupling and vortices in ultracold experiments [63, 64], in analogy to the phenomena encountered in condensed matter physics.

In preparation for our studies in this thesis, we present in this chapter, a brief review of the mean-field description of ultracold bosonic gases and how synthetic gauge fields can be engineered in these systems. Here, we will only present the essential details needed, namely the topics of rotation- and light-induced synthetic gauge potentials, as our focus for the most part, will be on how the dynamics of the condensate is modified through their introduction. Instead, we refer the reader to more comprehensive reviews on ultracold gases [14, 15, 19], and synthetic gauge potentials [46, 47].

2.2 The Gross-Pitaevskii equation

The mean-field description of a low-temperature weakly-interacting bosonic gas was first presented independently in the works of Gross and Pitaevskii in the early sixties [65, 66]. Since then, this model has proven to be a valuable tool in the study of quantum gases, validated not only by the successful production of ultracold gases in experiments [20–22], but also by several studies into predicted phenomena that have been verified experimentally. These include the emergence of vortex lattices under rotation [55–58], the properties of elementary excitations [67–71], and the generation of matter-wave solitons as prime examples [72–75]. This success is undoubtedly one of the greatest achievements of modern condensed matter physics, and one of the primary reasons for the growth and prominence of the field of ultracold gases in recent years.

To begin the derivation, we consider an ensemble of N interacting bosonic particles confined in an external trapping potential $V(\mathbf{r})$. The many-body Hamiltonian describing the atoms in second-quantised form, is given by

$$\begin{aligned}\hat{H} = &\int d\mathbf{r}\, \hat{\Phi}^{\dagger}(\mathbf{r},t)\left[-\frac{\hbar^2}{2m}\nabla^2 + V(\mathbf{r})\right]\hat{\Phi}(\mathbf{r},t) \\ &+ \frac{1}{2}\int d\mathbf{r}\int d\mathbf{r}'\, \hat{\Phi}^{\dagger}(\mathbf{r},t)\,\hat{\Phi}^{\dagger}(\mathbf{r}',t)\,V_{\text{int}}(\mathbf{r}-\mathbf{r}')\,\hat{\Phi}(\mathbf{r}',t)\,\hat{\Phi}(\mathbf{r},t)\,,\end{aligned} \tag{2.1}$$

where $\hat{\Phi}^{\dagger}(\mathbf{r},t)$ and $\hat{\Phi}(\mathbf{r},t)$ are the bosonic field operators and $V_{\text{int}}(\mathbf{r}-\mathbf{r}')$ represents the two-body interatomic potential between particles at positions $\mathbf{r}$ and $\mathbf{r}'$. The statistics and indistinguishability of the bosonic atoms are encoded in the commutation relations

$$\left[\hat{\Phi}(\mathbf{r},t),\hat{\Phi}^{\dagger}(\mathbf{r}',t)\right]=\delta(\mathbf{r}-\mathbf{r}'), \tag{2.2}$$

and

$$\left[\hat{\Phi}(\mathbf{r},t),\hat{\Phi}(\mathbf{r}',t)\right]=\left[\hat{\Phi}^{\dagger}(\mathbf{r},t),\hat{\Phi}^{\dagger}(\mathbf{r}',t)\right]=0. \tag{2.3}$$

The evolution of the field operator $\hat{\Phi}(\mathbf{r},t)$ can be determined directly from the Heisenberg equation, and reads as

$$\begin{aligned} i\hbar\frac{\partial}{\partial t}\hat{\Phi}(\mathbf{r},t)=&\left[-\frac{\hbar^2}{2m}\nabla^2+V(\mathbf{r})\right]\hat{\Phi}(\mathbf{r},t)\\ &+\int d\mathbf{r}'\,\hat{\Phi}^{\dagger}(\mathbf{r}',t)\,V_{\text{int}}(\mathbf{r}-\mathbf{r}')\,\hat{\Phi}(\mathbf{r}',t)\,\hat{\Phi}(\mathbf{r},t). \end{aligned} \tag{2.4}$$

To proceed, we assume that the gas of atoms is dilute and cooled to sufficiently low temperatures such that the interactions between atoms is dominated by low-energy binary collisions. Under these conditions, the interatomic potential can be approximated as a pseudo-potential of the form

$$V_{\text{int}}(\mathbf{r}-\mathbf{r}')=g\delta(\mathbf{r}-\mathbf{r}'), \tag{2.5}$$

where the coupling constant $g=4\pi\hbar^2a_s/m$ with s-wave scattering length a_s, characterises the strength of the interactions. Substituting the pseudo-potential into the equation obtained from the Heisenberg equation, then leads to the expression

$$i\hbar\frac{\partial}{\partial t}\hat{\Phi}(\mathbf{r},t)=\left[-\frac{\hbar^2}{2m}\nabla^2+V(\mathbf{r})+g\,\hat{\Phi}^{\dagger}(\mathbf{r},t)\,\hat{\Phi}(\mathbf{r},t)\right]\hat{\Phi}(\mathbf{r},t). \tag{2.6}$$

The final task involves decomposition of the field operators. For condensation to occur, a large population of the atoms must reside in the same single-particle quantum state. In this way, the field operator can be decomposed in the Bogoliubov approximation as

$$\hat{\Phi}(\mathbf{r},t)=\Phi(\mathbf{r},t)+\hat{\Phi}'(\mathbf{r},t), \tag{2.7}$$

where $\hat{\Phi}'(\mathbf{r},t)$ is a perturbation which describes the depletion away from the condensed state and $\Phi(\mathbf{r},t)=\langle\hat{\Phi}(\mathbf{r},t)\rangle$ is the mean-field order parameter, whose square

integral is related to the number of atoms

$$N = \int_{-\infty}^{\infty} d\mathbf{r} \, |\Phi(\mathbf{r}, t)|^2, \tag{2.8}$$

for the condensate density $\rho = |\Phi(\mathbf{r}, t)|^2$. Assuming that the quantum depletion is negligible at low temperatures, Eq. (2.6) becomes a zeroth-order theory for the condensed state, leading to the celebrated Gross-Pitaevskii equation

$$i\hbar \frac{\partial}{\partial t} \Phi(\mathbf{r}, t) = \left[-\frac{\hbar^2}{2m} \nabla^2 + V(\mathbf{r}) + g|\Phi(\mathbf{r}, t)|^2 \right] \Phi(\mathbf{r}, t) \tag{2.9}$$

In the absence of the trapping potential, Eq. (2.9) is formally equivalent to the nonlinear Schrödinger equation, which is encountered in numerous physical models, but principally in the field of nonlinear optics [9]. This similarity opens the possibility to study familiar topics known from nonlinear physics in the ultracold regime, and has been demonstrated in works detailing four-wave mixing [76], modulation instability [72], and the generation of matter-wave solitons [72–75]. The production of these phenomena in ultracold experiments, has served not only as a prime example for the applicability of nonlinear models in physics, but also as a validation for the semi-classical mean-field description of quantum gases.

2.3 Electromagnetism

The classical theory of electromagnetism is one of the simplest gauge theories encountered in theoretical physics, where the interaction of electrically charged particles is described by the electric and magnetic fields strengths, $\mathbf{E}(\mathbf{r}, t)$ and $\mathbf{B}(\mathbf{r}, t)$, via Maxwell's equations. This theory, in a similar manner to the nonlinear models that we will encounter in this thesis, is a classical field theory with the abelian $U(1)$ symmetry group, which describes the propagation of waves.

Using the techniques of Lagrangian mechanics, the dynamics of a non-relativistic particle in an electromagnetic field can be conveniently described by the Lagrangian function

$$L_{\text{em}} = \frac{1}{2} m\dot{\mathbf{r}}^2 + q\mathbf{A}(\mathbf{r}, t) \cdot \dot{\mathbf{r}} - qW(\mathbf{r}, t), \tag{2.10}$$

where the magnetic vector potential $\mathbf{A}(\mathbf{r}, t)$ and electrostatic scalar potential $W(\mathbf{r}, t)$ are defined through the relations

$$\mathbf{E}(\mathbf{r}, t) = -\nabla W(\mathbf{r}, t) - \frac{\partial \mathbf{A}(\mathbf{r}, t)}{\partial t}, \tag{2.11}$$

and

$$\mathbf{B}\left(\mathbf{r},t\right)=\nabla\times\mathbf{A}\left(\mathbf{r},t\right),\tag{2.12}$$

with the particle velocity $\mathbf{v}=\dot{\mathbf{r}}$. This Lagrangian can be minimised to obtain the more familiar Lorentz force

$$\mathbf{F}=q\left(\mathbf{E}+\mathbf{v}\times\mathbf{B}\right),\tag{2.13}$$

which shows that an electromagnetic field exerts two forces on a charged particle: one along the same linear orientation of the electric field and another perpendicular to the magnetic field.

Each of these gauge potentials possesses the property of gauge invariance, as their definitions are invariant under the transformations

$$W\left(\mathbf{r},t\right)\longrightarrow W\left(\mathbf{r},t\right)+\frac{\partial F\left(\mathbf{r},t\right)}{\partial t}+C\tag{2.14}$$

and

$$A\left(\mathbf{r},t\right)\longrightarrow A\left(\mathbf{r},t\right)-\nabla F\left(\mathbf{r},t\right)+C\tag{2.15}$$

for an arbitrary function $F\left(\mathbf{r},t\right)$ and constant C. This highlights an important property; that the choice of the gauge potentials is *not* unique and can lead to the same emergent electromagnetic field.

Using the techniques described later in Sec. 4.2.1, the corresponding electromagnetic Hamiltonian reads as

$$\hat{H}_{\mathrm{em}}=\frac{1}{2m}\left(\mathbf{p}-q\mathbf{A}(\mathbf{r},t)\right)^{2}+qW(\mathbf{r},t),\tag{2.16}$$

where each component of the mechanical momentum $\mathbf{p}=(p_x,p_y,p_z)$, is calculated from the expression

$$p_x=\frac{\partial L_{\mathrm{em}}}{\partial v_x}=mv_x+qA_x.\tag{2.17}$$

The prescription, $\mathbf{p}\longrightarrow\mathbf{p}-q\mathbf{A}(\mathbf{r},t)$, is often referred to in the literature as minimal coupling. Comparing the above Hamiltonian to the Gross-Pitaevskii equation, the task of realising an electromagnetic-type theory in ultracold gases can therefore be posed by requiring the appearance of the gauge potentials $\mathbf{A}(\mathbf{r},t)$ and $W(\mathbf{r},t)$ in the mean-field description of the condensate. However, as we will demonstrate in the next chapter, the form of these gauge potentials must be engineered carefully so that the emergent electromagnetic fields are non-trivial.

2.4 Rotation-induced gauge potentials

With the theories of ultracold bosonic gases and electromagnetism briefly reviewed, we can now turn our attention to the engineering of synthetic gauge potentials in these systems. The first example we will consider, is the case where a trapped gas is uniformly rotated with rotational frequency $\boldsymbol{\omega}_{\mathrm{rot}}$. The Hamiltonian describing the system in the rotating frame is given by

$$H_{\mathrm{rot}} = H - \boldsymbol{\omega}_{\mathrm{rot}} \cdot \mathbf{L} = \frac{\mathbf{p}^2}{2m} + V(\mathbf{r}) - \boldsymbol{\omega}_{\mathrm{rot}} \cdot \mathbf{L} + g|\Phi|^2, \tag{2.18}$$

with the angular momentum operator $\mathbf{L} = \mathbf{r} \times \mathbf{p}$. By rearranging the above equation into minimal-coupling form, one can obtain the new Hamiltonian

$$H_{\mathrm{rot}} = \frac{1}{2m} \left(\mathbf{p} - m\boldsymbol{\omega}_{\mathrm{rot}} \times \mathbf{r}\right)^2 + V(\mathbf{r}) - \frac{1}{2} m \left(\boldsymbol{\omega}_{\mathrm{rot}} \times \mathbf{r}\right)^2 + g|\Phi|^2. \tag{2.19}$$

This example demonstrates that in the rotating frame, the Coriolis force enters as an effective gauge potential on the mean-field level. However, this model features a drawback, in that as the system is rotated faster, the condensate becomes displaced due to the presence of an effective centrifugal term. It has been demonstrated experimentally that rotating the condensate beyond a critical value leads to the appearance of vortex lattices in the density profile of the condensate [55–58], which verifies the existence of an effective magnetic flux being generated in the gas.[ii]

2.5 Light-induced gauge potentials

The next example we consider is the generation of geometrical gauge potentials using light-matter interactions and the concept of adiabatic elimination [77]. To illustrate this, we consider a two-level system, where two internal states of the atoms are optically dressed by an external laser field. In the ultracold setting this can principally be achieved using two different light-matter interaction schemes, as pictured in Fig. 2.1. The first is a direct transition, which could for instance describe an intercombination line in alkaline-earth metals such as Strontium [24]. Whereas the second, a Λ-configuration, details a Raman transition between two hyperfine levels of the atomic ground state, such as in the case of Rubidium and other alkaline metals [54]. In both cases, the Hamiltonian describing the two-component non-interacting gas in the presence of the light-matter interactions can be written as

$$\hat{H} = \left(\frac{\hat{\mathbf{p}}^2}{2m} + V(\mathbf{r})\right) + \hat{H}_{\mathrm{lm}}, \tag{2.20}$$

[ii] Complete details on how vortices emerge through the introduction of angular momentum in the gas, can be found in Chap. 9 of Pethick and Smith [14].

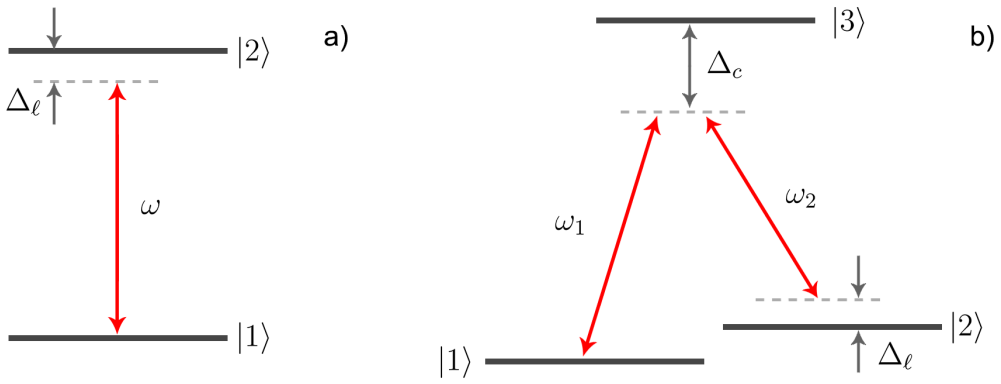

Figure 2.1: Light-matter interaction schemes for a two-level (a) and Λ-configuration (b), with laser frequencies ω_i, and laser detunings Δ_ℓ and Δ_c.

where the matrix

$$\hat{H}_{\rm lm} = \frac{\hbar\tilde{\Omega}}{2}\begin{pmatrix} \cos\theta & e^{-i\phi_\ell}\sin\theta \\ e^{i\phi_\ell}\sin\theta & -\cos\theta \end{pmatrix}, \tag{2.21}$$

describes the optical coupling between the two internal states the atom, characterised by five parameters: the laser phase angle ϕ_ℓ, laser detuning Δ_ℓ, mixing angle $\tan\theta = \left(-\tilde{\Omega}/\Delta_\ell\right)$, and the Rabi and generalised Rabi frequencies, Ω and $\tilde{\Omega} = \sqrt{\Delta_\ell^2 + \Omega^2}$, respectively.

The optical-coupling matrix $\hat{H}_{\rm lm}$ can be readily diagonalized for the eigenvectors

$$|\sigma_+\rangle = \begin{pmatrix} \cos(\theta/2) \\ e^{i\phi_\ell}\sin(\theta/2) \end{pmatrix} \tag{2.22}$$

and

$$|\sigma_-\rangle = \begin{pmatrix} -e^{i\phi_\ell}\sin(\theta/2) \\ \cos(\theta/2) \end{pmatrix}, \tag{2.23}$$

with eigenvalues $\lambda_\pm = \pm\hbar\tilde{\Omega}/2$, which are also called *'dressed states'* [78]. As Eq. (2.21) is self-adjoint, the eigenvectors $|\sigma_+\rangle$ and $|\sigma_-\rangle$ form a normalised orthogonal basis which satisfy the completeness relation

$$\hat{\mathbb{I}} = \sum_{n=+,-} |\sigma_n\rangle\langle\sigma_n| . \tag{2.24}$$

In the following, we will assume the adiabatic approximation, in which the particle is prepared initially in one of the optical dressed states and moves sufficiently slowly such that it remains proportional to that state for all time. In this way, the second dressed state may be adiabatically eliminated from the system dynamics, such that

the state vector in the two-component basis of the dressed states can be written as

$$|\Phi(\mathbf{r},t)\rangle = \sum_{n=+,-} \Phi_n(\mathbf{r},t)\,|\sigma_n(\mathbf{r})\rangle \overset{a}{\approx} \Phi_\pm\,|\sigma_\pm\rangle\,. \tag{2.25}$$

Here, we have introduced the amplitude coefficients Φ_n and the notation $\overset{a}{\approx}$ for the adiabatic approximation. To proceed, we project the adiabatic state vector onto the momentum operator to reveal

$$\begin{aligned}\mathbf{p}\,|\Phi(\mathbf{r},t)\rangle &= -i\hbar \sum_{n=+,-} \Big[(\nabla\Phi_n)\,|\sigma_n\rangle + \Phi_n \nabla\,|\sigma_n\rangle \Big] \\ &\overset{a}{\approx} \Big[\left(\mathbf{p} - i\hbar\,\langle\sigma_\pm|\nabla\sigma_\pm\rangle\right)\Phi_\pm \Big]\,|\sigma_\pm\rangle - i\hbar\Phi_\pm\,|\sigma_\mp\rangle\,\langle\sigma_\mp|\nabla\sigma_\pm\rangle\,,\end{aligned} \tag{2.26}$$

after a single application of the completeness relation. By projecting the adiabatic state vector onto the full Hamiltonian, one obtains the equation of motion

$$i\hbar\frac{\partial\Phi_\pm}{\partial t} \overset{a}{\approx} \left[\frac{1}{2m}\left(\mathbf{p} - \mathbf{A}_\pm\right)^2 + W + V \pm \frac{\hbar\tilde{\Omega}}{2}\right]\Phi_\pm, \tag{2.27}$$

in which two geometrical gauge potentials have appeared: a scalar potential

$$W \overset{a}{\approx} \frac{\hbar^2}{2m}|\,\langle\sigma_\mp|\nabla\sigma_\pm\rangle\,|^2 \overset{a}{\approx} \frac{\hbar^2}{8m}\left[(\nabla\theta)^2 + (\nabla\phi_\ell)^2\sin^2(\theta)\right], \tag{2.28}$$

and a vector potential

$$\mathbf{A}_\pm \overset{a}{\approx} i\hbar\,\langle\sigma_\pm|\nabla\sigma_\pm\rangle \overset{a}{\approx} \frac{\hbar}{2}\nabla\phi_\ell\,(\cos\theta - 1)\,. \tag{2.29}$$

The labelling of geometrical in this instance, highlights that these potentials depend not on the strength of the laser parameters, but their geometry via the vectorial coordinate $\mathbf{r}$. The first of these, the scalar potential, details the micromotion of the atom as it makes virtual transitions between the two dressed states. Whereas the vector potential takes the familiar form of the Mead-Berry connection [77], which is connected to the geometrical or 'Berry' phase

$$\gamma_n = \frac{1}{\hbar}\oint_{\mathcal{C}} d\mathbf{r}\cdot\mathbf{A}, \tag{2.30}$$

that the system obtains as it slowly moves around a contour in the parameter space.

2.6 Summary and outlook

In this chapter, we have provided a short review on the topic of engineering synthetic gauge potentials in ultracold atomic gases. At this brief conclusion, we emphasise

that the techniques reviewed in this chapter are only a small sample of the available methods for engineering synthetic gauge potentials. In particular we have only focused on the simplest models featuring abelian gauge theories and not considered more involved models that can realise non-abelian gauge potentials [46, 47]. In the next chapter, we will consider an extension to this work in the form of density-dependent gauge potentials.

Chapter 3

Simulating a density-dependent gauge theory

3.1 Introduction

So far in this thesis, we have detailed techniques which can engineer synthetic gauge potentials in ultracold gases. These methods however, suffer from a common drawback in that the synthetic gauge potential is defined by externally controlled parameters, such as the rotation frequency or laser parameters, without any explicit dependence on the matter-field of the condensate. These gauge potentials are therefore *static*, and do not describe a *dynamical* gauge theory which correctly captures the physics of electromagnetism.

To overcome this shortcoming, several proposals have appeared on the simulation of abelian and non-abelian gauge theories featuring dynamical gauge potentials in optical lattices [79–82]. In these works, focus is predominately aimed at the study of fermionic matter, so as to circumvent the problems encountered in quantum Monte Carlo simulations. In more modest approaches, proposals have also appeared on the engineering of density-dependent gauge potentials in both continuum and lattice models [48, 83, 84], which feature a back-action between the matter-field and gauge potential. In this case, the resulting gauge theory is not fully dynamical but represents a small step towards the eventual simulation of a complete theory. Very recently, the first series of experiments in this area have appeared, with a dynamical gauge theory realised in trapped ion systems [85], and a density-dependent gauge potential in a Bose-Einstein condensate loaded into a two-dimensional optical lattice [86].

In this chapter, we detail one of these methods, in which one can go beyond the static gauge potentials described previously and realise an interacting gauge theory in an ultracold gas. The key ingredient here, will be an effective spatial-detuning induced by a two-component interacting gas, which in the context of the techniques described in Sec. 2.5, can lead to the emergence of a density-dependent gauge potential. Although the resulting gauge theory will not be truly dynamical,

as the effective electromagnetic fields will vanish in the absence of the matter-field, the mean-field description of the condensate will possess many new features which greatly modify the dynamics of the gas.

3.2 Density-dependent gauge theory

In the previous chapter, we saw how a spatially-varying laser phase and optical detuning can give rise to geometric gauge potentials in a two-level model via adiabatic elimination. The first step in the construction of a set of dynamical, or more correctly speaking, density-dependent gauge potentials in the ultracold setting, therefore amounts to the situation in which the optical detuning depends on the local density of the gas.

To realise this, we consider the model studied in Ref. [48], in which a harmonically-trapped two-level Bose-Einstein condensate, with internal states $|1\rangle$ and $|2\rangle$, is optically dressed by an external laser field. The mean-field Hamiltonian describing the interacting trapped gas in the presence of the light-matter interactions can be written as

$$\hat{H} = \left(\frac{\hat{\mathbf{p}}^2}{2m} + V(\mathbf{r})\right)\hat{\mathbb{I}}_{2\times 2} + \begin{pmatrix} g_{11}|\Phi_1|^2 + g_{12}|\Phi_2|^2 & 0 \\ 0 & g_{12}|\Phi_1|^2 + g_{22}|\Phi_2|^2 \end{pmatrix} + \hat{H}_{\rm lm}, \quad (3.1)$$

where the coupling matrix

$$\hat{H}_{\rm lm} = \frac{\hbar\Omega}{2}\begin{pmatrix} 0 & e^{-i\phi_\ell} \\ e^{i\phi_\ell} & 0 \end{pmatrix}, \quad (3.2)$$

is simplified by setting the laser detuning to zero with $\Delta_\ell = 0$ [46, 47]. The mean-field interactions appearing in Eq. (3.1) take the familiar form for a two-component (spinor) condensate [14, 15], with the strength of the interactions between the atoms in states i and i' controlled by the scattering parameters $g_{ii'} = 4\pi\hbar^2 a_{s,ii'}/m$. Also appearing, is the harmonic trapping potential

$$V(\mathbf{r}) = \frac{1}{2}m\left(w_x^2x^2 + w_y^2y^2 + w_z^2z^2\right), \quad (3.3)$$

characterised by the length scale $\ell_\nu = \sqrt{\hbar/(m\omega_\nu)}$ with oscillation frequency ω_ν, for each spatial coordinate $\nu = \{x, y, z\}$.

To construct a density-dependent gauge theory, we will assume that the gas is sufficiently dilute such that mean-field interactions can be treated as a small perturbation to the laser coupling, with $\hbar\Omega \gg g_{ii'}|\Phi_{i'}|^2$. Then, following the techniques detailed in Sec. 2.5, we may describe the many-particle state of the system as a

Hartree product $|\Phi\rangle = \otimes^N |\sigma_n\rangle$, in which the optical dressed states

$$|\sigma_\pm^{(0)}\rangle = \frac{1}{\sqrt{2}}\left(|1\rangle \pm e^{i\phi_\ell}|2\rangle\right), \tag{3.4}$$

are weakly perturbed by the mean-field interactions. Then to proceed, we assume, as before, that the system is prepared and remains in one of the dressed states, such that the dynamics of the remaining dressed state can be adiabatically eliminated. The matrix describing the mean-field interactions can then be rewritten in the dressed basis using the unitary transformation $\mathcal{V}_\pm = U^\dagger \mathcal{V} U$, with $U = (\sigma_x + \sigma_z)/\sqrt{2}$ defined in terms of the Pauli matrices σ_x and σ_z, and reads as

$$\mathcal{V}_\pm \overset{a}{\approx} \begin{pmatrix} g & (g_{11} - g_{22})/4 \\ (g_{11} - g_{22})/4 & g \end{pmatrix} |\Phi_\pm|^2. \tag{3.5}$$

In writing Eq. (3.5), we have introduced the dressed scattering parameter $g = (g_{11} + g_{22} + 2g_{12})/4$, with the atomic populations in the dressed basis obtained from the projection

$$\Phi_{i=1,2} = \sum_{n=+,-} \langle i|\sigma_n^{(0)}\rangle \, \Phi_n \overset{a}{\approx} \langle i|\sigma_\pm^{(0)}\rangle \, \Phi_\pm. \tag{3.6}$$

The first-order corrections to the model can then be calculated directly from perturbation theory, leading to the perturbed or *'interacting'* dressed states

$$|\sigma_\pm\rangle \overset{a}{\approx} |\sigma_\pm^{(0)}\rangle \pm \frac{g_{11} - g_{22}}{8\hbar\Omega}|\Phi_\pm|^2 \, |\sigma_\mp^{(0)}\rangle, \tag{3.7}$$

with eigenvalues

$$E_\pm \overset{a}{\approx} \pm\frac{\hbar\Omega}{2} + g|\Phi_\pm|^2. \tag{3.8}$$

The state vector, in the basis of the interacting dressed states, can then be written in the adiabatic approximation as $|\Phi(\mathbf{r},t)\rangle \overset{a}{\approx} \Phi_\pm |\sigma_\pm\rangle$. Projecting this onto Eq. (3.1), leads to the effective Hamiltonian

$$\hat{H}_\pm \overset{a}{\approx} \frac{1}{2m}\left(\hat{\mathbf{p}} - \mathbf{A}_\pm\right)^2 + W + V \pm \frac{\hbar\Omega}{2} + \frac{g}{2}|\Phi_\pm|^2, \tag{3.9}$$

where the geometric potentials are given to leading order by

$$\mathbf{A}_\pm \overset{a}{\approx} i\hbar \langle \sigma_\pm|\nabla\sigma_\pm\rangle = \mathbf{A}^{(0)} \pm \mathbf{a}_1|\Phi_\pm|^2 + \mathcal{O}\left(\mathbf{a}_1\right)^2, \tag{3.10}$$

and

$$W \overset{a}{\approx} \frac{\hbar^2}{2m}|\langle \sigma_\mp|\nabla\sigma_\pm\rangle|^2 = \frac{|\mathbf{A}^{(0)}|^2}{2m} + \mathcal{O}\left(\mathbf{a}_1\right). \tag{3.11}$$

The form of the vector potential described by Eq. (3.10) highlights the central result of the model; that the effective detuning induced by the interacting gas can give rise to a density-dependent gauge potential, parametrised by the single-particle vector potential $\mathbf{A}^{(0)} = -(\hbar/2)\,\nabla\phi_\ell$ and strength $\mathbf{a}_1 = \nabla\phi_\ell\,(g_{11} - g_{22})\,/\,(8\hbar\Omega)$.

The equation of motion governing the evolution of the condensate amplitude $\Phi_\pm(\mathbf{r}, t)$ can then be found from variations of the Lagrangian functional

$$L_\pm \overset{a}{\approx} \int dr\ \left[\Phi_\pm^* \left(i\hbar\frac{\partial}{\partial t} - \hat{H}_\pm\right)\Phi_\pm\right], \tag{3.12}$$

with respect to $\Phi_\pm^*(\mathbf{r}, t)$ (see Sec. 4.2.1). After dropping the $\pm$ subscripts and the adiabatic notation, the mean-field Gross-Pitaevskii equation describing the condensate is then given by

$$i\hbar\frac{\partial\Phi}{\partial t} = \left[\frac{1}{2m}\left(\hat{\mathbf{p}}-\mathbf{A}\right)^2 + \mathbf{a_1}\cdot\mathbf{j} + W + V + \frac{\hbar\Omega}{2} + g|\Phi|^2\right]\Phi. \tag{3.13}$$

The density-dependent or *'interacting gauge theory'* described by Eq. (3.13) represents a novel nonlinear model in which the condensate dynamics is influenced by a back-action between the matter-field and the gauge potential. This is achieved through the appearance two geometric potentials on the mean-field level, but also by the presence of two nonlinearities: the standard cubic nonlinearity describing the contact interactions between the condensate atoms, and a new nonlinearity in the form of a probability current

$$\mathbf{j} = \frac{1}{2m}\left[\Phi\left(\hat{\mathbf{p}} + \mathbf{A}\right)\Phi^* - \Phi^*\left(\hat{\mathbf{p}} - \mathbf{A}\right)\Phi\right]. \tag{3.14}$$

Interestingly, this probability current is exactly the form known for a charged particle in an electromagnetic field, which in this model, acts as a collective drift of the condensate density $\rho(\mathbf{r}, t) = |\Phi(\mathbf{r}, t)|^2$, via the continuity equation

$$\frac{\partial\rho}{\partial t} = -\nabla\cdot\mathbf{j}. \tag{3.15}$$

Despite the structure of these equations, this model unfortunately does not describe a dynamical gauge theory, as the corresponding magnetic field vanishes in the absence of the interacting gas. However, Eq. (3.13) does represent an interesting model from a nonlinear dynamics perspective, due to the appearance of the current nonlinearity and gauge potentials. In other works, it has been demonstrated how these can lead to unconventional vortex dynamics in a two-dimensional system [87, 88], as well as various novel scenarios for the one-dimensional condensate which will be detailed in the next section.

3.3 One-dimensional reduction

One of the major advantages in the experimental control of ultracold gases is the ability to restrict the effective dimensionality of the system by controlling the individual oscillation frequencies of the trapping potential [30]. For our purposes, we will primarily be interested in the one-dimensional properties of the model, in order to study the soliton solutions of the interacting gauge theory.

To achieve this, we assume that the harmonic potential is tightly confined in the radial plane $\mathbf{r}_\perp(y,z)$, but weakly trapped along the axial x-axis, such that $\omega_\perp = \omega_y = \omega_z$ with $\omega_\perp \gg \omega_x$. In this regime, the condensate dynamics in the radial plane can be regarded as effectively stationary, with transitions to the excited states of the radial trap being energetically unfavourable, provided $\hbar\omega_\perp \gg g|\Phi|^2$. The total condensate wavefunction can then be factorised as [89, 90]

$$\Phi(\mathbf{r},t) = \Psi(x,t)\Psi_\perp(y,z)e^{-i\mu t/\hbar}e^{i\phi_\ell/2}, \tag{3.16}$$

where the radial wavefunction $\Psi_\perp(y,z)$ is approximately described by the ground-state solution

$$\Psi_\perp(y,z) = \frac{1}{\sqrt{\pi}\ell_\perp}e^{-(y^2+z^2)/2\ell_\perp}, \tag{3.17}$$

satisfying

$$\left[-\frac{\hbar^2}{2m}\left(\frac{\partial^2}{\partial y^2}+\frac{\partial^2}{\partial z^2}\right)+\frac{1}{2}m\omega_\perp^2\left(y^2+z^2\right)\right]\Psi_\perp(y,z) = \mu\Psi_\perp(y,z). \tag{3.18}$$

Substituting Eq. (3.16) into Eq. (3.13), multiplying by $\Psi_\perp(y,z)$, and integrating over the radial area of the gas leads to the quasi one-dimensional form

$$i\hbar\frac{\partial\Psi}{\partial t} = \left[\frac{1}{2m}\left(\hat{p}-a_1|\Psi|^2\right)^2 + a_1 j(x) + \tilde{W} + \frac{1}{2}m\omega_x^2x^2 + \frac{\hbar\Omega}{2} + g_{1\mathrm{D}}|\Psi|^2\right]\Psi, \tag{3.19}$$

and

$$j(x) = \frac{1}{2m}\left[\Psi\left(\hat{p}+a_1|\Psi|^2\right)\Psi^* - \Psi^*\left(\hat{p}-a_1|\Psi|^2\right)\Psi\right], \tag{3.20}$$

where the zeroth-order contribution to the vector potential has been eliminated by setting $\phi_\ell = q_\ell x$, with wave-vector q_ℓ. The scalar potential appearing in Eq. (3.19) is given by $\tilde{W} = \hbar^2 q_\ell^2/(8m)$, with the scattering parameters $g_{1\mathrm{D}} = g/(2\pi\ell_\perp^2)$ and $a_1 = q_\ell\left(g_{11}-g_{22}\right)/\left(16\pi\ell_\perp^2\Omega\right)$, rescaled by the radial area of the gas.

Rather than working with Eq. (3.19) directly, it will be favourable in most cases

to work instead in the complementary picture

$$i\hbar\frac{\partial\psi}{\partial t} = \bigg[-\frac{\hbar^2}{2m}\frac{\partial^2}{\partial x^2} - 2a_1 j'(x) + \frac{1}{2}m\omega_x^2 x^2 + g_{1\mathrm{D}}|\psi|^2 \bigg]\psi, \tag{3.21}$$

with

$$j'(x) = \frac{\hbar}{2mi}\bigg[\psi^*\frac{\partial\psi}{\partial x} - \psi\frac{\partial\psi^*}{\partial x}\bigg], \tag{3.22}$$

which is arrived at by using the nonlinear transformation

$$\Psi(x,t) = \psi(x,t)\exp\left(-\frac{i\tilde{W}t}{\hbar} - \frac{i\Omega t}{2} + \frac{ia_1}{\hbar}\int_{-\infty}^{x} dx'\rho(x',t)\right). \tag{3.23}$$

In the absence of the trapping potential and the cubic nonlinearity, Eq. (3.21) is often referred to in the literature as a *'chiral nonlinear Schrödinger equation',* which was originally studied in the context of one-dimensional anyons [91]. Compared to the standard Gross-Pitaevskii equation and several derivative-type nonlinear equations [92, 93], this model is generally *non-integrable*, due to failing both the Inverse Scattering and Painlevé tests [94–96]. Additionally, the model is not invariant under either a Galilean or parity transformation [97, 98], which consequently leads to breakdown of the conservation of canonical momentum. These properties in part, can then lead to many unconventional scenarios featuring chiral transport dynamics for the one-dimensional condensate, including the asymmetric expansion of the condensate envelope [48], collective modes which violate Kohn's theorem [99], and the central topic of this thesis; the emergence of *chiral* soliton solutions [52, 53, 97, 98].

At this stage, it is important to stress that Eq. (3.23) is *not* a gauge transformation, but rather a *nonlinear* transformation of the field, as several dynamical quantities, such as the momentum and energy densities, are modified in the transformed picture [97, 100] (see Sec. 4.4). This property will have profound consequences in the variational description of the chiral model and will be the main subject of the following chapter. Additionally, here and throughout the rest of this thesis, we will label the equations of motion, Eq. (3.19) and Eq. (3.21), as being in the *'standard'* and *'transformed'* pictures respectively, in preparation for these discussions.

As a final note before proceeding, it is important to discuss the practicalities of realising the one-dimensional interacting gauge theory in ultracold experiments, in addition to corrections of the one-dimensional model which arise from the residual dimensionality of the system. For the first point the principle criteria are:

(i) *The atomic lifetimes in both internal states should be long-lived and on the order of the condensate lifetime, to offset losses to spontaneous emission.*

(ii) *The coupling between the dressed states and any other atomic states should minimised, as set by the adiabatic approximation* $\hbar\Omega \gg g_{ii'}|\Phi_{i'}|^2$.

(iii) *The difference in the scattering parameters of the internal states should be significant in order for the strength of the gauge field to be meaningful, such that* $g_{11} \neq g_{22}$.

For these reasons, the use of standard alkali species such as Rubidium, which feature fast decay rates in addition to small differences in the scattering parameters of the hyperfine manifold, would render these systems unsuitable for realising the interacting gauge theory. Instead, condensates composed of Strontium, Calcium, or Ytterbium atoms would provide a more favourable option [48], due to their long radiative lifetimes. However, we should note that the drawbacks associated with alkali atoms could potentially be circumvented using dark states [46], as well as through careful tuning of Feshbach resonances [32]. More details are provided in Ref. [48].

In regards to the second point, there are two experimentally-relevant properties of the three-dimensional gas that are neglected in the one-dimensional model:

(i) *For a cylindrically-trapped condensate with attractive interactions* ($g < 0$)*, the number of condensate atoms must not exceed the critical value* $N_{\max} \leq 0.68\ell_\perp/|a_s|$*, in order to avoid critical collapse* [101].

(ii) *Three-body inelastic collisions, described by a cubic-quintic nonlinearity* [102, 103], *which arise from the fact that the condensate dynamics in the transverse plane are strictly speaking non-stationary.*

These two points are particularly important in the discussion of bright solitons, as the first imposes a strict stability criterion for the gas, with the second contributing not only to atomic losses, but also to the onset of non-integrable dynamics in the system. This latter point, in addition to the fact that a harmonic trapping potential also (albeit weakly) breaks the integrability of the system, can potentially have detrimental effects on the coherence of soliton collisions, including soliton bound states and fusion [102], in addition to a interaction-induced shift of the soliton oscillation frequency, as demonstrated in ultracold experiments [104].

3.4 Breakdown of Galilean invariance

In classical mechanics, the property of Galilean invariance is a common dynamical feature which states that the laws of motion are equivalent in all inertial reference frames. The same principle also applies for several wave equations, such as the

linear and non-linear Schrödinger equations, and the Korteweg-de Vries equation. As we will demonstrate, our interacting gauge theory is unfortunately not Galilean invariant, and will lead to contradictory dynamics between a stationary and moving condensate. Notably, a similar situation also appears in spin-orbit coupled condensates [105, 106].

To illustrate this, we consider two inertial reference frames, in which one of the reference frames is moving relative to the second at a constant velocity v. The transformation between the stationary-frame coordinates (x, t) and moving-frame coordinates (x_m, t_m), are given by the translations $x_m \to x - vt$ and $t_m \to t$, with the translated differential operators

$$\frac{\partial}{\partial t} \to \frac{\partial}{\partial t_m} - v\frac{\partial}{\partial x_m}, \tag{3.24}$$

and

$$\frac{\partial}{\partial x} \to \frac{\partial}{\partial x_m}. \tag{3.25}$$

In addition to this, an additional phase factor in the condensate wavefunction is required to describe the relative motion between the reference frames, and can be written using a Madelung transformation

$$\psi(x, t) = \varphi(x_m, t_m)e^{iS(x_m,t_m)}, \tag{3.26}$$

where $\varphi(x_m, t_m)$ and $S(x_m, t_m)$ are real functions corresponding to the envelope and phase of the condensate respectively. In the following, we impose no restrictions on the form of $\varphi(x_m, t_m)$ except that it must be a continuously differentiable function. Whereas for $S(x_m, t_m)$, we will explicitly assume that it is a linear function in the coordinates x_m and t_m, such that all derivatives of second-order and higher equate to zero.

By substituting the above set of translations into Eq. (3.21) and equating the real and imaginary parts, the interacting gauge theory can be rewritten as

$$\hbar v\varphi\frac{\partial S}{\partial x_m} - \varphi\frac{\partial S}{\partial t_m} = -\frac{\hbar^2}{2m}\left[\frac{\partial^2\varphi}{dx_m^2} - \varphi\left(\frac{\partial S}{\partial x_m}\right)^2\right] + \left[g_{1\mathrm{D}} - \frac{2a_1\hbar}{m}\frac{\partial S}{\partial x_m}\right]\varphi^3 \tag{3.27}$$

and

$$\hbar v\frac{\partial\varphi}{\partial x_m} = \frac{\hbar^2}{2m}\frac{\partial\varphi}{\partial x_m}\frac{\partial S}{\partial x_m}. \tag{3.28}$$

Then, by decoupling the phase function as $S(x_m, t_m) = S(x_m) + S(t_m)$, we can

directly integrate Eq. (3.28) to obtain the spatial contribution of the phase

$$S(x_m) = \frac{mvx_m}{\hbar} + \phi_0, \tag{3.29}$$

where ϕ_0 is an absolute phase arising from the initial condition $S(x_m)|_{x_m=0} = \phi_0$. Inserting this solution into Eq. (3.27) then leads to the expression

$$-\varphi \frac{d}{dt_m} S(t_m) + mv^2 = \underbrace{\left[-\frac{\hbar^2}{2m}\frac{d^2}{dx_m^2}\varphi + (g_{1\mathrm{D}} - 2a_1 v)\,\varphi^3 \right]}_{=\mu\varphi} + \frac{mv^2}{2}, \tag{3.30}$$

where the underbraced term is identified as the stationary equation for the condensate envelope with chemical potential μ. The temporal contribution of the phase can then be readily obtained as

$$S(t_m) = \frac{mv^2 t_m}{2\hbar} - \frac{\mu t_m}{\hbar}, \tag{3.31}$$

with the initial condition $S(t_m)|_{t_m=0} = 0$. Combining these results, the total phase profile for the moving-frame condensate then reads as

$$S(x_m, t_m) = \left(mvx_m + mv^2 t_m/2 - \mu t_m \right)/\hbar + \phi_0, \tag{3.32}$$

which takes the familiar form of a plane-wave which imprints a momentum boost onto the condensate envelope.

Returning to the topic at hand, we may now write the Galilean transformation for the moving-frame picture as

$$\psi(x,t) = \varphi(x_m, t_m) e^{i(mvx_m + mv^2 t_m/2)/\hbar}, \tag{3.33}$$

with the stationary transformation excluded. The dynamics of the condensate in the moving-frame is then described by the equation of motion

$$i\hbar \frac{\partial \varphi}{\partial t_m} = \left[-\frac{\hbar^2}{2m}\frac{\partial^2}{\partial x_m^2} - 2a_1 j'(x_m) + (g_{1\mathrm{D}} - 2a_1 v)\,|\varphi|^2 \right]\varphi. \tag{3.34}$$

The introduction of the renormalised scattering parameter $\tilde{g}_{1\mathrm{D}} = g_{1\mathrm{D}} - 2a_1 v$ highlights that Eq. (3.21) is not Galilean invariant, with the effective strength of the mean-field interactions dependent on both the magnitude and direction that the condensate is moving. The same result can also be obtained in a more modest calculation by applying the quotient rule to rewrite the current nonlinearity as

$$j'(x) = \frac{\hbar}{2mi}\left[\psi^* \frac{\partial \psi}{\partial x} - \psi \frac{\partial \psi^*}{\partial x} \right] = \frac{\hbar}{2mi}\left[\frac{d}{dx}\frac{\psi}{\psi^*} \right] |\psi|^2, \tag{3.35}$$

which highlights the introduction of an effective cubic nonlinearity when the condensate wave function is modulated by a spatially-varying phase. This feature details the chiral nature of the condensate dynamics, and as we will show later, will lead to the emergence of chiral soliton solutions [97, 98].

3.5 Breakdown of integrability

The property of integrability is arguably one of the most important and profound features for the dynamical behaviour of a given model. Many of the standard nonlinear wave equations, such as the nonlinear Schrödinger, Korteweg-de Vries, and Sine-Gordon equations, are integrable equations, and where each studied historically in the framework of the Inverse Scattering transform [3–5].

> **Definition 3.1:** *A partial differential equation is said to be fully integrable if the following conditions are true* [13]:
>
> (i) *The solution to a well-posed initial or boundary value problem can be expressed using elementary functions and obtained in a finite number of algebraic operations.*
>
> (ii) *The model contains an infinite number of conservation laws, where each integral of motion is in involution with another (i.e. their Poisson bracket commutes), and are periodically bounded in a compact phase-space; the Liouville-Arnol'd theorem.*

In the context of the Inverse Scattering transform, the first of these conditions details that the single- and N-soliton solutions to a suitable nonlinear equation can be constructed.[i] Whereas the second highlights that these models are highly constrained by the existence of an infinite number of conservations laws, with the dynamics experiencing periodic behaviour; the absence of chaotic motion as demonstrated in the Fermi-Pasta-Ulam-Tsingou problem [107].

In the case of the interacting gauge theory, the model is non-integrable as it fails both the Inverse Scattering and Painlevé tests [94–96]. As the proof of these is an involved calculation, we will not reproduce the results presented in these papers, but instead demonstrate how the integrability of the model can be restored in a more modest calculation. To show this, we consider a derivative nonlinear Schrödinger

[i] By suitable, we refer to an integrable nonlinear partial differential equation which supports a soliton solution.

equation counterpart to the interacting gauge theory

$$i\hbar\frac{\partial\Psi}{\partial t}=\left[-\frac{\hbar^2}{2m}\frac{\partial^2}{\partial x^2}-\frac{a_1\hbar}{mi}\left(2\Psi^*\frac{\partial\Psi}{\partial x}+\Psi\frac{\partial\Psi^*}{\partial x}\right)+g_{1\mathrm{D}}|\Psi|^2\right]\Psi, \tag{3.36}$$

which is an integrable model studied in the context of plasma physics and optical fibres [92, 108, 109]. By redefining the nonlinear transformation as

$$\Psi(x,t)=\psi(x,t)\exp\left(\frac{ia_1}{\hbar}\int_{-\infty}^{x}dx'\rho(x',t)\right), \tag{3.37}$$

and applying this expression to Eq. (3.36), one obtains the equation

$$i\hbar\frac{\partial\psi}{\partial t}=\left[-\frac{\hbar^2}{2m}\frac{\partial^2}{\partial x^2}-2a_1j'(x)+g_{1\mathrm{D}}|\psi|^2-\frac{3a_1^2}{2m}|\psi|^4\right]\psi. \tag{3.38}$$

As the nonlinear transformation defined above only involves a change of the dependent variable, the above equation is also integrable [96]; highlighting that the integrability of our model can be restored by adding the additional quintic term. However the solitons in that case will no longer be chiral [91]. Illustrative examples of how the non-integrability of the interacting gauge theory modifies the condensate dynamics will be shown when we study the interactions of chiral solitons in Chap. 7.

3.6 Summary and outlook

In this chapter, we have demonstrated how one can engineer a density-dependent or *'interacting gauge theory'* in an ultracold bosonic gas. This was achieved by the presence of an effective detuning in an optically dressed two-component interacting gas, where one of the interacting dressed states is adiabatically eliminated from the system dynamics. Although the resulting gauge theory was not completely dynamical, as the effective magnetic field vanishes in the absence of the interacting gas, the nonlinear model features new novel features, including the breakdown of both integrability and Galilean invariance, which greatly modify the dynamics of the gas. The study of these features will be the central topic for the remainder of this thesis, as we focus our attention to the study of solitons.

As a final note on the topic of synthetic gauge potentials, we note that although these artificial gauge theories fall short in correctly capturing all the features of a given model, they instead describe systems which are different than those present in nature; a property which emphasises their artificial origin [46]. With this, we can pose an alternative proposition for the field of synthetic gauge potentials; the engineering and simulation of exotic states of matter which have no analogues in nature. This idea has already been presented in the form of spin-orbit coupled

bosons with synthetic spin-1/2 statistics [110, 111], with future proposals aimed at how such a system can be used for strongly correlated topological matter, such as topological insulators which feature metallic surface states [112].

Chapter 4

Variational descriptions of a density-dependent gauge theory

4.1 Introduction

The techniques of Lagrangian and Hamiltonian mechanics, together with the calculus of variations, plays a historic role for the description and solutions of various dynamical problems in classical mechanics. These methods are powerful, offering insight not only of the motion of objects, but also providing an elegant description of the conservation laws and the corresponding symmetries underpinning a given dynamical model. In particular, the development from a discrete model to a continuum one, which amounts to a classical field theory, is important for the description of nonlinear wave equations and understanding how the integrability of such models manifests. Additionally, the quantisation of such a model as a quantum field theory, is central in the description of the fundamental forces between particles in the framework of the standard model [113, 114], as well as various topics in condensed matter physics such as superconductivity and the interacting bosonic gas [115, 116].

The details of formulating the one-dimensional interacting gauge theory in a variational framework were first presented in the original work by Aglietti et al. [91], borrowing principles known from the derivative nonlinear Schrödinger equation [108, 109]. A complete description detailing the symmetries and corresponding conservation laws was then later introduced by Jackiw [97], with a further extension to the hydrodynamic picture performed by Lee et al. [100]. For our purposes, we set out to further extend the above work in order describe our density-dependent gauge theory in the variational framework. At first, the proposition of this problem may seem trivial, merely amounting to the addition of the mean-field interactions and the trapping potential on the variational level. However, we will demonstrate that the mapping between the standard and transformed pictures requires care, as it can lead to non-trivial results for the variational functions and their corresponding conservation laws.

4.2 Preliminaries

Before proceeding to describe our model in the variational framework, it is instructive to first present a brief review of the calculus of variations and its application in the Lagrangian and Hamiltonian descriptions of a classical field theory. In the following proofs, we will draw inspiration from the details presented in the books by Greiner and Reinhardt [113], as well as Goldstein [117], but restricted to the case of only a single spatial coordinate.

4.2.1 Lagrangian field theory

The central concept in the description of a classical field theory lies in the definition of the action functional

$$\mathcal{S} \equiv \int_{t_1}^{t_2} dt\ L\left[\Psi, \Psi_t\right], \tag{4.1}$$

which describes all of the available paths that a system, defined by the Lagrangian $L\left[\Psi, \Psi_t\right]$, can traverse in the time interval $t = t_2 - t_1$. Here, we have introduced the compact notation, $\Psi_i = \partial\Psi/\partial i$, for the coordinates $i = \{x, t\}$. Hamilton's principle, or the *'principle of stationary action'*, states that the true path that the system evolves under, is the one which corresponds to a stationary point of the action. Mathematically speaking, this details that the optimal path is the solution for the minimisation problem

$$\frac{\delta\mathcal{S}}{\delta\Psi^*} = 0, \tag{4.2}$$

where $\delta/\delta\Psi^*$ represents the functional derivative, which will be derived as follows.

Definition 4.1: *The variation of a functional $F[\Psi]$ is defined as*

$$\delta F[\Psi] = \int dx\ \frac{\delta F}{\delta\Psi}\delta\Psi. \tag{4.3}$$

Applying the above definition to the action functional returns the expression

$$\delta\mathcal{S} = \int_{t_1}^{t_2} dt\ \left[\frac{\delta L}{\delta\Psi^*}\delta\Psi^* + \frac{\delta L}{\delta\Psi_t^*}\delta\Psi_t^*\right], \tag{4.4}$$

with $\delta\Psi_t^* = \partial/\partial t\left(\delta\Psi^*\right)$. Provided all of the available trajectories converge to a fixed point at each limit of the time interval, we may use integration by parts, together

with the boundary conditions $\delta\Psi^*(x,t_1) = \delta\Psi^*(x,t_2) = 0$, to rewrite the integral as

$$\delta\mathcal{S} = \int_{t_1}^{t_2} dt \left[\frac{\delta L}{\delta\Psi^*} - \frac{\partial}{\partial t}\frac{\delta L}{\delta\Psi_t^*}\right]\delta\Psi^* = 0, \tag{4.5}$$

where the bracketed term is the famous Euler-Lagrange equation encountered in the calculus of variations. The stationary solution can be determined from studying the variations of the Lagrange functional.

To describe a scalar field which extends over all space, the Lagrangian functional can be written as the spatial integral over a Lagrangian density

$$L(t) = \int dx\, \mathcal{L}\left(\Psi, \Psi_x, \Psi_t\right), \tag{4.6}$$

which describes the value and gradients of a field at each position at a given moment in time. Reusing Definition 4.1, one can then write the variation of the Lagrangian as

$$\delta L(t) = \int dx \left(\frac{\partial\mathcal{L}}{\partial\Psi^*}\delta\Psi^* + \frac{\partial\mathcal{L}}{\partial\Psi_x^*}\delta\Psi_x^* + \frac{\partial\mathcal{L}}{\partial\Psi_t^*}\delta\Psi_t^*\right) = 0. \tag{4.7}$$

Then, by using integration by parts as before, we obtain the variation

$$\delta L(t) = \int dx \left[\frac{\delta}{\delta\Psi^*}\mathcal{L}\left(\Psi, \Psi_x, \Psi_t\right)\right]\delta\Psi^* = 0, \tag{4.8}$$

where we identify the Fréchet or variational derivative

$$\frac{\delta}{\delta\Psi^*} = \frac{\partial}{\partial\Psi^*} - \frac{d}{dx}\frac{\partial}{\partial\Psi_x^*} - \frac{d}{dt}\frac{\partial}{\partial\Psi_t^*}. \tag{4.9}$$

The solution of the above Euler-Lagrange equation, is therefore the one for which Hamilton's principle is satisfied. Once the Lagrangian density is known, the corresponding field equations can be determined.

4.2.2 Hamiltonian field theory

To formulate the field theory in the Hamiltonian picture, we introduce the Legendre transformation

$$\mathcal{H}\left(\Psi, \Psi^*, \Pi, \Pi^*\right) = \Pi\frac{\partial\Psi}{\partial t} + \Pi^*\frac{\partial\Psi^*}{\partial t} - \mathcal{L}\left(\Psi, \Psi_x, \Psi_t\right), \tag{4.10}$$

where the Hamiltonian density $\mathcal{H}\left(\Psi, \Psi^*, \Pi, \Pi^*\right)$ is defined by the introduction of conjugate momentum fields $\Pi = \partial\mathcal{L}/\partial\Psi_t$ and $\Pi^* = \partial\mathcal{L}/\partial\Psi_t^*$. Substituting Eq. (4.10)

into Eq. (4.8) and equating the integrand to zero leads to Hamilton's first equation

$$\frac{\delta \mathcal{H}}{\delta \Psi^*} = \frac{\delta}{\delta \Psi^*}\left(\Pi \frac{\partial \Psi}{\partial t} + \Pi^* \frac{\partial \Psi^*}{\partial t}\right), \tag{4.11}$$

and Hamilton's second equation

$$\frac{\delta \mathcal{H}}{\delta \Pi} = \frac{\delta}{\delta \Pi}\left(\Pi \frac{\partial \Psi}{\partial t} + \Pi^* \frac{\partial \Psi^*}{\partial t}\right), \tag{4.12}$$

after a change of variables. The corresponding Hamiltonian, in a similar manner to the Lagrangian, is given by the spatial integral

$$H = \int dx\, \mathcal{H}\left(\Psi, \Psi_x\right), \tag{4.13}$$

which critically does not contain a time derivative of the field.

4.2.3 Noether's theorem

Conservation laws are important in our understanding of the dynamics and constraints of a given model. Most of the physical models we encounter in undergraduate studies feature these constraints, such as the conservation of momentum and energy in classical mechanics, and the conservation of probability in quantum mechanics. The description of these quantities in the field theory setting was derived in the celebrated work of Noether, and can be stated as:

> **Definition 4.2:** *For every continuous symmetry in which the action of a system is invariant, there exists a corresponding conservation law.*

Here, we will not detail the derivation of Noether's theorem extensively, and instead simply quote the essential results [13, 113].

By denoting the set of infinitesimal translations of the coordinates and the fields as $x \to x + \varepsilon x_c$, $t \to t + \varepsilon t_c$, and $\Psi \to \Psi + \varepsilon \Psi_c$, with the perturbation parameter $\varepsilon \ll 1$, it can be shown that the invariance of the action leads to the continuity equation

$$\frac{\partial Q}{\partial t} = -\frac{\partial J}{\partial x}. \tag{4.14}$$

This expression describes the conservation of the Noether charges

$$Q = \int dx f_t, \tag{4.15}$$

and Noether currents

$$J = \int dx f_x, \tag{4.16}$$

with

$$f_\nu = \left[\frac{\partial \mathcal{L}}{\partial \Psi_\nu} \left(\Psi_c - x_c \frac{\partial \Psi}{\partial x} - t_c \frac{\partial \Psi}{\partial t} \right) + c.c \right] + \nu_c \mathcal{L}. \tag{4.17}$$

Details on how the continuous symmetries lead to expressions for the conserved quantities will be shown later in the chapter.

4.3 Lagrangian and Hamiltonian formulations

With a review of the Lagrangian and Hamiltonian field theories concluded, we can now proceed to describe the interacting gauge theory in the variational framework. We draw particular attention to the results presented in this subsection, as the Lagrangian and Hamiltonian densities will be used frequently in the following chapters of the thesis.

To begin, we first consider the variational problem for the standard picture, Eq. (3.19). The corresponding Lagrangian density, in the absence of the trapping and scalar potentials, can be written as [91, 97, 98]

$$\mathcal{L}\left(\Psi, \Psi_x, \Psi_t\right) = \frac{i\hbar}{2} \left(\Psi \frac{\partial \Psi^*}{\partial t} - \Psi^* \frac{\partial \Psi}{\partial t} \right) + \frac{1}{2m} \left| \left(\hat{p} - a_1 |\Psi|^2 \right) \Psi \right|^2 + \frac{g}{2} |\Psi|^4. \tag{4.18}$$

It is straightforward to demonstrate that by substituting Eq. (4.18) into Eq. (4.8) and setting the integrand to zero, that the Lagrangian density correctly reduces to the equation of motion.

The Lagrangian density and Euler-Lagrange equations in the transformed picture can then be calculated directly from applying Eq. (3.37), and read as

$$\begin{aligned} \mathcal{L}\left(\psi, \psi_x, \psi_t\right) = \frac{i\hbar}{2} \left(\psi \frac{\partial \psi^*}{\partial t} - \psi^* \frac{\partial \psi}{\partial t} \right) + \frac{\hbar^2}{2m} \left| \frac{\partial \psi}{\partial x} \right|^2 \\ + \frac{g}{2} |\psi|^4 + a_1 |\psi|^2 \int_{-\infty}^{x} dx' \frac{\partial}{\partial t} \rho(x', t) \end{aligned} \tag{4.19}$$

and

$$\delta L(t) = \int dx \left[\frac{\delta}{\delta \psi^*} \mathcal{L}\left(\psi, \psi_x, \psi_t\right) \right] \delta \psi^* \tag{4.20}$$

respectively. A peculiar attribute of the transformed picture is highlighted here, with the appearance of a non-local contribution to the Lagrangian density. This term complicates the minimisation procedure of the transformed Lagrangian density, requiring several non-trivial steps in order to reduce correctly to the equation of motion, as we outline as follows.

> **Lemma 4.1:** *The reduction of the transformed Lagrangian density* $\mathcal{L}(\psi, \psi_x, \psi_t)$ *can be achieved using the Madelung transformation,* $\psi(x,t) = \varphi(x,t)e^{i\phi(x,t)}$, *where* $\varphi(x,t)$ *and* $\phi(x,t)$ *are real functions.*

Proof: The first step involves rewriting the non-local integral in term of the probability current, by using the continuity equation

$$\frac{\partial}{\partial t}\rho(x',t) = -\frac{\partial}{\partial x'}j'(x',t) \quad \Longrightarrow \quad \int_{-\infty}^{x} dx' \frac{\partial}{\partial t}\rho(x',t) = -j'(x,t). \tag{4.21}$$

Then, by substituting the resulting Lagrangian density into Eq. (4.20), one obtains the integral expression

$$\int dx \left[-i\hbar\frac{\partial\psi}{\partial t} + g|\psi|^2\psi - \frac{\hbar^2}{2m}\frac{\partial^2\psi}{\partial x^2} - \frac{a_1\hbar}{mi}\left(2\psi^*\frac{\partial\psi}{\partial x}\right)\psi \right] \delta\psi^*. \tag{4.22}$$

The final task requires the decomposition of the current term using integration by parts

$$\int dx \left[-\frac{a_1\hbar}{mi}\left(2\psi^*\frac{\partial\psi}{\partial x}\right)\psi \right] \delta\psi^* = \int dx \left[-\frac{a_1\hbar}{mi}\left(\psi^*\frac{\partial\psi}{\partial x} - \psi\frac{\partial\psi^*}{\partial x}\right)\psi \right] \delta\psi^*, \tag{4.23}$$

which can be proved using a Madelung transformation. Setting the integrand of Eq. (4.22) to zero together with this result, then leads to the transformed equation of motion, as required.[i]

Using the Lagrangian densities, the corresponding Hamiltonian densities can be directly obtained from applying the Legendre transformation, Eq. (4.10), and are given by

$$\mathcal{H}(\Psi, \Psi^*) = -\frac{1}{2m}\left| \left(\hat{p} - a_1|\Psi|^2\right)\Psi \right|^2 - \frac{g_{1\mathrm{D}}}{2}|\psi|^4, \tag{4.24}$$

and

$$\mathcal{H}(\psi, \psi^*) = -\frac{\hbar^2}{2m}\left|\frac{\partial\psi}{\partial x}\right|^2 - \frac{g_{1\mathrm{D}}}{2}|\psi|^4, \tag{4.25}$$

for the standard and transformed pictures respectively. Note, that it is critical that

[i] This refutes the claim in Ref. [98], that Eq. (3.21) cannot be obtained from a purely local Lagrangian density.

one obtains the transformed Hamiltonian density by applying the nonlinear transformation to Eq. (4.24), as one can encounter inconsistencies through the Legendre transformation approach.

At first glance, Eq. (4.25) would appear to be an incorrect Hamiltonian density as it does not contain any explicit dependence on the gauge field. This matter is resolved by noting that Hamilton's equations are also modified in the transformed picture as

$$\frac{\delta \mathcal{H}}{\delta \psi^*} = \frac{\delta}{\delta \psi^*}\left[\Pi\left(\frac{\partial \psi}{\partial t} - \frac{ia_1}{\hbar}\psi j'\right) + \Pi^*\left(\frac{\partial \psi^*}{\partial t} + \frac{ia_1}{\hbar}\psi^* j'\right)\right]. \tag{4.26}$$

Reusing the techniques described previously in Lemma 4.1, then correctly leads to the equation of motion. The minimisation for the standard picture, in a similar manner to the Lagrangian case, is straightforward to prove and is not presented.

4.4 Conservation laws

As detailed earlier in Definition 3.1, one of the defining properties of integrable models is that they possess an infinite number of conservation laws. As the chiral model is non-integrable, and therefore cannot be described in the framework of the Inverse Scattering transform, we unfortunately cannot determine the nature and number of conservation laws in this way. However, we can at the very least derive the principle conservations laws using Noether's theorem [97, 100], by considering the continuous symmetries of the model.

The first symmetry to consider is an infinitesimal change in the phase of the wavefunctions, which corresponds to the familiar $U(1)$ gauge symmetry encountered in electromagnetism. Setting the infinitesimal translations of the coordinates as $x_c = t_c = 0$ in Eq. (4.15), and identifying $\Psi_c = i\Psi/\hbar$ from the following first-order expansion

$$\Psi e^{i\varepsilon/\hbar} \approx \Psi + \frac{i\varepsilon}{\hbar}\Psi + \mathcal{O}(\epsilon)^2, \tag{4.27}$$

leads to the conserved quantity

$$N = \int_{-\infty}^{\infty} dx\ |\Psi|^2 = \int_{-\infty}^{\infty} dx\ |\psi|^2, \tag{4.28}$$

which describes the conservation of the particle number N in both the standard and transformed pictures. The corresponding Noether currents can then be calculated

from Eq. (4.16), and are given by

$$J_N = \frac{1}{2m}\left[\Psi\left(\hat{p}+a_1|\Psi|^2\right)\Psi^* - \Psi^*\left(\hat{p}-a_1|\Psi|^2\right)\Psi\right] = \frac{\hbar}{2mi}\left[\psi^*\frac{\partial\psi}{\partial x} - \psi\frac{\partial\psi^*}{\partial x}\right]. \quad (4.29)$$

These expressions are exactly the probability currents featured in Eqs. (3.20) and (3.22), for the standard and transformed equations of motion respectively.

The next symmetry to consider is translational invariance, in which the fields are unchanged under a small spatial translation, with $t_c = \Psi_c = 0$ and $x_c = 1$. The Noether charges and currents are given by

$$P = -i\hbar\int_{-\infty}^{\infty} dx\ \Psi^*\frac{\partial\Psi}{\partial x} = -i\hbar\int_{-\infty}^{\infty} dx\ \psi^*\frac{\partial\psi}{\partial x} + a_1\int_{-\infty}^{\infty} dx\ |\psi|^4, \quad (4.30)$$

and

$$\begin{aligned} J_P &= -\frac{1}{2m}\left|\left(\hat{p} - a_1|\Psi|^2\right)\Psi\right|^2 - \frac{\hbar^2}{4m}\frac{d^2}{dx^2}|\Psi|^2 + \frac{g}{2}|\Psi|^4 \\ &= -\frac{\hbar^2}{2m}\left|\frac{d\psi}{dx}\right|^2 - \frac{\hbar^2}{4m}\frac{d^2}{dx^2}|\psi|^2 + \frac{g}{2}|\psi|^4, \end{aligned} \quad (4.31)$$

which highlights an important dynamical property of the chiral model; that the canonical momentum is not a conserved quantity in the transformed picture. Instead, the momentum density features an additional term due to the action of the gauge field, in a similar manner to a classical particle travelling in an electromagnetic field. Additionally, this feature also emphasizes that Eq. (3.23) is *not* a gauge transformation, but rather a nonlinear transformation of the field.

Finally, for an infinitesimal temporal translation that leaves the fields unchanged, with $x_c = \Psi_c = 0$ and $t_c = 1$, we find the conserved quantities

$$\begin{aligned} E &= \int_{-\infty}^{\infty} dx\ \left(\frac{1}{2m}\left|\left(\hat{p} - a_1|\Psi|^2\right)\Psi\right|^2 + \frac{g_{1\mathrm{D}}}{2}|\Psi|^4\right) \\ &= \int_{-\infty}^{\infty} dx\left(\frac{\hbar^2}{2m}\left|\frac{\partial\psi}{\partial x}\right|^2 + \frac{g_{1\mathrm{D}}}{2}|\psi|^4\right), \end{aligned} \quad (4.32)$$

which describes the conservation of energy. The integrands in the above densities, are simply the corresponding Hamiltonian densities in the standard and transformed pictures, up to a minus sign, which are expected due to the fact that each model is

self-adjoint. Finally, the corresponding Noether currents are given by

$$\begin{aligned} J_E &= -\frac{\hbar}{2m}\left[i\frac{\partial\Psi^*}{\partial t}\left(\hat{p}-a_1|\Psi|^2\right)\Psi\right]+c.c \\ &= -\frac{\hbar^2}{2m}\left[\left(\frac{\partial\psi^*}{\partial t}+\frac{ia_1}{\hbar}j'\psi^*\right)\frac{\partial\psi}{\partial x}\right]+c.c, \end{aligned} \tag{4.33}$$

which together with the energy densities, further highlights that Eq. (3.23) is a nonlinear transformation.

In addition to the three conservation laws detailed above, a fourth symmetry of the chiral model also exists in the form of dilation invariance [97, 118], which details that the properties of a system are unchanged under a scaling transformation of the space-time coordinates and fields

$$x \to \sqrt{\varepsilon}x \quad , \quad t \to \varepsilon t \quad , \quad \psi(x,t) \to (\varepsilon)^{1/4}\psi(\sqrt{\varepsilon}x, \varepsilon t). \tag{4.34}$$

This means, that the physics of a model is the same at all length scales. It is straightforward to demonstrate that by inserting the above transformations into either Eq. (3.19) or Eq. (3.21), leads to an equivalent equation of motion provided the scattering coefficients are adjusted to compensate the scaling.

4.5 Ehrenfest's theorem and Poisson brackets

Although Noether's theorem guarantees that the integrals of motion are conserved quantities, it is a simple exercise to explicitly demonstrate by integration that the Noether charges do not vary in time. This inevitably amounts to proving Ehrenfest's theorem.

> **Theorem 4.1:** *The time-dependence of a Noether charge is given by Ehrenfest's Theorem*
>
> $$\frac{dQ}{dt} = -\frac{i}{\hbar}\int dx\ \psi^*\left[\mathcal{Q}, H\right]\psi + \int_{-\infty}^{\infty} dx\ \psi^*\frac{\partial\mathcal{Q}}{\partial t}\psi \tag{4.35}$$

Proof: We begin by first writing the Noether charges as

$$Q = \int_{-\infty}^{\infty} dx\ \psi^*\mathcal{Q}(t)\psi, \tag{4.36}$$

where $\mathcal{Q}(t)$ is a time-dependent self-adjoint operator inferred from the explicit form of the Noether charge. Taking the derivative of both sides with respect to time and

substituting the time derivatives of the fields leads to

$$\frac{dQ}{dt} = -\frac{i}{\hbar}\int dx\ \psi^*\left(\mathcal{Q}H - H\mathcal{Q}\right)\psi + \int dx\ \psi^*\frac{\partial \mathcal{Q}}{\partial t}\psi. \tag{4.37}$$

Using the definition of the commutator $[\mathcal{Q}, H] = \mathcal{Q}H - H\mathcal{Q}$, then leads to Ehrenfest's theorem as required. From this, one can conclude that a Noether charge is a conserved quantity if $[\mathcal{Q}, H]$ and $\partial\mathcal{Q}/dt$ both equate to zero.

The same principles can also be determined through the use of Poisson brackets.

Definition 4.3: *The Poisson bracket between a pair of functionals*

$$F = \int dx\ \mathcal{F}(\psi, \Pi) \quad , \quad G = \int dx\ \mathcal{G}(\psi, \Pi), \tag{4.38}$$

is defined as

$$\{F, G\}_{\mathrm{PB}} = \int dx \left[\frac{\delta \mathcal{F}}{\delta \psi}\frac{\delta \mathcal{G}}{\delta \Pi} - \frac{\delta \mathcal{G}}{\delta \psi}\frac{\delta \mathcal{F}}{\delta \Pi}\right]. \tag{4.39}$$

Explicitly taking the derivative of Q, together with Leibniz's rule and the multivariable chain rule leads to the integral expression

$$\frac{dQ}{dt} = \int dx\ \left[\frac{\partial Q}{\partial \psi}\frac{\partial \psi}{\partial t} + \frac{\partial Q}{\partial \psi_x}\frac{\partial \psi_x}{\partial t} + \{\psi \to \Pi\}\right] \tag{4.40}$$

Then by using integration by parts on the spatial-derivative terms, one obtains

$$\frac{dQ}{dt} = \int dx\ \left[\frac{\delta Q}{\delta \psi}\frac{\partial \psi}{\partial t} + \{\psi \to \Pi\}\right]. \tag{4.41}$$

Finally, substituting Hamilton's equations for the temporal derivatives leads to the expression

$$\begin{aligned}\frac{dQ}{dt} &= -\frac{i}{\hbar}\int dx\ \left[\frac{\delta \mathcal{Q}}{\delta \psi}\frac{\delta \mathcal{H}}{\delta \Pi} - \frac{\delta \mathcal{H}}{\delta \psi}\frac{\delta \mathcal{Q}}{\delta \Pi}\right] \\ &= -\frac{i}{\hbar}\{Q, H\}_{\mathrm{PB}},\end{aligned} \tag{4.42}$$

which is equivalent to Ehrenfest's theorem for $\partial Q/\partial t = 0$. Importantly, if the Poisson bracket between two observables equates to zero, then these quantities are said to be in *involution*, which in the case of a projection onto the Hamiltonian, proves that Q is a conserved quantity, as hinted in Definition 3.1.

4.6 Summary and outlook

In this chapter, we have constructed the one-dimensional interacting gauge theory in the formalism of both a Lagrangian and a Hamiltonian field theory. From this, we were able to derive the principle conservation laws for the chiral model and demonstrate through the methods of Poisson brackets and Ehrenfest's theorem, that the Noether charges do not evolve in time. Importantly, we found that the variational descriptions can differ in the standard and transformed pictures, highlighting that Eq. (3.23) is a *nonlinear* transformation, but not a gauge transformation.

The variational models and their conservations laws will be studied more in the following chapters when we consider the properties of the soliton solutions in our interacting gauge theory. In particular, we will find that the symmetries of the model will appear in the solutions of the linear stability analysis, reinforcing the results concluded in this chapter.

Chapter 5

Chiral matter-wave solitons

5.1 Introduction

Many of the nonlinear partial differential equations which describe the propagation of waves possess solitary wave solutions. These waves are one of the hallmark features of nonlinear dynamics, appearing in the fields of nonlinear optics [9, 10], condensed matter physics [11, 13–15], and biology [7, 8], in addition to their historical beginnings in hydrodynamics [6, 119]. A universal definition of a soliton is an awkward problem to present, as details can vary depending on the integrability of the model, the topology of the boundary conditions, and what field of physics the model is applied to. Notably, the terms *'soliton'* and *'solitary wave'*, are often abused and used interchangeably in physics, particularly in the study of ultracold gases. Here, we present and expand on the definitions provided by Drazin and Johnson [6], as well as Scott [13].

> **Definition 5.1:** *In an integrable model, a solitary wave is a solution with the following properties:*
>
> (i) *Of permanent form, due to a balance between the dispersive and interaction forces of the model, or through topological protection.*
>
> (ii) *Travels at a constant velocity up to a Galilean transformation.*
>
> *Whereas a soliton is a solitary wave with the additional property that:*
>
> (i) *Passes through and emerges from the collision with another soliton unperturbed, except for a possible phase shift or drift of the centre of mass. Or in other words, that the collision between two solitons is elastic.*

This last property details that a soliton is a solitary wave which behaves like a classical particle. In addition to this, several studies have also demonstrated that

under certain conditions, solitons can tunnel classically through a potential barrier [120–123], which also hints at their particle-like behaviour. While in non-integrable models, stable solitary wave solutions which behave similar to solitons can also exist [2, 124], but their classification as solitons is often a debatable topic due to their collision dynamics being generally inelastic.

The types of soliton solutions that one can encounter in nonlinear dynamics is incredibly rich [8, 13]. Generally, one can categorize these into either continuum solitons as solutions to a wave equation, or lattice (discrete) solitons as found in the Toda lattice [125]. In the former case, this can be further classified into three distinct types:

(i) *Envelope solitons, which are composed of an envelope signal modulated by a carrier wave, with the soliton formed by the delicate balance between the nonlinearity and dispersion, as found in the nonlinear Schrödinger equation.*

(ii) *Non-topological solitons, where the boundary conditions are topologically equivalent for the soliton and vacuum state, with the soliton also formed by the balance between nonlinearity and dispersion, as found in the Korteweg-de Vries equation.*

(iii) *Topological solitons or 'kinks', where the boundary conditions are not topologically equivalent, and can lead to soliton structures which are topologically protected due to the degeneracy of the vacuum state, as found in the sine-Gordon equation.*

For our purposes, we will only be concerned with the topic of envelope solitons, which generally come in distinct two flavours: bright solitons, where the square modulus of the envelope is single-humped and positive everywhere, and dark solitons, where the square modulus features a dip on top of a background.

The successful realisation of envelope solitons in ultracold experiments was a defining achievement for the mean-field description of the condensed state. For bright solitons, this was first achieved independently in the groups of Salomon [73] and Hulet [72]. In both cases, a gas of ^{7}Li atoms was prepared in the $|F = 1, m_f = 1\rangle$ hyperfine state, with the soliton formed by tuning the interactions from repulsive to attractive using a Feshbach resonance. Similarly, the first experimental realisation of dark solitons was demonstrated independently by two consortia of researchers, one in a gas of ^{87}Rb atoms [74], and a second with ^{23}Na [75]. This was achieved in both systems by the method of phase imprinting [126], where one half of the trapped condensate is illuminated by a far-detuned laser beam and acquires an additional phase factor.

In the following years, this success has been further demonstrated through several key experiments on both bright and dark trapped solitons [104, 127–129], which critically agreed with predictions from the one-dimensional Gross-Pitaevskii equation. Whereas on the theoretical side, many papers have also appeared which propose the existence of unconventional solitons in more exotic ultracold systems. These include two-component solitons in spinor condensates [130, 131], gap solitons in lattices [27], and for condensates featuring dipolar [132–134], as well as spin-orbit interactions [135–138]. In this chapter, we show how the density-dependent gauge theory can support another set of soliton solutions in the ultracold setting which are called *'chiral'* solitons.[i]

5.2 Chiral soliton solutions

For integrable models, the derivation of soliton solutions is most commonly known to be obtainable using the Inverse Scattering transform [3–5], and in some instances, through the use of Bäcklund transformations and Hirota's bilinear method [139, 140]. However, for some nonlinear equations, the soliton solutions can also be obtained more directly using standard integration techniques [2], as we will demonstrate as follows.

The key idea to note, is that an envelope soliton is composed of a stationary envelope function that is modulated by a carrier wave. Therefore, in order to derive an expression for the soliton envelope, we may consider the problem in the moving-frame in order to eliminate the momentum boost described by the carrier wave. Returning to Eq. (3.33), and further setting $\varphi_{\rm S} = \varphi e^{-i\mu t_m/\hbar}$, leads to the stationary eigenvalue problem

$$\left[-\frac{\hbar^2}{2m}\frac{d^2}{dx_m^2} - \mu + \tilde{g}_{\rm 1D}\varphi_{\rm S}^2\right]\varphi_{\rm S} = 0. \tag{5.1}$$

As the above equation takes the form of a stationary Gross-Pitaevskii equation but with a trivial redefinition of the scattering parameter as $\tilde{g}_{\rm 1D} = g_{\rm 1D} - 2a_1 v$, we may simply write down the soliton solutions of the interacting gauge theory in the form of the standard matter-wave solitons with the mapping $g_{\rm 1D} \to g_{\rm 1D} - 2a_1 v$. However, for completeness, we will present a formal derivation of the soliton solutions as follows.

To proceed, we multiply the above equation by $d\varphi_{\rm S}/dx_m$ and integrate the resulting expression with respect to x_m to obtain the first-order mechanical energy

[i] In the following work, we will conform to the practice in referring to the solitary wave solutions of the density-dependent gauge theory as solitons, despite the fact that they are strictly speaking *not* solitons.

equation

$$\frac{\hbar^2}{m\tilde{g}_{1D}}\left(\frac{d\varphi_S}{dx_m}\right)^2 = V(\varphi_S), \tag{5.2}$$

which effectively describes the motion of a particle in the one-dimensional potential

$$V(\varphi_S) = \varphi_S^4 - \frac{2\mu}{\tilde{g}_{1D}}\varphi_S^2 + C, \tag{5.3}$$

with integration constant C.[ii] Details on the properties of this polynomial potential can be found in Ref. [96], but will not be required to proceed.

5.2.1 Bright chiral solitons

For the boundary conditions $\varphi_S|_{x\to\pm\infty} \to 0$ and $d\varphi_S/dx|_{x\to\pm\infty} \to 0$, which describes a localised solution which is bounded as $x \to \pm\infty$, the integration constant C can be taken to zero. Eq. (5.2) can then be reduced to the separation of variables problem

$$\int \frac{d\varphi_S}{\varphi_S\sqrt{\varphi_S^2 - 2\mu/\tilde{g}_{1D}}} = -\sqrt{\frac{m\tilde{g}_{1D}}{\hbar^2}}\int dx_m, \tag{5.4}$$

for which the integral on the left hand side can be solved directly using the hyperbolic substitution

$$\varphi_S = \sqrt{\frac{2\mu}{\tilde{g}_{1D}}}\,\mathrm{sech}(u) \quad \Longrightarrow \quad d\varphi_S = -du\sqrt{\frac{2\mu}{\tilde{g}_{1D}}}\tanh(u)\,\mathrm{sech}(u). \tag{5.5}$$

The bright soliton solution then reads as

$$\psi_B = \sqrt{\frac{2\mu}{\tilde{g}_{1D}}}\,\mathrm{sech}\left(\sqrt{-\frac{2m\mu}{\hbar^2}}\,(x - vt)\right)e^{i\left(mvx - mv^2t/2 - \mu t\right)/\hbar}, \tag{5.6}$$

with $\tilde{g}_{1D} = g - 2a_1 v < 0$, in which we have transformed back into the stationary-frame. Illustrations of the bright soliton envelope, phase profile, and propagation dynamics obtained numerically from a explicit central-difference algorithm, are presented in Fig. 5.1. Here, one can see that the solution retains its shape as it propagates at a constant velocity, which justifies their classification as a soliton by Definition 5.1.

Due to the breakdown of Galilean invariance, both the chemical potential $\mu =$

[ii] The general solution to both the first- and second-order differential equations described here can be written in terms of the Jacobi elliptic functions [96, 141]. However, we will not require the use of these special functions in the following derivations as they reduce to hyperbolic functions when the elliptic modulus approaches unity.

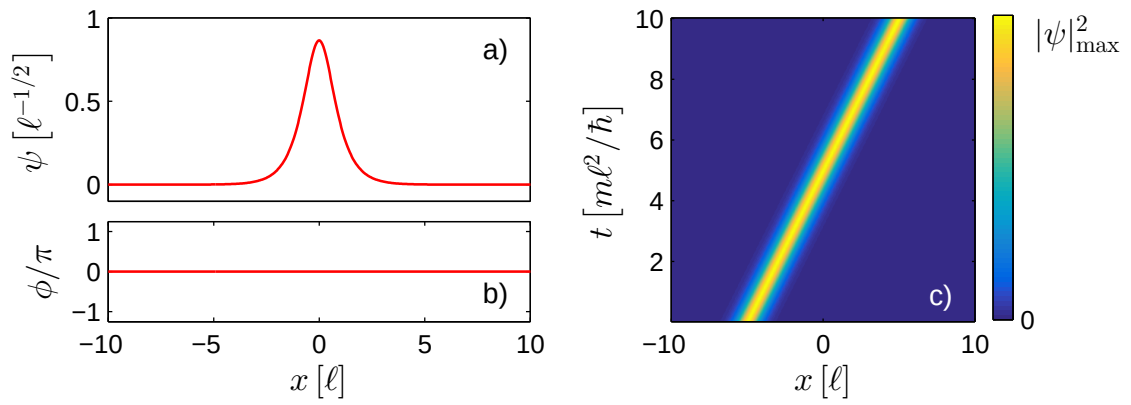

Figure 5.1: Envelope (a), phase profile (b), and propagation of a bright chiral soliton (c), with $g_{1D}m\ell/\hbar^2 = -1$, $vm\ell/\hbar = 1$, and $a_1/\hbar = 1$.

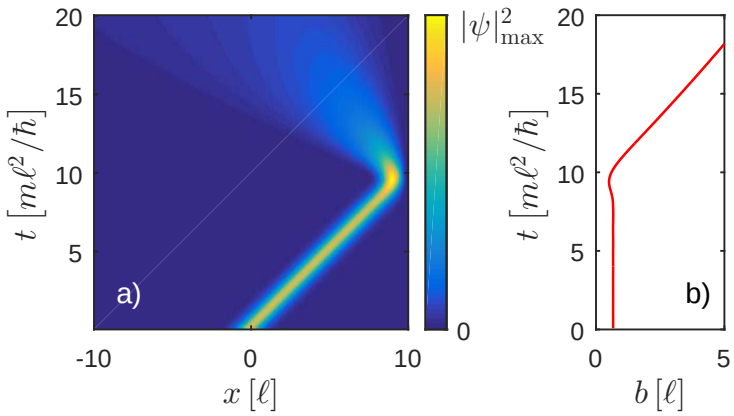

Figure 5.2: (a) Reflection of a chiral soliton off a hard-wall, with the corresponding time evolution of the soliton width (b). The soliton parameters are $g_{1D}m\ell/\hbar^2 = -1$, $vm\ell/\hbar = 1$, and $a_1/\hbar = 1$.

$-m\tilde{g}_{1D}^2/(8\hbar^2)$ and effective width $b = -2\hbar^2/(m\tilde{g}_{1D})$ of the soliton will depend on the direction of motion. The soliton solution described above is therefore *chiral*, such that under appropriate conditions, the soliton can either be stable or unstable in a given direction. An illustrative example of this can be demonstrated by the reflection of a chiral soliton off a hard wall, as pictured in Fig. 5.2 [48]. In this case, the propagation of the soliton becomes unstable due to the renormalised scattering parameter, $\tilde{g}_{1D} = g_{1D} - 2a_1 v$, switching sign under a change of direction. Consequently, this demonstrates that in contrast to the standard solitons described in the Gross-Pitaevskii equation, a chiral soliton cannot arbitrarily reduce its velocity without undergoing an instability [97, 98].

5.2.2 Dark chiral solitons

For the boundary conditions $\varphi_S|_{x\to\pm\infty} \to \pm\sqrt{\rho_0}$ and $d\varphi_S/dx|_{x\to\pm\infty} \to 0$, which describes a delocalised solution that approaches a constant value at $x = \pm\infty$.

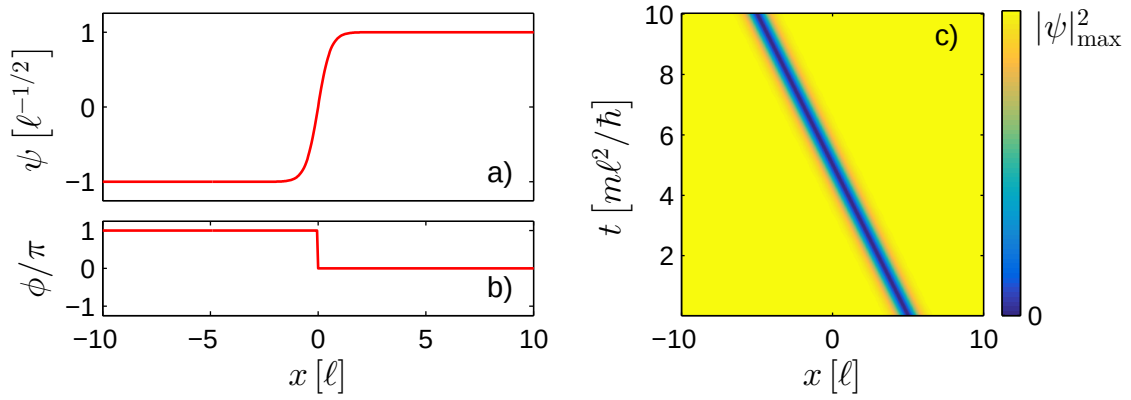

Figure 5.3: Envelope (a), phase profile (b), and propagation of a dark chiral soliton (c), with $g_{1D}m\ell/\hbar^2 = 1$, $vm\ell/\hbar = -1$, $a_1/\hbar = 1$, and $\rho_0\ell = 1$.

Eqs. (5.1) and (5.2) then infer that $\mu = \tilde{g}_{1D}\rho_0$ and $C = 2\mu\rho_0/\tilde{g}_{1D} - \rho_0^2$ respectively. The right-hand side of Eq. (5.2) can then be factorised as

$$\varphi_S^4 - \frac{2\mu}{\tilde{g}_{1D}}\varphi_S^2 + \left(\frac{\mu}{\tilde{g}_{1D}}\right)^2 = \left(\varphi_S^2 - \frac{\mu}{\tilde{g}_{1D}}\right)^2, \tag{5.7}$$

which subsequently leads to the separation of variables problem

$$\int \frac{d\varphi_S}{\varphi_S^2 - \mu/\tilde{g}_{1D}} = -\sqrt{\frac{m\tilde{g}_{1D}}{\hbar^2}} \int dx_m, \tag{5.8}$$

where we have taken the negative root. The above differential equation can also be solved directly by hyperbolic substitution

$$\varphi_S = \sqrt{\frac{\mu}{\tilde{g}_{1D}}}\tanh(u) \quad \Longrightarrow \quad d\varphi_S = du\sqrt{\frac{\mu}{\tilde{g}_{1D}}}\,\mathrm{sech}^2(u), \tag{5.9}$$

and leads to the chiral dark soliton solution

$$\psi_D = \sqrt{\frac{\mu}{\tilde{g}_{1D}}}\tanh\left(\sqrt{\frac{m\mu}{\hbar^2}}\,(x - vt)\right) e^{i\left(mvx - mv^2t/2 - \mu t\right)/\hbar}, \tag{5.10}$$

with $\tilde{g}_{1D} = g - 2a_1 v > 0$, and complementary illustrations presented in Fig. 5.3. In a similar manner to the bright soliton case, here we can see that this solution propagates at a constant velocity while maintaining the shape of its envelope. However, since the envelope of the dark soliton approaches different values depending on the direction that one takes in the asymptotic limit, a phase jump exists at the root of the solution, with

$$\Delta\phi = \lim_{n\to 0} \; -2\tan^{-1}\left(\frac{\sqrt{\rho_0}}{n}\right) = -\pi. \tag{5.11}$$

5.3 Integrals of motion

To characterise these soliton solutions, we begin by first evaluating the conservation laws derived in Sec. 4.4. As these solitons are only defined in the transformed picture, we will not need to consider the conservation laws in the standard picture.

We start, by parametrising the bright soliton in terms of the soliton width as

$$\psi_{\mathrm{B}}\left(x;b\right)=\sqrt{\frac{N}{2b}}\operatorname{sech}\left(\left(x-vt\right)/b\right)e^{i\left(mvx-mv^{2}t/2-\mu t\right)/\hbar}, \tag{5.12}$$

which will be subsequently derived in the variational calculation. The integrals of motion can then be directly calculated as

$$N_{\mathrm{B}}=N, \tag{5.13}$$

$$P_{\mathrm{B}}=mvN+\frac{a_{1}N^{2}}{3b}, \tag{5.14}$$

and

$$E_{\mathrm{B}}=\frac{1}{2mN}\left(P_{\mathrm{B}}-\frac{a_{1}N^{2}}{3b}\right)^{2}+\frac{\hbar^{2}N}{6mb^{2}}+\frac{g_{1\mathrm{D}}N^{2}}{6b}. \tag{5.15}$$

These results elegantly demonstrate the particle nature of the soliton, as well as illustrating the properties of the gauge field. Eq (5.14), takes the familiar form for the mechanical momentum of a classical particle travelling in an electromagnetic field, composed by a canonical and a field momentum term. The same concept is also present in the energy equation, with each term corresponding to the kinetic, binding, and interaction energy of the soliton successively [142]. Note, that the scalar potential term is absent in Eq. (5.15), as this was previously eliminated via a gauge transformation in the model.

For the case of the dark solitons, it is clear that the above expressions will not be finite, as the solution is not square-integrable. Instead, we must renormalise the integrals of motion by subtracting the contribution from the background density [103, 143]. Then by setting

$$\psi_{\mathrm{D}}\left(x;b\right)=\sqrt{-\frac{N}{2b}}\tanh\left(\left(x-vt\right)/b\right)e^{i\left(mvx-mv^{2}t/2-\mu t\right)/\hbar}, \tag{5.16}$$

which again, will be derived later in the variational calculation, we calculate the

renormalised integrals

$$N_{\mathrm{D}} = \int_{-\infty}^{\infty} dx \ \left(|\psi|^2 - \rho_0\right) = N, \tag{5.17}$$

$$\begin{aligned} P_{\mathrm{D}} &= -i\hbar \int_{-\infty}^{\infty} dx \ \psi^* \frac{\partial \psi}{\partial x} \left(1 - \frac{\rho_0}{|\psi|^2}\right) + a_1 \int_{-\infty}^{\infty} dx \ \left(|\psi|^2 - \rho_0\right)^2 \\ &= mvN + \frac{a_1 N^2}{3b}, \end{aligned} \tag{5.18}$$

and

$$\begin{aligned} E_{\mathrm{D}} &= \int_{-\infty}^{\infty} dx \ \left(\frac{\hbar^2}{2m} \left[\left| \frac{\partial \psi}{\partial x} \right|^2 + \rho_0 \left| \frac{\partial}{\partial x} \frac{\psi}{|\psi|} \right|^2 \right] + \frac{g_{1\mathrm{D}}}{2} \left(|\psi|^2 - \rho_0\right)^2 \right) \\ &= \frac{1}{2mN} \left(P_{\mathrm{D}} - \frac{a_1 N^2}{3b} \right)^2 - \frac{\hbar^2 N}{3mb^2} + \frac{g_{1\mathrm{D}} N^2}{6b}. \end{aligned} \tag{5.19}$$

Note, that in writing these integrals of motion, we have defined the renormalised density as $|\psi|^2 - \rho_0$, in contradiction to the conventional choice $\rho_0 - |\psi|^2$. In this case, the square-integral of the renormalised dark soliton is taken as *negative*, instead of positive. Additionally, an extra term is present in the kinetic portion of Eq. (5.19) for the kinetic energy to be finite, due to the requirement that the chiral soliton must be moving.

These equations are equivalent to the bright soliton case, except for an additional factor for the binding term in Eq. (5.19) and the property that N is taken as negative for the dark soliton. This can be further understood by calculating the effective mass,

$$m_{\mathrm{eff}} = \frac{\partial P_{\mathrm{D}}}{\partial v} = -m|N|, \tag{5.20}$$

which highlights a key attribute; that the dark soliton is dynamically equivalent to a bright soliton, but with a *negative* effective mass.

5.4 Variational equations

In addition to the integrals of motion, we may also describe the chiral solitons in a variational, or *'collective coordinate'* framework. This versatile method provides a classical description of a model, by reducing the often infinite number of degrees of freedom to a finite set of key variables, such as the centre of mass motion and velocity [8]. In this way, the resulting equations of motion for the reduced set of parameters

can provide viable insight into problems which generally do not admit analytical solutions, as demonstrated for the dynamics of a trapped condensate [144, 145]. As before, we will consider the case of the bright soliton first and conclude with the dark soliton calculation.

The central idea behind this method, in analogy with the techniques discussed in the previous chapter, lies in the principle of least action

$$\frac{\delta}{\delta s_n}\int_{t_1}^{t_2} dt\; L\left[s_n, \dot{s}_n, \ldots\right], \tag{5.21}$$

where we seek to derive a set of equations for the variational or *'collective'* coordinates $s_n(t)$, which correspond to a stationary point of the action. The first, and most important step for this calculation, involves carefully choosing an appropriate ansatz for the condensate wavefunction, as a general solution for the dynamics of the gas is not known. Typically, this is achieved by approximating the trapped condensate as a Gaussian in the weak scattering regime $g_{1\mathrm{D}} \approx 0$, or as a Thomas-Fermi solution for $\mu/\hbar\omega_\nu \gg 1$, with chemical potential μ and trapping frequency ω_ν. Fortunately in our case, we can use the exact analytical expressions for the chiral solitons as a basis to begin the calculation. Therefore, to accurately describe the dynamics of the bright soliton, we will write a general variational ansatz of the form [146, 147]

$$\psi \equiv a\,\mathrm{sech}\left(\left(x-\xi\right)/b\right) e^{i\left(k(x-\xi)+w(x-\xi)^2+\phi\right)}, \tag{5.22}$$

where $a(t)$, $b(t)$, $\xi(t)$, $k(t)$, $w(t)$, and $\phi(t)$ are a set of time-dependent variational parameters corresponding to the amplitude, width, centre-of-mass coordinate, velocity, curvature, and absolute phase of the soliton. At this point, it is important to highlight the limitations of this choice of ansatz. Since Eq. (5.22) presumes that the soliton retains its shape for all time, effects like radiation emission and fracturing of the soliton envelope cannot be described, and will generally lead to inconsistencies in the results. However, provided these discrepancies are small in magnitude, we will still obtain sensible results.

Following the variational techniques described in the previous chapter, we proceed by writing the Lagrangian density in the transformed picture as

$$\begin{aligned}\mathcal{L}\left(\psi,\psi_x,\psi_t\right) = \frac{i\hbar}{2}\left(\psi\frac{\partial\psi^*}{\partial t} - \psi^*\frac{\partial\psi}{\partial t}\right) + \frac{\hbar^2}{2m}\left|\frac{\partial\psi}{\partial x}\right|^2 + \frac{1}{2}m\omega_x^2x^2|\psi|^2 \\ + \frac{g}{2}|\psi|^4 + a_1|\psi|^2\int_{-\infty}^{x} dx'\frac{\partial}{\partial t}\rho(x',t),\end{aligned} \tag{5.23}$$

where we have reintroduced the harmonic trapping potential. Substituting the vari-

ational ansatz into Eq. (5.23) leads to the new Lagrangian density [iii]

$$\mathcal{L}_{\mathrm{B}} = \frac{a^4}{2}\left(g_{1\mathrm{D}} - \frac{2a_1\hbar k}{m}\right)\operatorname{sech}^4\chi + \frac{\hbar^2 a^2}{2m}\left(\frac{1}{b^2}\tanh^2\chi + k^2 + 4w^2b^2\chi^2\right)\operatorname{sech}^2\chi$$
$$+ \frac{1}{2}m\omega_x^2 a^2\left(b^2\chi^2 + \xi^2\right)\operatorname{sech}^2\chi + \hbar a^2\left(\dot{\phi} + \dot{w}b^2\chi^2 - k\dot{\xi}\right)\operatorname{sech}^2\chi, \tag{5.24}$$

with the change of variables $\chi = (x-\xi)/b$. Note, that in writing Eq. (5.24), we have explicitly excluded terms which have odd-symmetry as these will equate to zero in the subsequent integration. At this stage, we can already see some of the expected dynamics, with the appearance of the renormalised scattering parameter in the first term of Eq. (5.24). Integrating the above Lagrangian density then leads to the averaged Lagrangian

$$L_{\mathrm{B}} = \frac{2a^4 b}{3}\left(g_{1\mathrm{D}} - \frac{2a_1\hbar k}{m}\right) + \frac{\hbar^2 a^2 b}{m}\left(\frac{1}{3b^2} + k^2 + \frac{w^2b^2\pi^2}{3}\right)$$
$$+ m\omega_x^2 a^2 b\left(\frac{b^2\pi^2}{12} + \xi^2\right) + 2\hbar a^2 b\left(\dot{\phi} + \frac{\dot{w}b^2\pi^2}{12} - k\dot{\xi}\right), \tag{5.25}$$

from which equations of motion can be extracted.

Applying the principle of least action, Eq (5.21), one obtains the set of coupled differential equations

$$k = \frac{m\dot{\xi}}{\hbar} + \frac{a_1 N}{3\hbar b}, \tag{5.26}$$

$$\frac{m\pi^2}{12}\left(\ddot{b} + \omega_x^2 b\right) = \frac{\left(g_{1\mathrm{D}} - 2a_1\hbar k/m\right)N}{6b^2} + \frac{\hbar^2}{3mb^3}, \tag{5.27}$$

and

$$m\left(\ddot{\xi} + w_x^2\xi\right) = \frac{Na_1\dot{b}}{3b^2}, \tag{5.28}$$

[iii] The evaluation of the non-local term in the Lagrangian density can be achieved in two ways:

(i) Simplifying using Leibniz's integral rule and integrating

$$\int_{-\infty}^{x} dx' \frac{\partial}{\partial t}\rho\left(x',t\right) = \frac{d}{dt}\int_{-\infty}^{x} dx' \rho\left(x',t\right)$$

(ii) Recasting in terms of the probability current using the continuity equation

$$\frac{\partial\rho}{\partial t} = -\frac{\partial j'}{\partial x'} \quad \Longrightarrow \quad \int_{-\infty}^{x} dx' \frac{\partial\rho}{\partial t} = -j'$$

which collectively describe the dynamics of the trapped soliton. To obtain these equations, we have used the definitions $a^2 = N/(2b)$ and $w = m\dot{b}/(2\hbar b)$, which are determined from variations of the action with respect to the coordinates $a(t)$ and $w(t)$.

The Newtonian structure of these equations provides a key insight into the dynamics of the bright soliton. The first equation, which describes the velocity of the bright soliton, is equivalent in form to the expression derived from the momentum density, Eq. (5.14). In this case, and similarly to before, the momentum of the soliton contains an extra contribution from the gauge field, as expected from classical electrodynamics. The second equation for the soliton width does not drastically differ from the standard case, as it simply describes the effects of the binding and interaction energy under the restoring force of the harmonic trap. The equation for the centre of mass motion $\xi(t)$ is intriguing, as one finds that the gauge field enters as a driving force to the harmonic motion provided the width of the soliton is perturbed. For these reasons, the evolution of a trapped chiral soliton is expected to lead to a loss of coherence [148].

Although this set of differential equations cannot be solved analytically due to the coupling of the variational parameters, we can still obtain exact solutions in the limiting case where the width of the untrapped soliton does not vary in time, with $\omega_x = 0$ and $\dot{b}(t) = 0$. In this case, the set of differential equations decouple completely, enabling us to solve Eq. (5.28) for the soliton trajectory

$$\xi = vt + \xi_0 \quad \Longrightarrow \quad \dot{\xi} = v, \tag{5.29}$$

which reiterates that the unperturbed soliton travels at a constant velocity. Furthermore, from Eq. (5.27), we can also determine expressions for the width $b = -2\hbar^2/\left(m\tilde{g}_{1\mathrm{D}}N\right)$ and chemical potential $\mu = -m\tilde{g}_{1\mathrm{D}}^2N^2/\left(8\hbar^2\right)$ of the bright soliton, as introduced previously in Eq. (5.12). The case for $\dot{b} \neq 0$, which details the situation where the soliton is perturbed, will be studied briefly in the numerical simulations presented in Sec. 6.4.

Using the renormalisation techniques discussed previously, the effective Lagrangian

density for the dark soliton can be written as [149][iv]

$$\mathcal{L}\left(\psi,\psi_x,\psi_t\right)=\frac{i\hbar}{2}\left(\psi\frac{\partial\psi^*}{\partial t}-\psi^*\frac{\partial\psi}{\partial t}\right)\left(1-\frac{\rho_0}{|\psi|^2}\right)+\frac{\hbar^2}{2m}\left[\left|\frac{\partial\psi}{\partial x}\right|^2+\rho_0\left|\frac{\partial}{\partial x}\frac{\psi}{|\psi|}\right|^2\right]$$

$$+\frac{g_{1\mathrm{D}}}{2}\left(|\psi|^2-\rho_0\right)^2-a_1\left(|\psi|^2-\rho_0\right)j'(x)\left(1-\frac{\rho_0}{|\psi|^2}\right), \tag{5.30}$$

Following the success of the bright soliton case, we write the variational ansatz for the dark soliton as

$$\psi_{\mathrm{D}}\equiv a\tanh((x-\xi)/b)e^{i\left(k(x-\xi)+w(x-\xi)^2\right)}, \tag{5.31}$$

where we have reused the notation for the variational parameters. Inserting the ansatz into the renormalised Lagrangian density leads to the expression

$$\mathcal{L}_{\mathrm{D}}=\frac{a^4}{2}\left(g_{1\mathrm{D}}-\frac{2a_1\hbar k}{m}\right)\operatorname{sech}^4\chi+\frac{\hbar^2a^2}{2m}\left(\frac{1}{b^2}\operatorname{sech}^2\chi-k^2-4w^2b^2\chi^2\right)\operatorname{sech}^2\chi$$

$$-\hbar a^2\left(\dot{\phi}+\dot{w}b^2\chi^2-k\dot{\xi}\right)\operatorname{sech}^2\chi, \tag{5.32}$$

where again we have explicitly excluded terms which have odd-symmetry. Integrating the Lagrangian density then leads to the averaged Lagrangian

$$L_{\mathrm{D}}=\frac{2a^4b}{3}\left(g_{1\mathrm{D}}-\frac{2a_1\hbar k}{m}\right)+\frac{\hbar^2a^2b}{m}\left(\frac{2}{3b^2}-k^2-\frac{w^2b^2\pi^2}{3}\right)$$

$$-2\hbar a^2b\left(\dot{\phi}+\frac{\dot{w}b^2\pi^2}{12}-k\dot{\xi}\right). \tag{5.33}$$

Applying the principle of least action, as before, leads to the set of coupled equations

$$k=\frac{m\dot{\xi}}{\hbar}+\frac{a_1N}{3\hbar b}, \tag{5.34}$$

$$\frac{m\pi^2}{12}\ddot{b}=\frac{\left(g_{1\mathrm{D}}-2a_1\hbar k/m\right)N}{6b}-\frac{2\hbar^2}{3mb^3}, \tag{5.35}$$

[iv]The harmonic trapping potential is excluded in this example, as it leads to a contradiction in the asymptotic behaviour of the dark soliton envelope and inconsistencies in the corresponding variational equations; notably, an incorrect value for the oscillation frequency of the dark soliton instead of the known result $\omega_{\mathrm{osc}}=\omega_x/\sqrt{2}$ for $a_1=0$ [129].

and

$$m\ddot{\xi} = \frac{Na_1\dot{b}}{3b^2}, \tag{5.36}$$

for the trapped dark soliton. These equations are equivalent to those for the bright-soliton except for an additional factor in the binding term of Eq. (5.35). This consequently leads to the expressions for the width $b = 4\hbar^2/(m\tilde{g}_{1\mathrm{D}}N)$ and chemical potential $\mu = m\tilde{g}_{1\mathrm{D}}^2N^2/(8\hbar^2)$ of the dark soliton, which allows us to rewrite the dark soliton solution, as shown earlier in Eq. (5.16).

5.5 Lyapunov stability

Lyapunov, or orbital stability, is one of the fundamental stability theories for dynamical systems, which details the behaviour of a solution around the stationary points of the model [150].

> **Definition 5.2:** *For a solution $f(x(t))$ which starts in the neighbourhood of a stationary point x_s of a system, such that $|x(0) - x_s| = x_\Delta$, the solution is:*
>
> (i) *'Lyapunov' stable, if $f(x(t))$ remains in the neighbourhood of x_s for all time, with $|x(t) - x_s|_{t\to\infty} \leq x_\Delta$.*
>
> (ii) *Asymptotically stable, if $f(x(t))$ converges to the solution at the stationary point, with $|x(t) - x_s|_{t\to\infty} = 0$.*
>
> (iii) *Unstable, if $f(x(t))$ diverges from the solution at the stationary point, with $|x(t) - x_s|_{t\to\infty} \geq x_\Delta$.*

The task of proving the Lyapunov stability of the soliton solutions, therefore requires the identification and study of the stationary points of the Hamiltonian functional. In the following we will only demonstrate the former, which hints at, but does not strictly prove the Lyapunov stability. Instead we refer the reader to Refs. [151–153] for a rigorous calculation using Sobolev integral estimates, although in passing, we note that the Lyapunov stability will be proven implicitly when we consider the linear stability analysis in Chap. 6.

> **Theorem 5.1:** *The soliton envelope $\varphi_{\mathrm{S}}(x_m)$, corresponds to a stationary point of the moving-frame Hamiltonian*

$$H_m = -\int_{-\infty}^{\infty} dx_m\, \mathcal{H}_m = \int_{-\infty}^{\infty} dx_m\, \left(\frac{\hbar^2}{2m}\left|\frac{\partial\varphi_{\mathrm{S}}}{\partial x_m}\right|^2 + \frac{(g_{1\mathrm{D}} - 2a_1v)}{2}|\varphi_{\mathrm{S}}|^4 \right), \tag{5.37}$$

for a fixed number of particles.

Proof: This theorem was already hinted at in Sec. 5.2, but can be proven rigorously using the method of Lagrange multipliers. The corresponding Lagrange functional for the minimisation problem can be written as

$$H\left(\varphi_{\mathrm{S}}; b(\mu)\right) = \int_{-\infty}^{\infty} dx_m \, \left(-\mathcal{H}_m - \mu|\varphi_{\mathrm{S}}|^2\right). \tag{5.38}$$

where the chemical potential μ plays the role of a Lagrange multiplier for the normalisation constraint. Inserting the soliton envelopes into Eq. (5.38) and integrating leads to the Hamiltonian functions

$$H_{\mathrm{B}}(b) = \frac{\hbar^2}{6mb^2} + \frac{\tilde{g}_{1\mathrm{D}}}{6b} - \mu \tag{5.39}$$

and

$$H_{\mathrm{D}}(b) = -\frac{\hbar^2}{3mb^2} + \frac{\tilde{g}_{1\mathrm{D}}}{6b} - \mu, \tag{5.40}$$

for the bright and dark chiral solitons respectively. These functions take the familiar form of an interatomic potential, in which a stationary point is formed by the competition of two terms with differing length scales. The exact values of these stationary points can be determined by varying the Hamiltonian functions with respect to the soliton width, and read as

$$\frac{\hbar^2}{3mb^3} + \frac{\tilde{g}_{1\mathrm{D}}}{6b^2} = 0 \quad \Longrightarrow \quad b = -\frac{2\hbar^2}{m\tilde{g}_{1\mathrm{D}}} \tag{5.41}$$

and

$$-\frac{2\hbar^2}{3mb^3} + \frac{\tilde{g}_{1\mathrm{D}}}{6b^2} = 0 \quad \Longrightarrow \quad b = \frac{4\hbar^2}{m\tilde{g}_{1\mathrm{D}}}, \tag{5.42}$$

as well as being illustrated in Fig. 5.4. These expressions correspond exactly to the definitions of the soliton widths derived from the variational calculations, and therefore demonstrates that the soliton envelope corresponds to a stationary point of the Hamiltonian, as required.

5.6 Summary and outlook

In this chapter, we have derived and characterised the chiral soliton solutions described in the one-dimensional interacting gauge theory. By calculating the integrals of motion, we have illustrated the particle nature of both the bright and dark solitons, and in particular, showed how the synthetic gauge potential behaves in the

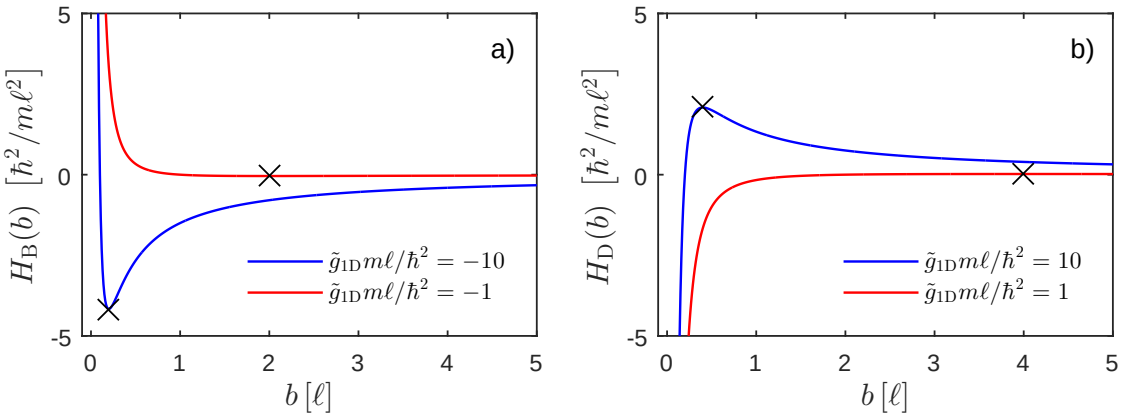

Figure 5.4: Potential energy curves highlighting the Lyapunov stability of the bright (a) and dark (b) chiral solitons. The stationary points of each curve are highlighted by black crosses, with $\mu = 0$ set for simplicity.

classical limit. This was further understood when considering a variational description, which provided exact expressions for the widths and chemical potentials of the solitons, as well as providing some insight into the effects of perturbations. Lastly, we showed that the chiral solitons correspond to a stationary point of the Hamiltonian, which hints at, but does not strictly prove their stability in the Lyapunov sense.

A notable absence in our set of solutions, and also in the literature presented over the years by various authors, is the grey soliton solution [14, 103]. In this case, the soliton envelope is complex and therefore presents difficulty in deriving an analytical solution in the context of the density-dependent gauge theory. However, a numerical solution may still be feasible. In this case, it would be interesting to determine whether the grey soliton is dynamically stable due to the interplay of its diffusive motion and the breakdown of Galilean invariance in the model.

Additionally, it is also interesting as to whether the current nonlinearity can support the existence of higher-dimensional solitons [154], or at least help to prevent the critical collapse of the condensate. Very recently, it has been demonstrated that stable solitons can form in two- and three-dimensional condensates featuring spin-orbit coupling [136, 137, 155], offering promising potential in this direction. For this purpose, the Galilean group of transformations, which describes the effects of uniform motion, translations, and rotations in Euclidean space, may lead to exotic dynamical properties for the condensate [156].

Chapter 6

Linear stability of bright chiral solitons

6.1 Introduction

The stability of solitons in the presence of perturbations represents one of the fundamental problems in the study of solitary waves. Only solitons which are generally robust to perturbations are suitable for study in a physical setting, and by extension, implementing into potential applications in both science and industry [17, 18]. Over the years, this topic has been studied extensively for various nonlinear models, with analysis generally falling into two frameworks: the study of small (linear) perturbations of the soliton envelope via a linear stability analysis [2, 10, 153, 157], or the study of additional perturbative terms in the model through a perturbation theory or variational analysis [158–163]. The motivation here is twofold: to establish the intrinsic stability of the soliton in a given model, but also to consider the effect of physically relevant perturbations which may influence or potentially damage the soliton. The latter point is of particular importance, as realistic systems are generally described by non-integrable models, in which solitons can potentially be unstable.

In the traditional setting of nonlinear optics, described by the generalized nonlinear Schrödinger equation, understanding the stability of solitons in the presence of perturbations has been a fundamental area of research in the design of soliton-based optical communications [9, 16]. Most notable is the Vakhitov-Kolokolov criterion [151, 164], which connects the linear stability of bright solitons to two key properties: the number of negative eigenvalues in the spectral problem, and the behaviour of the power integral with respect to the propagation constant. In addition to this pioneering work, several studies have addressed the addition of perturbative terms in the model, such as but not limited to, the excitation of internal modes in non-Kerr media [124, 165, 166], the effects of third-order dispersion and self-steepening [161, 167], and more recently for $\mathcal{PT}$-symmetric potentials [168–171], which describe media with complex refractive indices.

In ultracold atomic gases, the linear stability framework is more commonly referred to as the Bogoliubov-de Gennes equations and plays a historic role in understanding the superfluid properties of the gas [14, 19, 172]. Following the first experimental realisation of these ultracold gases, considerable work was centered around studying the response of the trapped condensate to small perturbations [67–71], which highlighted that the low-lying excitations of the system had a collective nature. The second generation of studies extended to the case of both dark and bright solitons [72, 73, 89, 103, 129, 173], and subsequently lead to a number of key works illustrating the stability of solitons in ultracold gases, including: the interactions between trapped bright solitons [104, 174], the generation of soliton trains in an attractive condensate [72, 175, 176], the friction induced by a cloud of thermal atoms [177], and understanding the snake instability of dark solitons [178, 179].

As the design of these ultracold systems becomes more involved, it is important to understand how the dynamics and stability of the condensate is modified, as retaining the coherent property of the gas is of vital importance for the purposes of interferometry and future atomtronic based technologies [49–51]. In particular, with the introduction of synthetic gauge potentials in these systems, the properties of the gas can be drastically altered, with the emergence of vortices and spin-orbit coupling [63, 64], as well as the breakdown of both Galilean invariance and integrability. The question of the dynamical stability of a chiral soliton is therefore an important topic in preparation for a future experimental implementation, but also from a purely nonlinear dynamics perspective. To study this, we will consider three complementary methods which are standard in the analysis of linear stability: the stability spectrum of the Bogoliubov de-Gennes equations, the Vakhitov-Kolokolov criterion, and numerical simulations of a perturbed chiral soliton. In each case, we will find that the stability properties of the soliton will be similar to those of *integrable* models, despite the interacting gauge theory being generally *non-integrable*. This property will in part, lead to the principle conclusion of this thesis; that the dynamics of the interacting gauge theory is *near*-integrable for the case of a single-soliton.

6.2 Bogoliubov-de Gennes equations

For the first method, we will study the linear stability of the bright soliton in the framework of the Bogoliubov de-Gennes equations [14, 15, 19], which describe the response of the condensate to small deviations in the order parameter away from the equilibrium state. To achieve this, we proceed in the standard way by introducing the condensate wave function in the *moving-frame* as [14, 124]

$$\varphi = \left(\varphi_{\mathrm{B}} + (u+v)\, e^{-i\omega t_m} - (u-v)^*\, e^{i\omega t_m}\right) e^{-i\mu t_m/\hbar}, \tag{6.1}$$

where the bright soliton envelope $\varphi_{\rm B}$ is perturbed by small-amplitude excitations, $u(x_m)$ and $v(x_m)$, with frequency ω. Substituting Eq. (6.1) into Eq. (3.34) and linearising to first-order in $u(x_m)$ and $v(x_m)$, leads to the zeroth-order equation

$$L_1\varphi_{\rm B} = 0, \tag{6.2}$$

and the pair of Bogoliubov-de Gennes equations [99]

$$\hat{L}\begin{pmatrix} u \\ v \end{pmatrix} = \begin{pmatrix} 2\mathcal{J}_0 & L_3 \\ L_1 & 0 \end{pmatrix}\begin{pmatrix} u \\ v \end{pmatrix} = \hbar\omega\begin{pmatrix} u \\ v \end{pmatrix}, \tag{6.3}$$

which feature the standard linear operators

$$L_n = -\frac{\hbar^2}{2m}\frac{d^2}{dx_m^2} - \mu + n\tilde{g}_{\rm 1D}|\varphi_{\rm B}|^2, \tag{6.4}$$

for $n \in \mathbb{Z}_0^+$, in addition to the current operator

$$\mathcal{J}_0 = \frac{ia_1\hbar}{m}\left[|\varphi_{\rm B}|^2\frac{d}{dx_m} - \frac{1}{2}\frac{d}{dx_m}|\varphi_{\rm B}|^2\right]. \tag{6.5}$$

Together, Eqs. (6.2) and (6.3) describe the perturbation dynamics of the soliton, with the stability properties determined by the nature of the eigenvalues, or *'stability spectrum'*, of the Bogoliubov-de Gennes equations. A key feature of these equations is highlighted by the property that in the moving-frame, the current operator does not explicitly couple to the envelope of the soliton, but does couple to the excitations around it. In turn, this leads to the zeroth-order equation for the stationary soliton being described by the *integrable* Gross-Pitaevskii equation, despite Eq. (3.21) being generally *non-integrable*. Therefore, it is expected that the spectrum of excitations around the chiral soliton will be similar to that of integrable models, with only their form modified slightly due to the coupling of the current operator, as per Eq. (6.5). This proposition will be a key underlying point in the analysis to follow.

Before solving the Bogoliubov de-Gennes equations, it is instructive to first review the key properties of the linearised operator $\hat{L}$.

> **Theorem 6.1:** *The linearised operator $\hat{L}$ is not a self-adjoint matrix, but is $\mathcal{PT}$-symmetric.*

Proof: This can be determined by directly computing the adjoint matrix using the following definitions:

> **Definition 6.1:** *For a pair of square-integrable functions $f_n(x)$ and*

$f_{n'}(x)$, the inner-product is defined as

$$\langle f_n, f_{n'} \rangle \equiv \int_{-\infty}^{\infty} dx \; f_n^\dagger f_{n'}. \tag{6.6}$$

Definition 6.2: *The transpose of a block matrix A is given by*

$$\begin{pmatrix} a & b \\ c & d \end{pmatrix}^{\mathrm{T}} = \begin{pmatrix} a^{\mathrm{T}} & c^{\mathrm{T}} \\ b^{\mathrm{T}} & d^{\mathrm{T}} \end{pmatrix}. \tag{6.7}$$

Taking the conjugate-transpose of Eq. (6.3) and using the property that L_1 and L_3 are self-adjoint operators, leads to the adjoint eigenvalue problem

$$\begin{pmatrix} u & v \end{pmatrix}^* \hat{L}^\dagger = \begin{pmatrix} u & v \end{pmatrix}^* \begin{pmatrix} 2\mathcal{J}_0^\dagger & L_1 \\ L_3 & 0 \end{pmatrix} = \begin{pmatrix} u & v \end{pmatrix}^* \hbar\omega^*, \tag{6.8}$$

for the conjugate eigenvalues $\hbar\omega^*$. The adjoint current operator appearing in Eq. (6.8) is given by

$$\mathcal{J}_0^\dagger = \frac{ia_1\hbar}{m}\left[|\varphi_{\mathrm{B}}|^2 \frac{d}{dx_m} + \frac{3}{2}\frac{d}{dx_m}|\varphi_{\mathrm{B}}|^2\right], \tag{6.9}$$

and can be determined using Definition 6.1, together with integration by parts. The fact that $\hat{L} \neq \hat{L}^\dagger$, due to the interchange of the off-diagonal terms and the result $\mathcal{J}_0 \neq \mathcal{J}_0^\dagger$, proves that $\hat{L}$ is not a self-adjoint operator.

For the topic of $\mathcal{PT}$-symmetry, it is straightforward to demonstrate that both $\hat{L}$ and $\hat{L}^\dagger$ are invariant under the transformation

$$\mathcal{PT}\hat{L}^{(\dagger)} = \hat{L}^{(\dagger)}, \tag{6.10}$$

with $\mathcal{P}\hat{L}(x_m) = \hat{L}(-x_m)$ and $\mathcal{T}\hat{L}(x_m) = \hat{L}^*(x_m)$. The linearised operator $\hat{L}$ therefore belongs to a class of $\mathcal{PT}$-symmetric, or equivalently *pseudo-hermitian* operators [180], with the following properties for the eigenspectrum:

(i) *The eigenvalues appear in pairs or quadruples; if $\hbar\omega$ is an eigenvalue, so is $-\hbar\omega$, $\hbar\omega^*$, and $-\hbar\omega^*$.*

(ii) *The right-eigenvectors of $\hat{L}^\dagger$ are the adjoint of the left-eigenvectors of $\hat{L}$.*

(iii) *The set of right-eigenvectors and left-eigenvectors of $\hat{L}$ is not guaranteed to form a bi-orthogonal basis, as $\hat{L}$ is generally not diagonalisable.*

These properties will be demonstrated in the subsequent sections.

We can also conclude several additional properties of the excitations by studying the matrix

$$\hat{L} = \begin{pmatrix} (ia_1\hbar/mb)\,\mathrm{sech}^2\,(x_m/b)\,(d/dx_m) - iW(x_m) & L_0 + 3V(x_m) \\ L_0 + V(x_m) & 0 \end{pmatrix}, \tag{6.11}$$

which is obtained by substituting the soliton solution into Eq. (6.3). Appearing in Eq. (6.11) are two potential functions

$$V(x_m) = \frac{\tilde{g}}{2b}\,\mathrm{sech}^2(x_m/b), \tag{6.12}$$

and

$$iW(x_m) = i\frac{\tilde{g}_{1\mathrm{D}}}{2b}\frac{a_1}{\hbar}\tanh(x_m/b)\,\mathrm{sech}^2(x_m/b), \tag{6.13}$$

which are a standard reflectionless potential [147, 181] and a gain-loss distribution for the excitations respectively [168–171]. Together, they form a modified (hyperbolic) Scarf-II potential which is convergent in the limit $x_m \to \pm\infty$, with $V(x_m)$ and $W(x_m) \to 0$. This highlights, that the soliton acts as a complex effective potential for the excitations, with bound states and scattering states supported for the attractive potential $V(x_m)$, and the gains and losses of the excitations balanced by the symmetry of the imaginary potential $\int_{-\infty}^{\infty} dx_m\, W(x_m) = 0$.

6.2.1 Numerical solution

With the Bogoliubov-de Gennes equations derived and their properties reviewed, we can now proceed in solving for the stability spectrum of the soliton. To achieve this, we first consider a numerical solution, in which Eq. (6.3) is discretised with periodic boundary conditions and solved using a sparse eigenvalue solver. The resulting eigenvalues and eigenvectors are shown in Figs. 6.1 and Fig. 6.2 respectively.

As expected, we find that the eigenspectrum retains several characteristic features commonly encountered in integrable models [2]. The eigenvalues consist of the union of two sets: a continuous spectrum with two symmetric branches each gapped from the origin by $|\hbar\omega| = |\mu|$, and a discrete spectrum with one pair of eigenvalues located at $\hbar\omega = 0$ and another pair displaced from the origin by a small imaginary component. At first glance, this pair of imaginary eigenvalues would indicate an instability mode where the soliton state can collapse. However, this component arises instead due to the discreteness of the numerical analysis and subsequently vanishes in the continuum limit, where the length of the numerical domain $L \to \infty$ and domain spacing $\Delta x_m \to 0$. This feature is a common occurrence in the study of

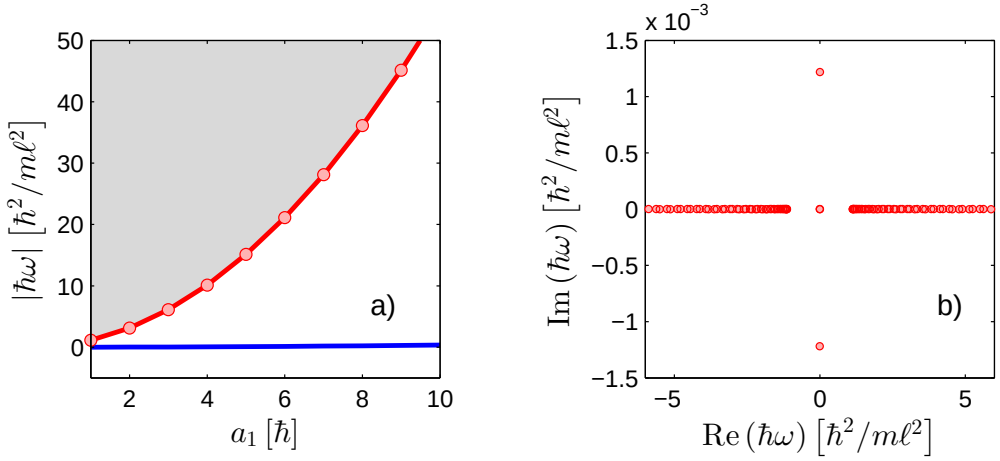

Figure 6.1: (a) Numerically obtained eigenvalue spectrum of the Bogoliubov-de Gennes equations with discrete states (blue) and continuous states (grey). The band edge of the continuous spectrum is highlighted in red, for both numerical (solid) and analytical (dots) results. The soliton parameters are taken as $g_{1D}m\ell/\hbar^2 = -1$, and $vm\ell/\hbar = 1$. (b) Subset of (a) taken at $a_1/\hbar = 1$.

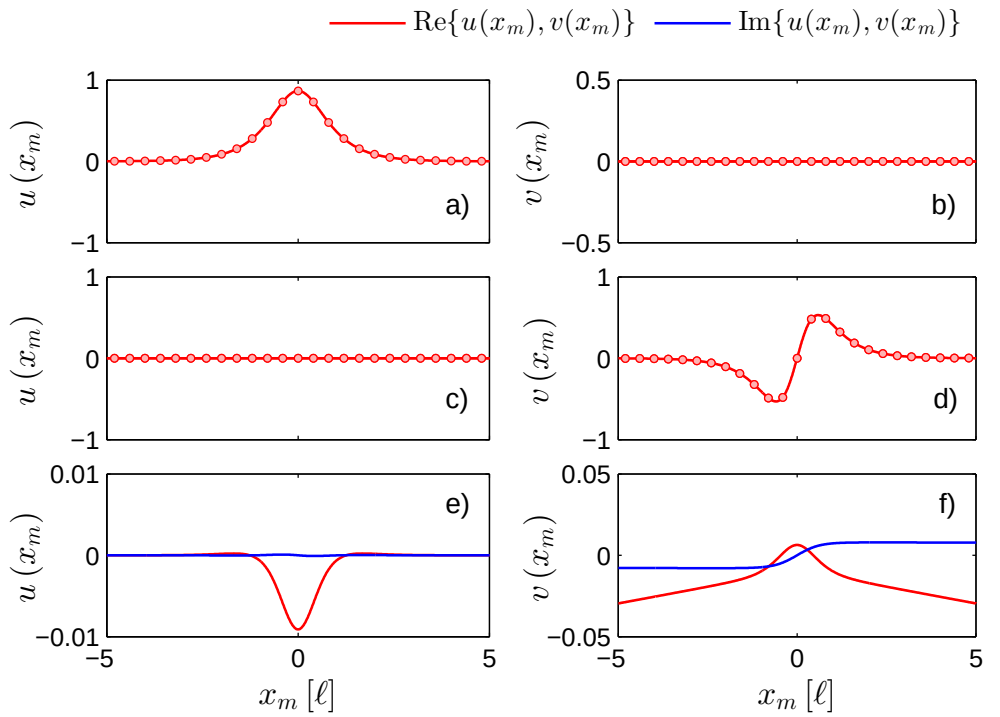

Figure 6.2: Bogoliubov-de Gennes eigenvectors $(u\ \ v)^{\mathrm{T}}$ for $g_{1D}m\ell/\hbar^2 = -1$, $vm\ell/\hbar = 1$, and $a_1/\hbar = 1$. Pictured are the degenerate bound states, (a-b) and (c-d), corresponding to the discrete spectrum and the first continuous state (e-f). All eigenvectors are scaled to units of $\ell^{-1/2}$ for both numerical (solid-line) and analytical (dots) results.

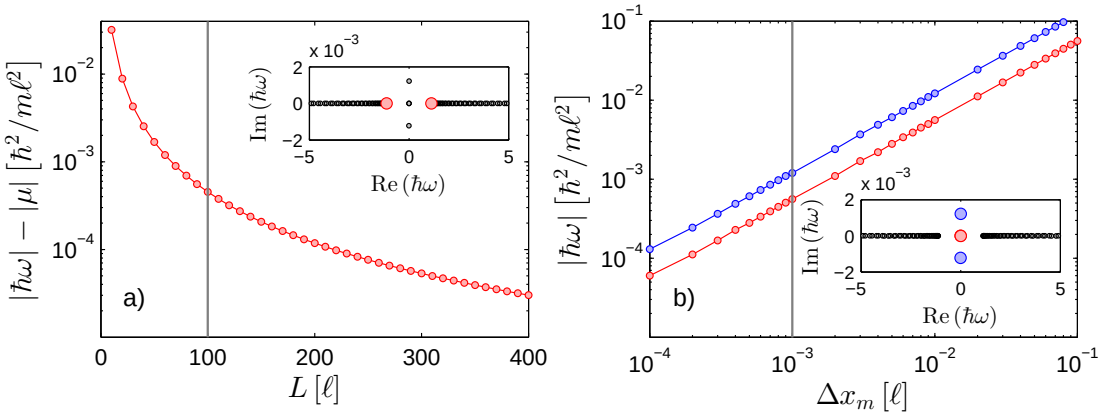

Figure 6.3: Numerical convergence of the Bogoliubov de-Gennes eigenvalues in the continuum limit. (a) The continuous state band-edge eigenvalue compared to the chemical potential for increasing domain length, and (b) discrete eigenvalues for decreasing domain spacing. The soliton parameters are fixed at $g_{1D}m\ell/\hbar^2 = -1$, $vm\ell/\hbar = 1$, and $a_1/\hbar = 1$, with the grey line of each plot corresponding to the spectrum shown in the respective inset with the eigenvalues colour-coded.

spectral stability and arises from the numerical model being ill-conditioned; that the soliton, which is strictly speaking a solution in free space, is discretised and truncated in the numerical picture. Details of the numerical convergence of the eigenvalues is presented in Fig. 6.3.[i] The eigenvalues of Eq. (6.3) are therefore entirely real, with a four-fold degenerate eigenvalue at $\hbar\omega = 0$, in an identical manner as for the Gross-Pitaevskii equation. We can therefore conclude that in the continuum limit, the chiral soliton is stable to linear perturbations.

The eigenvectors of Eq. (6.3) are also consistent with that of integrable models, with the discrete spectrum corresponding to localised real-valued solutions in the vicinity of the soliton (Fig. 6.2(a-d)), while the continuous states are complex-valued and generally oscillatory as $x_m \to \pm\infty$ (Fig. 6.2(e-f)). In fact, the discrete states pictured are exactly the same as for the Gross-Pitaevskii equation, with the first and second states taking the form of the envelope of the soliton and its derivative respectively. This similarity, or rather, the invariance of the form of the discrete states in the presence of the current operator, will become clear from the analytical results in the next section.

These numerical results therefore validate the proposition posed earlier, that the stability spectrum of the chiral soliton is similar to that of integrable models. As such, the interacting gauge theory represents a non-integrable model in which the soliton solutions are stable to linear perturbations. The absence of instability modes in the model will be revisited in the numerical simulations at the end of the chapter.

[i]For these reasons, we may conclude that for the fixed chemical potential in Fig. 6.3, a reasonably accurate solution for the eigenspectrum can be obtained with a modest domain length of $L = 100$ and spacing $\Delta x_m = 10^{-3}$, corresponding each to an error of $\approx 10^{-3}$.

6.2.2 Analytical solution

For several integrable models, the spectrum of excitations around the soliton solution can be derived analytically [157, 158, 182]. This can be generally achieved either through a connection to the squared eigenfunctions of the associated eigenvalue problem [183], in analogy to the Zakharov-Shabat system [4], or in some cases, by direct methods. As our model is generally non-integrable, it is unclear whether the former method would be applicable. However, using the numerical results obtained previously as a basis, we can at the very least obtain expressions for the discrete spectrum using traditional methods, as well as details on the continuous states in the asymptotic limit.

Discrete Spectrum - Bound States

As was demonstrated numerically, the discrete spectrum of the excitations correspond to a set of bound states which are a zero-eigenvalue solution of Eq. (6.3). For this reason, the Bogoliubov-de Gennes equations can be written as

$$L_1 u = 0, \tag{6.14}$$

and

$$L_3 v = -2\mathcal{J}_0 u. \tag{6.15}$$

The above set of differential equations can be solved exactly, with the homogeneous eigenvalue problem solvable using either a hypergeometric series approach [14, 184–186] or by operator methods [187], together with the method of variation of parameters for the inhomogeneous problem. As the latter of these is an established technique in the study of differential equations, we will only present details for the complementary solution using the hypergeometric series approach as follows.

By introducing the soliton width $b = -2\hbar^2/(m\tilde{g}_{1\mathrm{D}})$ as a scaling parameter, the homogeneous part of the Bogoliubov-de Gennes equations can be written as

$$\left[-\frac{d^2}{dx_m^2} - \ell\,(\ell+1)\,\mathrm{sech}^2(x_m/b)\right] f(x_m/b) = E f(x_m/b), \tag{6.16}$$

with $\ell \in \mathbb{Z}^+$ and eigenvalue E. The potential function appearing in Eq. (6.16) is commonly referred to in the literature as a *'modified Pöschl-Teller'* or *'Eckart'* potential, which has been studied in the context of reflectionless scattering [147, 181] and supersymmetry [187, 188]. As this potential is attractive, and converges to zero when $x_m \to \pm\infty$, the corresponding eigenspectrum will consist of two sets: a bound-

state spectrum for $E < 0$, and scattering states with $E > 0$. For our purposes, we will only be concerned with the bound-state spectrum and instead refer the reader to Refs. [6, 184, 185] for details on the continuous spectrum and reflectionless properties of the potential.

To proceed, we follow the method outlined by Flügge [184], in which we seek to transform Eq. (6.16) into hypergeometric form by introducing the change of variables $y = \cosh^2(x_m/b)$. The resulting transformed differential equation reads as

$$y\,(1-y)\,\frac{d^2f}{dy^2} + \left[\frac{1}{2} - y\right]\frac{df}{dy} - \left[\frac{\ell\,(\ell+1)}{4y} + \frac{E}{4}\right] f = 0. \tag{6.17}$$

Then, by further setting $f = wy^{(\ell+1)/2}$, we arrive at the hypergeometric differential equation

$$y\,(1-y)\,\frac{d^2w}{dy^2} + [\gamma - (\alpha+\beta+1)\,y]\,\frac{dw}{dy} - \alpha\beta w = 0, \tag{6.18}$$

with the abbreviations $\alpha = (\ell+1-i\sqrt{E}\,)/2$, $\beta = (\ell+1+i\sqrt{E}\,)/2$, and $\gamma = \ell+3/2$. For the domain $0 \leq |x_m/b| \leq \infty \rightarrow 1 \leq y \leq \infty$, the general solution around the singular point $y = 1$ is given by

$$\begin{aligned} f/y^{(\ell+1)/2} = {} & A\ {}_2F_1\,(\alpha,\beta;\gamma';1-y) \\ & + (1-y)^{-\gamma'+1}\,B\ {}_2F_1\,(\gamma-\beta,\gamma-\alpha;2-\gamma';1-y)\,, \end{aligned} \tag{6.19}$$

where A and B are arbitrary constants with $\gamma' = \alpha+\beta-\gamma+1$. A derivation of the above solution, as well as a review on the properties of the hypergeometric differential equation is provided in Appendix A.

As we require the general solution described by Eq. (6.19) to converge to zero in the $\lim_{x_m\rightarrow\pm\infty}$ for $E < 0$, we can proceed in deriving an expression for the allowed eigenvalues by studying the asymptotic behaviour of the solution. To this end, we introduce the asymptotic form $y = \cosh^2(x_m/b) \sim e^{2|x_m/b|}/4$, which together with Kummer's solutions,[ii] allows us to write the set of fundamental solutions as

$$\lim_{|x_m|\rightarrow\infty} w_3 \sim y^{-\alpha}\frac{\Gamma\,(\gamma')\,\Gamma\,(\beta-\alpha)}{\Gamma\,(\beta)\,\Gamma\,(\beta-\gamma+1)} + y^{-\beta}\frac{\Gamma\,(\gamma')\,\Gamma\,(\alpha-\beta)}{\Gamma\,(\alpha)\,\Gamma\,(\alpha-\gamma+1)}, \tag{6.20}$$

[ii]The connection formulas between the sets of solutions $\{w_3, w_4\}$ and $\{w_5, w_6\}$ are given by

$$w_3(z) = \frac{\Gamma(\gamma')\Gamma(\beta-\alpha)}{\Gamma(\beta)\Gamma(\beta-\gamma+1)}w_5(z) + \frac{\Gamma(\gamma')\Gamma(\alpha-\beta)}{\Gamma(\alpha)\Gamma(\alpha-\gamma+1)}w_6(z),$$

and

$$w_4(z) = \frac{\Gamma(2-\gamma')\Gamma(\beta-\alpha)}{\Gamma(1-\alpha)\Gamma(\gamma-\alpha)}w_5(z) + \frac{\Gamma(2-\gamma')\Gamma(\alpha-\beta)}{\Gamma(1-\beta)\Gamma(\gamma-\beta)}w_6(z),$$

up to a overall phase factor.

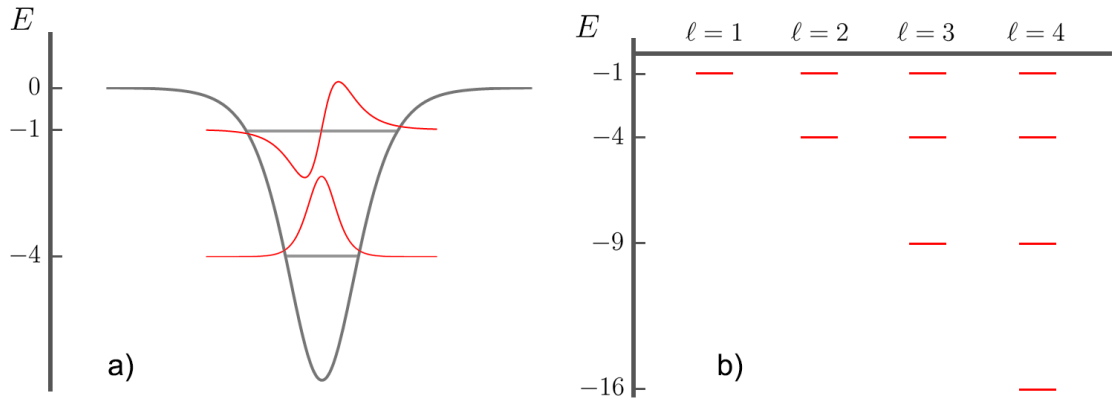

Figure 6.4: (a) Modified Pöschl-Teller potential for $\ell = 2$ illustrating the bound-state spectrum and corresponding eigenfunctions (red-solid). (b) Bound-state spectrum for the first four values of ℓ as per Eq. (6.24).

and

$$\lim_{|x_m|\to\infty} w_4 \sim y^{-\alpha}\frac{\Gamma\left(2-\gamma'\right)\Gamma\left(\beta-\alpha\right)}{\Gamma\left(1-\alpha\right)\Gamma\left(\gamma-\alpha\right)} + y^{-\beta}\frac{\Gamma\left(2-\gamma'\right)\Gamma\left(\alpha-\beta\right)}{\Gamma\left(1-\beta\right)\Gamma\left(\gamma-\beta\right)}, \tag{6.21}$$

where the hypergeometric functions reduce in the asymptotic limit as

$$\lim_{|x_m|\to\infty} {}_2F_1(\alpha, \alpha-\gamma+1; \alpha-\beta+1; 4e^{-2|x_m/b|}) \sim$$

$$1 + \frac{\alpha\left(\alpha-\gamma+1\right)}{(\alpha-\beta+1)}4e^{-2|x_m/b|} + \frac{\alpha(\alpha+1)\left(\alpha-\gamma+1\right)\left(\alpha-\gamma+2\right)}{(\alpha-\beta+1)(\alpha-\beta+2)}2e^{-4|x_m/b|} + \ldots \sim 1, \tag{6.22}$$

and similarly for

$$\lim_{|x_m|\to\infty} {}_2F_1(\beta, \beta-\gamma+1; \beta-\alpha+1; 4e^{-2|x_m/b|}) \sim 1. \tag{6.23}$$

The pair of asymptotic forms described above converge provided the ratio of Γ-functions vanishes. Therefore we require $\beta-\gamma+1 = -n$ (even) and $1-\alpha = -n$ (odd), for the fundamental solutions w_3 and w_4 respectively, with $n \in \mathbb{Z}_0^+$ provided $E < 0$. The resulting expression for the eigenvalues can then be determined iteratively and takes the form

$$E = -\left(\ell - n\right)^2, \tag{6.24}$$

with the constraint $0 \leq n \leq \ell - 1$. The energy spectrum is illustrated in Fig. 6.4.

To solve for the eigenvectors of Eq. (6.16), it is instructive to consider specific values of ℓ and E to obtain the solutions as required. For the operator L_1, which corresponds to setting $\ell = 1$ and $E = -1$ in Eq. (6.16), we find the complementary

solution

$$f = A\,\mathrm{sech}(x_m/b) + i\frac{B}{2}\left[(x_m/b)\,\mathrm{sech}(x_m/b) + \sinh(x_m/b)\right], \tag{6.25}$$

with the hypergeometric identities

$${}_2F_1\left(1/2, 3/2; 1/2; -\sinh^2(x_m/b)\right) = \mathrm{sech}^3(x_m/b), \tag{6.26}$$

and

$${}_2F_1\left(2, 1; 3/2; -\sinh^2(x_m/b)\right) = \frac{1}{2}\,\mathrm{sech}^2(x_m/b)\left[(x_m/b)\,\mathrm{csch}(x_m/b)\,\mathrm{sech}(x_m/b) + 1\right]. \tag{6.27}$$

Similarly for $\ell = 2$ and $E = -1$, which corresponds to the operator L_3, we find the complementary solution

$$\begin{aligned} f = \frac{A}{2}\,\mathrm{sech}(x_m/b)\left[3 - 3(x_m/b)\tanh(x_m/b) - \cosh^2(x_m/b)\right] \\ + iB\tanh(x_m/b)\,\mathrm{sech}(x_m/b), \end{aligned} \tag{6.28}$$

with

$$\begin{aligned} &{}_2F_1\left(1, 2; 1/2; -\sinh^2(x_m/b)\right) = \\ &\frac{3}{2}\,\mathrm{sech}^4(x_m/b)\left[1 - (x_m/b)\tanh(x_m/b) - (1/3)\cosh^2(x_m/b)\right], \end{aligned} \tag{6.29}$$

and

$${}_2F_1\left(5/2, 3/2; 3/2; -\sinh^2(x_m/b)\right) = \mathrm{sech}^5(x_m/b). \tag{6.30}$$

This completes the derivation of the complementary solution.

Collating these results, we denote the zero-eigenvalue solutions as $\zeta_n = \begin{pmatrix} u & v \end{pmatrix}^{\mathrm{T}} = n \in \mathbb{Z}^+$, and find

$$\zeta_1 = \begin{pmatrix} c_1\,\mathrm{sech}(x_m/b) \\ 0 \end{pmatrix}, \tag{6.31}$$

and

$$\zeta_2 = \begin{pmatrix} 0 \\ c_4\tanh(x_m/b)\,\mathrm{sech}(x_m/b) \end{pmatrix}, \tag{6.32}$$

where c_n are set of arbitrary constants. Due to the four-fold degeneracy of the

zero-eigenvalue, two linearly-independent solutions, $\zeta_3 = 2\left(\zeta_{3,-} + \zeta_{3,+}\right)$ and $\zeta_4 = 2\left(\zeta_{4,-} + \zeta_{4,+}\right)$, are also required for completeness, where

$$\zeta_{3,-} = c_2 \operatorname{sech}(x_m/b) \begin{pmatrix} x_m/b \\ ia_1/\left(2\hbar\right) \end{pmatrix}, \tag{6.33}$$

$$\zeta_{3,+} = c_2 \begin{pmatrix} \sinh(x_m/b) \\ -\left(2ia_1/\hbar\right) \operatorname{sech}(x_m/b)\left[(x_m/b)\tanh(x_m/b) - 3/4\right] \end{pmatrix}, \tag{6.34}$$

$$\zeta_{4,-} = \begin{pmatrix} 0 \\ c_3 \operatorname{sech}(x_m/b)\left[(x_m/b)\tanh(x_m/b) - 1\right] \end{pmatrix}, \tag{6.35}$$

and

$$\zeta_{4,+} = \begin{pmatrix} 0 \\ (c_3/3)\cosh(x_m/b) \end{pmatrix}, \tag{6.36}$$

are a set of generalized eigenvectors which satisfy the eigenrelations, $\hat{L}\zeta_{3,\pm} = \pm 2\zeta_2$ and $\hat{L}\zeta_{4,\pm} = \pm 2\zeta_1$, up to a constant [158, 189].

> **Definition 6.3:** *For a defective $n \times n$ matrix A, which contains an eigenvalue whose geometric multipiclity is larger than the algebraic multiplcity, a generalised eigenvector* $\mathbf{y}$ *of rank m, is defined by the eigenrelation*
>
> $$\left(A - \lambda \hat{\mathbb{I}}_{n\times n}\right)^m \mathbf{y} = 0,$$
>
> *such that*
>
> $$\left(A - \lambda \hat{\mathbb{I}}_{n\times n}\right) \mathbf{y} = \mathbf{x},$$
>
> *for the ordinary eigenvector* $\mathbf{x}$ *and $n \times n$ identity matrix $\hat{\mathbb{I}}_{n\times n}$.*

Together, these states compose the discrete spectrum of Eq. (6.3), corresponding each to small variations of the soliton with respect to its four free parameters: phase, position, velocity, and chemical potential. In turn, this leads to the identification of four continuous symmetries of the chiral model, namely: the gauge symmetry, translational symmetry, Galilean symmetry, and dilation symmetry for each free parameter respectively [97, 118]. As an example, by expanding the soliton solution around a infinitesimal spatial translation $x_m \to x_m + \varepsilon x_c$, one finds to first-order

that

$$\operatorname{sech}((x_m + \varepsilon x_c)/b) = \operatorname{sech}(x_m/b) - \frac{\varepsilon x_c}{b}\tanh(x_m/b)\operatorname{sech}(x_m/b) + \mathcal{O}(\varepsilon)^2, \quad (6.37)$$

which is captured by $\zeta_2(x_m)$ with respect to Eq. (6.1). The same procedure follows for the remaining eigenvectors.

Surprisingly, this set of discrete states is identical to that of the Bogoliubov-de Gennes equations for the Gross-Pitaevskii equation, except for $\zeta_3(x_m)$ which features current-dependent terms due to the width of the chiral soliton being defined in part by its velocity. This similarity becomes clear when obtaining the solutions, as one finds that the soliton envelope is a zero eigenvalue solution of not only the linear operator $L_1\varphi_{\mathrm{B}} = 0$, but also the current operator $\mathcal{J}_0\varphi_{\mathrm{B}} = 0$. Therefore, the eigenvalue problem for both $\zeta_1(x_m)$ and $\zeta_2(x_m)$ effectively reduces to the standard case, which naturally leads to the form of the solutions pictured in Fig. 6.2.

Discrete Spectrum - Adjoint Bound States

In addition to the standard eigenvalue problem, we can also solve the corresponding adjoint problem using the same analytical techniques. This will then enable us to derive the left-eigenvectors of $\hat{L}$, and subsequently construct a dual-basis for the eigenspace. Although this system does not have any physical relevance, the equivalence of both eigenvalue problems will be a key property which we will exploit when deriving the Vakhitov-Kolokolov criterion in the next section.

Using the same techniques as before, we denote the left-eigenvectors of $\hat{L}$ as $\vartheta = (u \quad v)^* = n \in \mathbb{Z}^+$, and find the pair of adjoint solutions

$$\vartheta_1 = \begin{pmatrix} 0 \\ c_5 \operatorname{sech}(x_m/b) \end{pmatrix}^\dagger, \quad (6.38)$$

and

$$\vartheta_2 = c_8 \operatorname{sech}(x_m/b) \begin{pmatrix} \tanh(x_m/b) \\ -(ia_1/\hbar)\operatorname{sech}^2(x_m/b) \end{pmatrix}^\dagger. \quad (6.39)$$

Again, due to the degeneracy of the zero-eigenvalue, two additional solutions, $\vartheta_3 = 2(\vartheta_{3,-} + \vartheta_{3,+})$ and $\vartheta_4 = 2(\vartheta_{4,-} + \vartheta_{4,+})$, are also required for completeness, where

$$\vartheta_{3,-} = \begin{pmatrix} 0 \\ c_6(x_m/b)\operatorname{sech}(x_m/b) \end{pmatrix}^\dagger, \quad (6.40)$$

$$\vartheta_{3,+} = \begin{pmatrix} 0 \\ c_6 \sinh(x_m/b) \end{pmatrix}^{\dagger}, \tag{6.41}$$

$$\vartheta_{4,-} = c_7 \operatorname{sech}(x_m/b) \begin{pmatrix} (x_m/b)\tanh(x_m/b) - 1 \\ -(ia_1/\hbar)\left[(x_m/b)\operatorname{sech}^2(x_m/b) - \tanh(x_m/b)\right] \end{pmatrix}^{\dagger}, \tag{6.42}$$

and

$$\vartheta_{4,+} = \frac{c_7}{3} \begin{pmatrix} \cosh(x_m/b) \\ (2ia_1/\hbar)\,(x_m/b)\operatorname{sech}(x_m/b) \end{pmatrix}^{\dagger}, \tag{6.43}$$

are the set of generalized eigenvectors satisfying the eigenrelations, $L^{\dagger}\vartheta_{3,\pm} = \pm 2\vartheta_2$ and $L^{\dagger}\vartheta_{4,\pm} = \pm 2\vartheta_1$, up to a constant.

Discrete Spectrum - Inner products and Wronskians

With the set of right and left eigenvector derived, we are now in a position to construct a dual-basis for the eigenspace and compare our analytical results to the numerical ones obtained earlier. Before proceeding with this, it is practical to first prove that our sets of solutions are complete, as follows.

> **Lemma 6.1** *The set of eigenvectors ζ_n form a complete basis for the discrete spectrum of the Bogoliubov-de Gennes equations, and likewise for ϑ_n for the adjoint problem.*

Proof: As the zero-eigenvalue of the Bogoliubov-de Gennes equations has a geometric multiplicity of four, it is sufficient to prove that each of the four eigenvectors are linearly independent to each other.

> **Definition 6.4** *The Wronskian between a pair of two-component vectors $\mathbf{x}(x_1, x_2)$ and $\mathbf{y}(y_1, y_2)$ is given by*
>
> $$\mathcal{W}(\mathbf{x}, \mathbf{y}) = \det \begin{vmatrix} x_1 & y_1 \\ x_2 & y_2 \end{vmatrix}, \tag{6.44}$$
>
> *such that $\mathcal{W}(\mathbf{x}, \mathbf{y}) \neq 0$ indicates a pair of vectors that are linearly independent.*

Using Definition 6.4, it is straightforward to verify that the solutions are linearly independent

$$\mathcal{W}\left(\zeta_1, \zeta_2\right) = \det \begin{vmatrix} \operatorname{sech}(x_m/b) & 0 \\ 0 & \tanh(x_m/b)\operatorname{sech}(x_m/b) \end{vmatrix} \neq 0, \tag{6.45}$$

and likewise for the remaining solutions in ζ_n and ϑ_n.

In the sub-space of ordinary eigenvectors, with $n = \{1, 2\}$, the corresponding inner-products can be readily calculated, with

$$\langle \zeta_n, \zeta_m \rangle = \langle \vartheta_n, \vartheta_m \rangle = \delta_{n,m}, \tag{6.46}$$

and

$$\langle \vartheta_n, \zeta_m \rangle = 0, \tag{6.47}$$

where in Eq. (6.46), each inner-product is constrained by the normalisation condition, Eq. (4.28), with $N = 1$. The fact that $\langle \vartheta_n, \zeta_m \rangle \neq \delta_{n,m}$, highlights that the pair of eigenvectors $\{\vartheta_n, \zeta_n\}$, does not form a bi-orthogonal basis. Note, that the inner-products in the generalised eigenspace, with $n = \{3, 4\}$, do not need to be considered as these states are not square-integrable solutions and are therefore unphysical.

From Eq. (6.46), one can then calculate the values of $|c_1|^2 = 1/(2b)$ and $|c_4|^2 = 3/(2b)$ for the arbitrary constants in $\zeta_1(x_m)$ and $\zeta_2(x_m)$ respectively. This in turn, now allows us to directly compare our analytical results to those obtained numerically, as shown in Fig. 6.2. Here, we find exact agreement between the analytical (dots) and numerical (solid-line) results for the discrete states $\zeta_1(x_m)$ and $\zeta_2(x_m)$. This then reinforces the statement that the discrete eigenvalues in the stability spectrum are four-fold degenerate at $\hbar\omega = 0$, with the imaginary component attributed to numerical artifacts. Therefore we may conclude, with confidence, that due to the consistency in the results obtained, that the chiral soliton is stable to linear perturbations.

Continuous States

For the continuous states, we are unfortunately unable to derive a closed-form solution due to the complexity of the eigenvalue problem. As a result, we cannot address questions related to the properties of the soliton potential, particularly on the topic of reflectionless scattering. Although we may be able to study this using a power series method or supersymmetry techniques [187, 190, 191], the complicated nature of the calculation presents little benefit for the knowledge gained, since the

continuous states are irrelevant for addressing the stability of the soliton. However, we can obtain some details of the continuous spectrum by studying the asymptotic behaviour of the Bogoliubov de-Gennes equations.

The key point to note, is that for large distances away from the soliton's centre of mass, the soliton density asymptotically approaches zero as $\lim_{x_m \to \pm\infty} |\varphi_{\mathrm{B}}|^2 \sim 0$. In this limit, the Bogoliubov-de Gennes equations decouple into a pair of identical fourth-order equations

$$L_0^2 \begin{pmatrix} u \\ v \end{pmatrix} \sim (\hbar\omega_c)^2 \begin{pmatrix} u \\ v \end{pmatrix}, \tag{6.48}$$

for the continuous eigenvalues $\hbar\omega_c$. As these equations are simply the square of a typical free-particle Schrödinger equation, we may approximate the solutions in the asymptotic limit as plane waves of the form

$$\lim_{x \to \pm\infty} \begin{pmatrix} u \\ v \end{pmatrix} \sim \pm \begin{pmatrix} e^{iqx} \\ e^{iqx} \end{pmatrix}, \tag{6.49}$$

with wave-number q. Then, by substituting Eq. (6.49) into Eq. (6.48), one finds the continuous eigenvalue expression

$$\hbar\omega_c \sim \pm \left(\frac{\hbar^2 q^2}{2m} - \mu \right), \tag{6.50}$$

which as expected, is simply a free-particle dispersion relation gapped by the chemical potential of the soliton. In Fig. 6.1, we compare both the numerical (red solid-line) and analytic (red dots) values for the continuous state band edge ($q = 0$) which as shown, is in exact agreement.

6.3 Vakhitov-Kolokolov criterion

As the chiral solitons present in our model are solutions to a generalized Gross-Pitaevskii equation with a real-positive envelope, we can also establish their stability properties using the Vakhitov-Kolokolov criterion [151, 164].

> **Theorem 6.2:** *For the standard Gross-Pitaevskii equation, the bright soliton solution is stable to linear perturbations provided:*
>
> (i) *The eigenspectrum of the operators L_1 and L_3, should contain at most only a single negative eigenvalue, which is sufficient.*
>
> (ii) *The slope of the power integral, $dN/d\mu \geq 0$, should be non-negative for $\mu < 0$, which is necessary.*

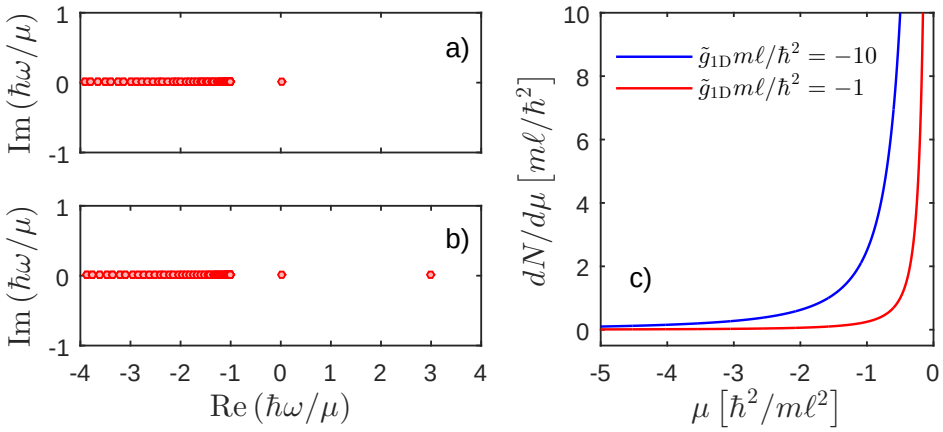

Figure 6.5: Numerically obtained eigenvalues of the linear operators L_1 (a) and L_3 (b), with $g_{1D}m\ell/\hbar^2 = -1$, $vm\ell/\hbar = 1$, and $a_1/\hbar = 1$, and Vakhitov-Kolokolov slope condition (c) for a bright chiral soliton. Note, that the eigenvalues in (a) and (b) are scaled by the chemical potential with $\mu < 0$.

Proof: The first condition can be verified analytically using the hypergeometric techniques presented earlier, or more readily by calculating the eigenvalues numerically. The second condition can be determined from direct integration by setting the unconstrained soliton as $\varphi_{\rm B}(x_m;\mu) \equiv \mathrm{sech}(x_m/b)$, such that

$$N = \int_{-\infty}^{\infty} dx_m\ |\varphi_{\rm B}(x_m;\mu)|^2 \Longrightarrow \frac{dN}{d\mu} = -\frac{\tilde{g}_{1D}}{4\mu^2}. \tag{6.51}$$

These results are summarised in Fig. 6.5, and will be proved in the following analysis in the context of the interacting gauge theory.

As the eigenvalues of $\hat{L}$ and $\hat{L}^\dagger$ are conjugate to each other, we can without loss of generality, consider the spectral properties of either eigenvalue problem. To this end, it will prove advantageous to work in the adjoint picture, as the following stability analysis is simpler while also exploiting the property that the operators L_1 and L_3 are self-adjoint.

We start, by restating the adjoint eigenvalue problem

$$2\mathcal{J}_0^\dagger u^* + L_1 v^* = \hbar\omega^* u^*, \tag{6.52}$$

and

$$L_3 u^* = \hbar\omega^* v^*, \tag{6.53}$$

where the asterisks in $u^*(x_m)$ and $v^*(x_m)$ are suppressed for brevity. Taking the inner-product of Eq. (6.52) with $\varphi_{\rm B}\,(x_m)$ leads to the expression

$$2\langle\varphi_{\rm B}, \mathcal{J}_0^\dagger u^*\rangle + \langle\varphi_{\rm B}, L_1 v^*\rangle = \hbar\omega^*\langle\varphi_{\rm B}, u^*\rangle. \tag{6.54}$$

As L_1 is a self-adjoint operator with $L_1\varphi_{\rm B} = 0$, the above expression is true $\forall\omega^*$, provided the orthogonality condition

$$\langle\varphi_{\rm B}, \mathcal{J}_0^\dagger u^*\rangle = \langle\varphi_{\rm B}, u^*\rangle = 0, \tag{6.55}$$

is satisfied. Therefore, for the non-zero eigenvalues in the stability analysis, we may restrict ourselves to the function space

$$\mathcal{M} \equiv \{h\,(x_m) : \langle\varphi_{\rm B}, \mathcal{J}_0^\dagger u^*\rangle = \langle\varphi_{\rm B}, u^*\rangle = 0\}, \tag{6.56}$$

where the inverse operators L_1^{-1} and L_3^{-1} are definable. In addition, we normalise the inner-product, $\langle h, h\rangle = 1$, to unity.

Returning to Eqs. (6.52) and (6.53), we can now proceed in constructing the stability criterion for the chiral soliton by combining both equations into the fourth-order equation

$$L_1 L_3 h = (\hbar\omega^*)^2\, h - 2\hbar\omega^*\,\mathcal{J}_0^\dagger h, \tag{6.57}$$

in the function space $\mathcal{M}$. Multiplying Eq. (6.57) by L_1^{-1}, taking the inner product with respect to $h(x_m)$, and completing the square leads to the expression

$$(\hbar\omega^*)^2 = \frac{\gamma}{\alpha} + \frac{2\beta^2}{\alpha^2} \pm \frac{\beta}{\alpha}\left(\frac{\beta^2}{\alpha^2} + \frac{\gamma}{\alpha}\right)^{1/2}, \tag{6.58}$$

with $\alpha = \langle h, L_1^{-1}\, h\rangle$, $\beta = \langle h, L_1^{-1}\mathcal{J}_0^\dagger\, h\rangle$, and $\gamma = \langle h, L_3\, h\rangle$. Note, that we have reused the Greek notation in these inner-products and should not be confused with the hypergeometric function arguments presented earlier. The condition of stability is now set by requiring that the right-hand side of Eq. (6.58) be non-negative, such that $\hbar\omega^*$, by extension, is real. Otherwise for negative values, $\hbar\omega^*$ would be imaginary, thereby indicating an instability. To determine this, we will study the definiteness of each linear operator as follows.

> **Lemma 6.2:** *The adjoint current operator $\mathcal{J}_0^\dagger$, is nilpotent in the domain of the soliton, i.e. $\mathcal{J}_0^\dagger h = 0$, such that all the eigenvalues of $\mathcal{J}_0^\dagger$ are zero.*

Proof: This can be proven directly by solving the eigenvalue equation

$$\mathcal{J}_0^\dagger h(x_m) = \lambda h(x_m), \tag{6.59}$$

for eigenfunction $h(x_m)$ and eigenvalue λ.[iii] Using separation of variables, the general

[iii] A numerical solution of the eigenspectrum is unfortunately ill-conditioned, as the matrix $\mathcal{J}_0^\dagger$ is singular in the continuum limit.

solution of Eq. (6.59) can be readily obtained

$$h(x_m) = C\cosh^3(x_m/b)\ \ \exp\left[-i\epsilon\lambda\left(x_m/b + \frac{1}{2}\sinh(2x_m/b)\right)\right], \tag{6.60}$$

where $\epsilon = mb^2/a_1\hbar$, and C is an arbitrary constant. For a ring domain of length (circumference) L, with periodic boundary conditions $h(-L/2) = h(L/2)$, the eigenvalues form a continuous spectrum

$$\lambda = \frac{2\pi\upsilon}{\epsilon\left(L/b + \sinh(L/b)\right)}, \tag{6.61}$$

with $\upsilon \in \mathbb{Z}_0$. Then, in the combined limit where $L \to \infty$ and $\upsilon \to \pm\infty$, the eigenvalues of Eq. (6.59) coalesce at $\lambda = 0$, highlighting that in the continuum limit, the adjoint current operator $\mathcal{J}_0^\dagger$ is nilpotent, as required. Using this result, the stability criterion for the chiral soliton is greatly simplified, and reduces to the case of the standard Gross-Pitaevskii equation

$$(\hbar\omega^*)^2 = \frac{\langle h, L_3\, h\rangle}{\langle h, L_1^{-1}h\rangle}, \tag{6.62}$$

requiring us to study the definiteness of the operators L_1^{-1} and L_3. This leads to the conclusion, that in the linear-stability framework of the chiral soliton, the gauge-field does not contribute to dynamical instabilities.

> **Lemma 6.3:** *The linearised operator L_1 and it's inverse is positive definite in the function space $\mathcal{M}$.*

Proof: As the eigenvalues of the operator L_1 are entirely real and positive in the space $\mathcal{M}$ (see Fig. 6.5), both L_1 and L_1^{-1} are by definition positive-definite operators.

> **Definition 6.5:** *For a self-adjoint matrix A with eigenvectors $\mathbf{x}$ and eigenvalues λ satisfying*
>
> $$A\mathbf{x} = \lambda\mathbf{x} \quad \Longrightarrow \quad \mathbf{x}^\dagger A\mathbf{x} = \lambda||\mathbf{x}||^2,$$
>
> *the quantity $\mathbf{x}^\dagger A\mathbf{x}$ is positive for $\lambda \in \mathbb{R}^+$, such that A, by definition, is a positive-definite operator.*

The condition of stability therefore requires that $\{\min\langle h, L_3 h\rangle\} \geq 0$, such that L_3 should be either positive or positive semi-definite in the space $\mathcal{M}$.

> **Lemma 6.4:** *The linearised operator L_3 is positive semi-definite in the function space $\mathcal{M}$.*

Proof: The definiteness of the operator L_3 can be determined using the method of Lagrange multipliers, and will subsequently lead to the Vakhitov-Kolokolov criterion. We begin by defining the Lagrange functional

$$\mathscr{L}(h(x_m);\kappa,\tau) \equiv \langle h, L_3 h\rangle - \kappa\langle h, \varphi_{\rm B}\rangle - \tau\langle h, h\rangle, \tag{6.63}$$

where κ and τ, are Lagrange multipliers for the orthogonality and normalisation constraints respectively. Minimising the above functional with respect to $h^*(x_m)$ leads to the expressions

$$L_3 h = \kappa\varphi_{\rm B} + \tau h = 0, \tag{6.64}$$

and

$$\langle h, L_3 h\rangle = \tau\langle h, h\rangle, \tag{6.65}$$

with the second obtained by taking the inner-product of the first. The definiteness of L_3 is then determined by the sign of τ, as detailed in Eq. (6.65), and must be studied for the cases $\kappa = 0$ and $\kappa \neq 0$ separately.

In the first instance, with $\kappa = 0$, Eq. (6.64) reduces to the eigenvalue equation

$$L_3 h = \tau h, \tag{6.66}$$

such that τ is an eigenvalue of the linear operator L_3, with eigenfunction $h(x_m)$. However, as the only discrete eigenvalue of L_3 in the function space $\mathcal{M}$ is the ground state solution $h_0 = \mathrm{sech}^2(x_m/b)$, with $\langle h_0, \varphi_{\rm B}\rangle \neq 0$, we require $\tau = 0$ to avoid a contradiction in the constraints. In turn, this reveals that $\{\min\langle h, L_3 h\rangle\} = 0$, such that L_3 is a positive semi-definite operator in the function space $\mathcal{M}$, as stated in Lemma 6.3.

The case of $\kappa \neq 0$ is more involved and requires care. As L_3 is a self-adjoint operator, we can expand the eigenfunctions $h(x_m)$ into a complete set of orthogonal functions

$$h(x_m) = \sum_n c_n p_n(x_m) + \int_{-\mu}^{-\infty} d\Lambda\, Cp(x_m), \tag{6.67}$$

where the summation and integration runs over the discrete and continuous states respectively. Substituting Eq. (6.67) into Eq. (6.64), leads to the following values of the expansions coefficients

$$c_n = \frac{\kappa\langle p_n, \varphi_{\rm B}\rangle}{\Lambda_n - \tau}, \tag{6.68}$$

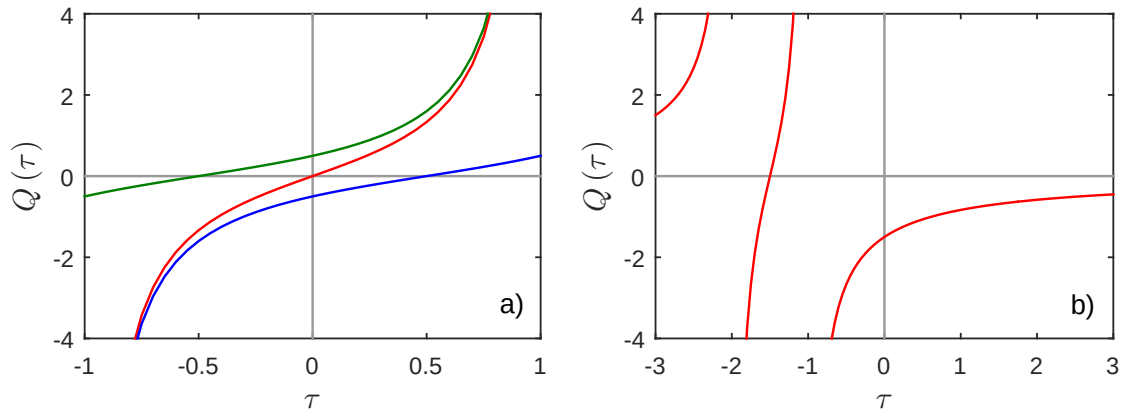

Figure 6.6: Plots of the $Q(\tau)$ function, Eq. (6.71), detailing the behaviour of the minimum roots $\tau_{\min}$ for the case of a single negative eigenvalue (a), and two negative eigenvalues (b). Pictured in (a) are the three possible scenarios: $|\Lambda_0| = |\Lambda_2|$ (red), $|\Lambda_0| < |\Lambda_2|$ (green), and $|\Lambda_0| > |\Lambda_2|$ (blue).

and

$$C = \frac{\kappa \langle p, \varphi_{\mathrm{B}} \rangle}{\Lambda - \tau}, \tag{6.69}$$

provided $L_3 h = \Lambda h$. Eq. (6.67) can then be rewritten as

$$h(x_m) = \sum_n \frac{\kappa \langle p_n, \varphi_{\mathrm{B}} \rangle}{\Lambda_n - \tau} p_n + \int_{-\mu}^{-\infty} d\Lambda \, \frac{\kappa \langle p, \varphi_{\mathrm{B}} \rangle}{\Lambda - \tau} p, \tag{6.70}$$

which when inserted into the orthogonality condition, becomes

$$Q(\tau) = \sum_n \frac{\kappa |\langle p_n, \varphi_{\mathrm{B}} \rangle|^2}{\Lambda_n - \tau} + \int_{-\mu}^{-\infty} d\Lambda \, \frac{\kappa |\langle p, \varphi_{\mathrm{B}} \rangle|^2}{\Lambda - \tau} = 0. \tag{6.71}$$

The possible values of τ can now be determined from examining the roots of $Q(\tau)$.

> **Lemma 6.5:** *If the linear operator L_3 contains only a single negative eigenvalue, the value of the function $Q(\tau)$ at $\tau = 0$, determines the sign of the minimal root $\tau_{\min}$, such that:*
>
> (i) *$Q(0) > 0$, then $\tau_{\min} < 0$, which indicates an instability.*
>
> (ii) *$Q(0) \leq 0$, then $\tau_{\min} \geq 0$, which indicates stability.*
>
> *Otherwise, if L_3 contains more than one negative eigenvalue, $\tau_{\min}$ is guaranteed to be negative.*

Proof: This can be determined readily, by studying the function $Q(\tau)$ graphically as a function of the number of negative eigenvalues in L_3.

For the case of a single negative eigenvalue, we know that $c_0 = \langle \varphi_{\mathrm{B}}, p_0 \rangle \neq 0$ and $c_1 = \langle \varphi_{\mathrm{B}}, p_1 \rangle = 0$, due to the positivity of φ_{B}, such that the eigenvalues can be

ordered $\Lambda_0 < 0 < \Lambda_2$, with continuous eigenvalues $\Lambda_{n>1}$. The function $Q(\tau)$ then increases monotonically from $Q(\Lambda_0) = -\infty$ to $Q(\Lambda_2) = \infty$, with a single root at $Q(\tau_{\min}) = 0$, as illustrated in Fig. 6.6(a). Then, depending on the values of Λ_0 and Λ_2, three possible scenarios can occur:

(i) $|\Lambda_0| = |\Lambda_2|$ (red), $Q(0) = 0$, such that $\tau_{\min} = 0$.

(ii) $|\Lambda_0| < |\Lambda_2|$ (green), $Q(0) > 0$, such that $\tau_{\min} < 0$.

(iii) $|\Lambda_0| > |\Lambda_2|$ (blue), $Q(0) < 0$, such that $\tau_{\min} > 0$.

Therefore, one can conclude that the value of $Q(0)$ determines the sign of $\tau_{\min}$. If we propose that L_3 contained two or more negative eigenvalues, one can see in Fig. 6.6(b), that $\tau_{\min}$ is guaranteed to be negative. This then demonstrates the first Vakhitov-Kolokolov criterion, that the spectral problem should only contain a single negative eigenvalue for the soliton to be stable to linear perturbations.

The second stability criterion can be determined from an elegant representation of the function

$$Q(0) = \sum_n \frac{|\langle p_n, \varphi_{\mathrm{B}}\rangle|^2}{\Lambda_n} + \int_{-\mu}^{-\infty} d\Lambda \, \frac{|\langle p, \varphi_{\mathrm{B}}\rangle|^2}{\Lambda}. \tag{6.72}$$

Using the completeness relation, together with the eigenvalue equation $L_3 h = \Lambda h$, one can rewrite Eq. (6.72) as the inner-product

$$Q(0) = \langle \varphi_{\mathrm{B}}, L_3^{-1} \varphi_{\mathrm{B}}\rangle. \tag{6.73}$$

To calculate $L_3^{-1}\varphi_{\mathrm{B}}$, one can differentiate the zeroth-order equation for the soliton envelope with respect to the propagation constant

$$L_3 \frac{d\varphi_{\mathrm{B}}}{d\mu} = \varphi_{\mathrm{B}}, \tag{6.74}$$

to obtain $d\varphi_{\mathrm{B}}/d\mu = L_3^{-1}\varphi_{\mathrm{B}}$. Substituting these definitions then leads to the Vakhitov-Kolokolov slope-condition

$$Q(0) = \langle \varphi_{\mathrm{B}}, \frac{d}{d\mu}\varphi_{\mathrm{B}}\rangle = \frac{1}{2}\frac{dN}{d\mu}. \tag{6.75}$$

with $\mu < 0$. The stability of the soliton is then determined by the sign of $dN/d\mu$. For $dN/d\mu \geq 0$, $\tau_{\min} \geq 0$ such that the soliton in linearly stable. Whereas $dN/d\mu < 0$, $\tau_{\min} < 0$, indicating an instability. This completes the derivation of the Vakhitov-Kolokolov criterion.

To summarize these results, we return to the full stability criterion described by

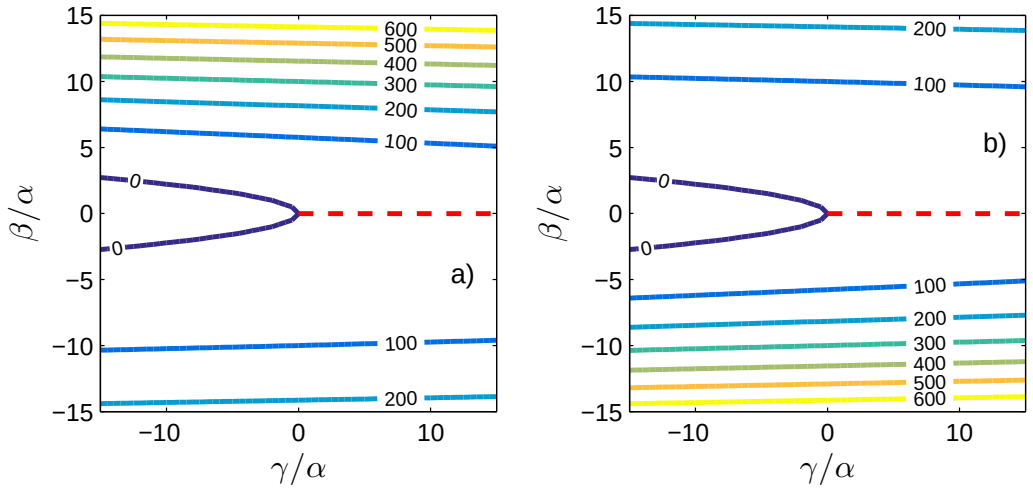

Figure 6.7: Contour plots of the stability eigenvalues $(\hbar\omega^*)^2$ for the positive (a) and negative (b) branches of Eq. (6.58). The dashed red line in both plots correspond to analytic result with $\beta/\alpha = 0$ and $\gamma/\alpha \geq 0$.

Eq. (6.58), which can be viewed as an energy surface in the generalised parameter space $\{\gamma/\alpha, \beta/\alpha\} \in \mathbb{R}$. In doing so, the stability of the soliton can be inferred from the regions of the energy surface which are positive, with negative and complex regions corresponding to regions of instability. In Fig. 6.7, we plot the energy surfaces of Eq. (6.58) for both the positive and negative branches of the stability criterion. In both cases, we find that the eigenvalues are entirely positive except for a region bounded by the $(\hbar\omega^*)^2 = 0$ contour in which the Eq. (6.58) becomes complex. However, this region does not intersect with the contour describing the analytical results for the definiteness of γ/α and β/α (red-dashed), and is therefore irrelevant. Interestingly, these plots highlight that the conditions of stability can be relaxed, as the energy surfaces are positive $\forall\ \beta/\alpha \in \mathbb{R}$, even though $\mathcal{J}_0^\dagger$ was found to be nilpotent in our analysis.

6.4 Numerics

As a final demonstration of the stability of the soliton, we consider a set of numerical simulations which illustrate the propagation of the chiral soliton under the influence of a perturbation. To achieve this, we follow the standard numerical scheme in which the initial number of atoms (power) of the soliton differs from the exact solution and observe whether the soliton collapses or retains its shape [2, 10]. As such, we define the perturbed soliton state as

$$\varphi_\Delta = \varphi_\mathrm{B}\,(1 + \Delta\varphi)\,, \tag{6.76}$$

and show two examples of the perturbation dynamics in Fig. 6.8, each for a different sign of the perturbation parameter $\Delta\varphi$.

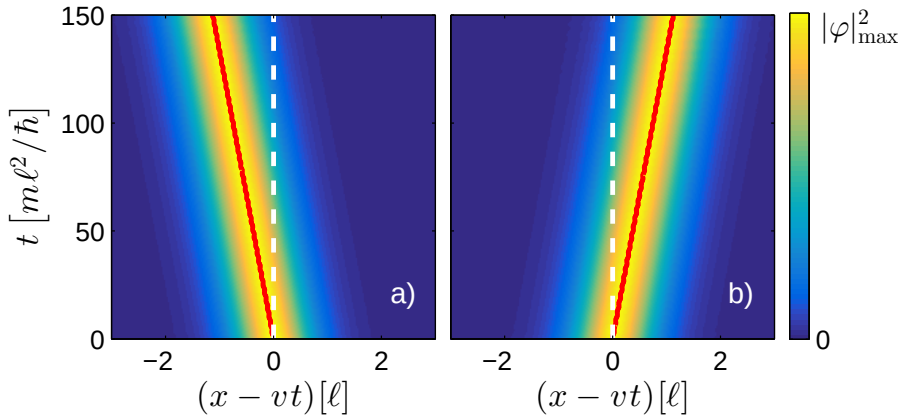

Figure 6.8: (colour online). Propagation of a chiral soliton, in the *moving-frame*, whose initial envelope is perturbed due to a change in the initial number of atoms. Shown, are the predicted trajectories from the variational equations (red-solid) in comparison to the full numerics (colour) and the unperturbed case (white-dash). The soliton parameters are $g_{1D}m\ell/\hbar^2 = -1$, $vm\ell/\hbar = 1$, and $a_1/\hbar = 1$, with the mismatch parameters $\Delta\varphi = +0.01$ (a), and $\Delta\varphi = -0.01$ (b).

In both cases, the soliton maintains its shape over the course of the simulation and does not collapse, disperse, or oscillate due to the excitation of an internal mode [10, 166]. Instead, the soliton emits a small (non-visible) amount of radiation and decays to the stable low-amplitude solution, in a similar manner to solitons of the Gross-Pitaevskii equation. However, as the initial width of the soliton changes due to the perturbation, with g_{1D} and a_1 both fixed, the velocity of the perturbed soliton will differ from the frame velocity set by Eq. (3.33). This results in the soliton drifting in the moving frame, with the direction controlled by the sign of the perturbation. This effect is not captured by the stability spectrum of the Bogoliubov-de Gennes equations, as Eq. (6.1) explicitly assumes that the excitations do not couple to the envelope of the soliton. Instead, we are required to return to the variational equations presented in Sec. 5.4 to explain the presence of the soliton drift.

Upon inspection, the source of the moving-frame drift is now clear from the coupling between Eqs. (5.27) and (5.28), that a time-dependent variation of the soliton's width, induced by a perturbation, can lead to a change in the soliton's centre-of-mass proportional to the strength of the gauge field. Therefore, for either an increase or decrease in the particle number, it is expected that the soliton will drift in the moving frame, with the trajectory of the soliton set by Eq. (5.26). However, as the form of these equations explicitly assumes that the shape and particle number of the soliton is conserved, the interplay of radiation is therefore absent in the variational model. Nevertheless, provided the magnitude of the perturbation is kept small, this discrepancy will not have significant implications.

To illustrate the above reasoning, we solve the set of variational equations numerically using a fourth-order Runge-Kutta method and plot the predicted soliton

trajectories (red solid-line) in Fig. 6.8. Both the direction and magnitude of the drift is captured correctly by the variational equations and therefore validates that the drift of the soliton arises due to how the initial state is prepared. In addition, these results show that in this weak perturbation regime, the emission of radiation from the soliton plays no significant role in the dynamics. Despite this, its absence in the variational description does lead to inconsistencies, as demonstrated by the presence of small-amplitude oscillations in the predicted trajectories which persist indefinitely.

To conclude, although we cannot strictly say that the chiral soliton is stable due to the presence of the drift, we stress that it is a manageable feature which does not destroy or damage the envelope of the soliton. This result therefore demonstrates the Lyapunov stability of the soliton, as alluded to in Sec. 5.5. Therefore, we may view the soliton as *effectively stable*, with the absence of the traditional instability mechanisms consistent with the spectrum of the Bogoliubov-de Gennes equations.

6.5 Summary and outlook

In this chapter, we have studied the linear stability of chiral bright solitons in an interacting gauge theory. Despite being described by a non-integrable model, we found that the stability properties of the chiral soliton effectively reduced to the standard integrable case, with the absence of imaginary eigenvalues in the linear stability spectrum. This was then further understood by formulating the stability problem using the Vakhitov-Kolokolov criterion, which highlighted that the linearised current operator was nilpotent in the numerical domain and therefore could not contribute to dynamical instabilities.

One of the most intriguing aspects of the soliton dynamics highlighted in the linear stability analysis, is that a chiral soliton drifts in the moving-frame when its initial envelope is weakly perturbed. By generalising the study to a broader class of perturbations, several questions are inspired not only in regards to the stability of the soliton in an experimental context, but also to features which could be exploited in order to control the soliton [9, 192]. For example, could the role of atom losses in the condensate driven by heating and interactions [193, 194], or the residual dimensionality of the gas [102], enable the soliton to accelerate or decelerate? Or, could the competition between perturbations compensate the drift the soliton and potentially enhance the stability? These questions, together with the linear stability properties concluded in this chapter, offers a promising candidate for practical transport dynamics in atomtronic systems [51, 195], where retaining the coherent properties of the gas can be an important factor.

Chapter 7

Interactions of bright chiral solitons

7.1 Introduction

One of the defining properties of solitons in integrable models, such as the nonlinear Schrödinger and Korteweg-de Vries equations, is that they pass through and emerge from the collision with another soliton unperturbed [6, 13]. All of the dynamical quantities of the solitons, such as their velocities, masses, and amplitudes, are conserved during the collision except for a possible phase shift or drift of the centre of mass due to the nonlinear interaction. The elastic nature of these collisions directly follows from the property that integrable models possess an infinite number of conservation laws [2, 4], which heavily restricts the soliton dynamics to fixed trajectories in the phase space.

In non-integrable models, the restrictions imposed by the conservation laws is generally relaxed and often leads to inelastic collisions featuring chaotic scattering trajectories [2, 13]. The defining feature here, is the existence of a short-lived bound state in which the number of collision events depends fractally on the initial conditions. Generally, this mechanism arises from the excitation of an internal mode of the soliton, either with [183, 196–199], or without radiation losses [200, 201], as well as through the presence of a weak perturbation [202–204]. In addition to this, solitons in non-integrable models can also fracture or merge into new products through fission and fusion events [134, 205, 206], particularly in the context of three-soliton and soliton-breather collisions [160]. Together, these effects present a strong contrast to the typical soliton dynamics encountered in integrable models, which are interesting not only from a fundamental point of view, but also provide valuable insight into the description of realistic systems which are generally described by non-integrable models.

Following the success of realising single solitons in ultracold experiments, the study of two-soliton physics in these gases has been a notable area of research in recent years. In the case of experiments, this was first studied, although somewhat

primitively, in the context of soliton trains [72, 175, 176], where the solitons collided in a random and uncontrollable fashion. However, upon improvements in the experimental method, a set of controlled collisions was demonstrated in the pioneering work conducted by the Hulet group [104], which critically highlighted the success of the mean-field description of matter-wave solitons. This work was accompanied by several theoretical papers [174, 207–209], which detailed how the breaking of integrability due to the harmonic trapping potential, can lead to the onset of chaotic dynamics for the solitons. In other theoretical works, soliton interactions have also been studied in the case of higher-dimensional [210] and two-component systems [129, 131, 211], and more recently for condensates featuring dipolar [132–134, 212] and spin-orbit interactions [136–138]. From this, several proposals have appeared which centre on the collisions of matter wave solitons, particularly on the topic of interferometry [49, 50], with extended applications for nonlinear splitters [213] and the creation of Bell states [214].

With the breakdown of both Galilean invariance and integrability in the interacting gauge theory, the collision dynamics between pairs of chiral solitons is therefore expected to be highly unconventional, but interesting from a nonlinear dynamics perspective. However, as a consequence of the non-integrability, the analytical techniques afforded to us by the Inverse Scattering Transform are unfortunately unavailable. Instead, in order to study the interactions of chiral solitons, we must rely on the use of numerical simulations and variational techniques. By performing these, we will find that the collision dynamics can feature several non-integrable phenomena; from inelastic collisions in the presence of population transfer and radiation losses, to short-lived bound states and soliton fission. The emergence of these phenomena, will then conclude the principle result of this thesis; that the density-dependent gauge theory features *near*-integrable for the case of a single-soliton, but is dominated by *non*-integrable dynamics in the two-soliton case.

7.2 Numerics

For our initial studies into the interactions of chiral solitons, we consider a series of numerical solutions in order to visualize how the non-integrability of the interacting gauge theory modifies the interactions. To achieve this, we write the initial two-soliton state as

$$\psi_{\text{int}}\left(x, t=0\right) \equiv \sum_{n=1,2} \frac{1}{2\sqrt{b_n}} \operatorname{sech}\left(\left(x-\xi_n\right)/b_n\right) e^{imv_n x/\hbar + i\phi_n}, \tag{7.1}$$

provided the solitons are initially well-separated in the far-field, such that $\xi_1 - \xi_2 \gg b_n$, for the linear approximation to hold. The two-soliton width $b_n = -4\hbar^2/(m\tilde{g}_{1\text{D}})$,

is chosen such that $\int_{-\infty}^{+\infty} dx\ \psi_{\rm int} = N$, with each soliton containing half the number of atoms.

Since a full parameter scan detailing the interactions of chiral solitons for every degree of freedom presents a formidable and intractable problem, we restrict our analysis to two parameter regimes, each set by a ratio of interaction strengths which illustrates the essential physics present in the model:

(i) *Strong-chiral regime,* $|g_{\rm 1D}| \ll |a_1 (v_1 + v_2)|$*, where the collision dynamics is dominated by effects stemming from the current nonlinearity*

(ii) *Weak-chiral regime,* $|g_{\rm 1D}| \gg |a_1 (v_1 + v_2)|$*, where the current nonlinearity is treated as a small perturbation to the mean-field dynamics.*

Then, to integrate Eq. (3.21) numerically, we construct an explicit central-difference algorithm for the evolution of the wave function and compared our results to those produced by a split-step Fourier method to ensure consistency. Critically, the numerical domain is chosen to be two orders of magnitude larger than the widths of the soliton, to avoid radiation back-reflecting to the interaction centre.

At this stage, it is important to point out that in the standard Gross-Pitaevskii equation, the absolute phase difference of the solitons is a conserved quantity which is invariant to the initial separation of the centre of masses [215]. As we will demonstrate in the following numerics, this property will not translate into the chiral model, as the gauge field will modify the absolute phases difference of the solitons after the collision. Therefore, each result we present is defined up to a choice of the initial phase difference and separation, although altering these parameters does not yield a qualitative difference.

7.2.1 Strong-chiral regime

For the strong-chiral regime, we present in Fig. 7.1, a set of density plots detailing the collision dynamics of two co-moving chiral solitons. In each case, the interaction strength induced by the current nonlinearity dominates over the mean-field effects due to the fast velocities of the solitons.

The top row of Fig (7.1) provide two examples of the collision dynamics in the extreme limit, where the dynamics are influenced solely by the current nonlinearity with the mean-field contact interaction set as $g_{\rm 1D} m\ell/\hbar^2 = 0$. Surprisingly, the collisions in these two instances are similar to those produced by the standard Gross-Pitaevskii equation, with the solitons surviving the collision with the general shape

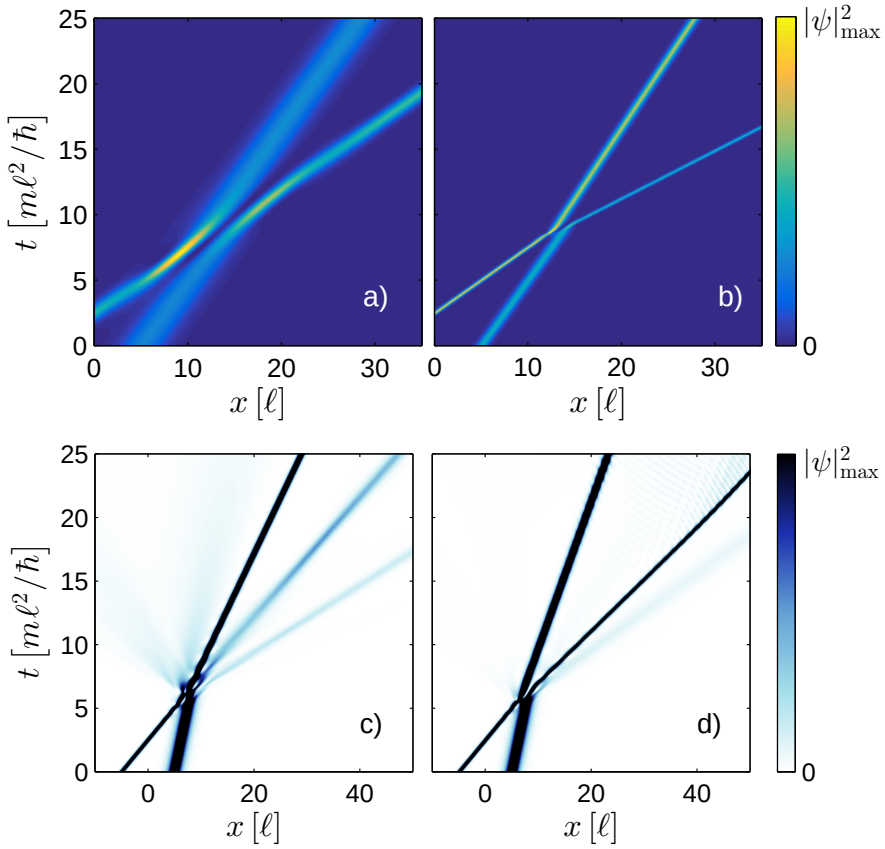

Figure 7.1: Examples of the collision dynamics between two chiral solitons in the strong-chiral regime. Note, that the colourbar limit has been intentionally lowered in these plots to display the solitons more clearly.

(Top row) Inelastic trajectories with $g_{1D}m\ell/\hbar^2 = 0$, $v_1 m\ell/\hbar = 2$, $v_2 m\ell/\hbar = 1$, and $\delta = 0$, where the gauge field strength varies as $a_1/\hbar = 1$ (a), and $a_1/\hbar = 4$(b).

(Bottom row) Soliton fission with $g_{1D}m\ell/\hbar^2 = 2$, $v_1 m\ell/\hbar = 2$, $v_2 m\ell/\hbar = 0.5$, $a_1/\hbar = 5$, with $\delta = 0$ (c), and $\delta = \pi$(d).

of their envelopes intact. However, two key differences are visible in these plots, particularly in the case of $a_1/\hbar = 4$, Fig. 7.1(b). The first are a pair of inelastic trajectories, where the outgoing velocities of the solitons is different from their initial velocities, with the top soliton post collision decreasing its velocity and the bottom soliton increasing its velocity. The second difference, is the appearance of a density node at the interaction centre, which is reminiscent of a repulsive interaction, despite the initial phase difference taken as $\delta = 0$, which is conventionally an attractive interaction. Each of these effects is a consequence of the non-integrability of the model, which permits the transfer of stored interaction energy into kinetic energy, and the possibility of a non-trivial shift of the soliton phase difference. The presence of the population transfer is directly linked to this phase shift, as both quantities are mutually conjugate. The energy exchange, or rather the inelasticity of the collision, appears to be minimised when the collision parameters are chosen so that the solitons interact repulsively. This is evident from comparisons between the two figures, where we note that $a_1/\hbar = 1$ leads to a repulsive interaction with elastic trajectories, while $a_1/\hbar = 4$ gives rise to a more attractive interaction which features inelastic trajectories.

The lower row of Fig. 7.1 illustrates the case where the collision dynamics is destructive, with the solitons fracturing into multiple products in a similar manner to a fission event. In both cases, three solitons emerge from the collision (the third soliton in Fig. 7.1(d) with $\delta = \pi$ is located at the leading edge of the other two) with the populations and velocities of each outgoing soliton dependent on the initial phase difference. In addition, a modest amount of radiation is ejected during the collision, as seen in the trailing edge in Fig. 7.1(c), and the interference pattern located between the slowest two solitons in Fig. 7.1(d). The main difference here as compared to the previous case, is a larger difference in the initial velocities, which when coupled with a larger gauge-field strength, produces two soliton envelopes with a greater disparity of widths. As such, in the course of the collision, the solitons effectively interact over a longer period, which enhances the effects stemming from the interaction.

7.2.2 Weak-chiral regime

In the previous subsection, it was demonstrated that the chiral solitons can collide inelastically while retaining the general shape of their envelopes. To quantify the elasticity of the collisions going forward, we introduce the coefficient of restitution [134]

$$\eta = \frac{\sum_{n=1,2} m_n v_n^2|_{t=\infty}}{\sum_{n=1,2} m_n v_n^2|_{t=0}}, \tag{7.2}$$

which quantifies the change in kinetic energy before and after the collision. Here, m_n and v_n play the role of the masses (particle number) and velocities of the solitons in our semi-classical description, and are calculated from the expectation values

$$m_n = N \int dx\ |\psi|^2, \tag{7.3}$$

and

$$v_n = -\frac{i\hbar}{m_n} \int dx\ \psi^* \frac{\partial \psi}{\partial x}. \tag{7.4}$$

The integration in each case at either the initial ($t = 0$) or final time ($t \to \infty$) is performed locally around each soliton's centre of mass to exclude contributions from radiation and the overlap with the other soliton. For $\eta = 1$, the collision is perfectly elastic with the masses and velocities of the solitons conserved, whereas $\eta \neq 1$ indicates an inelastic collision involving an element of energy exchange. As the populations and velocities of the solitons are not conserved in an inelastic collision, one cannot distinguish whether the chiral solitons pass through or rebound off each other. Therefore, to remain consistent, we label the solitons located in regions $x \in (-\infty, 0]$ and $x \in [0, \infty)\ \forall\ t$, as the first and second respectively.

By varying the strength of the gauge-field, we have performed a detailed parameter scan of the soliton-soliton collisions as a function of the initial phase difference. The coefficient of restitution is calculated and plotted in Fig. 7.3 with corresponding examples of the dynamics shown in Fig. 7.2. For each value of the gauge-field strength, three regimes of collision dynamics can be identified depending on the initial phase difference between the solitons. The first is an elastic scattering regime highlighted by a plateau in the restitution data at $\eta = 1$, with an example of the dynamics shown in Fig. 7.2(a). Here, the interaction is notably repulsive, with a distinct node in the density at the interaction centre and the soliton parameters conserved after the collision. Away from this plateau, two distinct regimes of inelastic dynamics are found with $\eta > 1$, as illustrated in Fig. 7.2(b) and Fig. 7.2(d). Here, the dynamics are also similar to the case of strong interactions, with inelastic trajectories that feature a redistribution of the soliton masses, as well as an evolution of the absolute phases which results in shifts of the in- and out-of-phase collision points. Comparing these two plots, one notices that depending on the direction in which one moves away from the plateau in the parameter space, the soliton mass can be transferred chiefly in either the left Fig. 7.2(d) or right-hand Fig. 7.2(b) outgoing soliton. The final inelastic regime, indicated by the 'resonance' peak in the restitution data and the plot in Fig. 7.2(c), features the turning point of this population transfer. Here, a peculiar soliton state is formed, where there is a strong interplay between the excitation of an oscillatory mode in the left- and right-hand

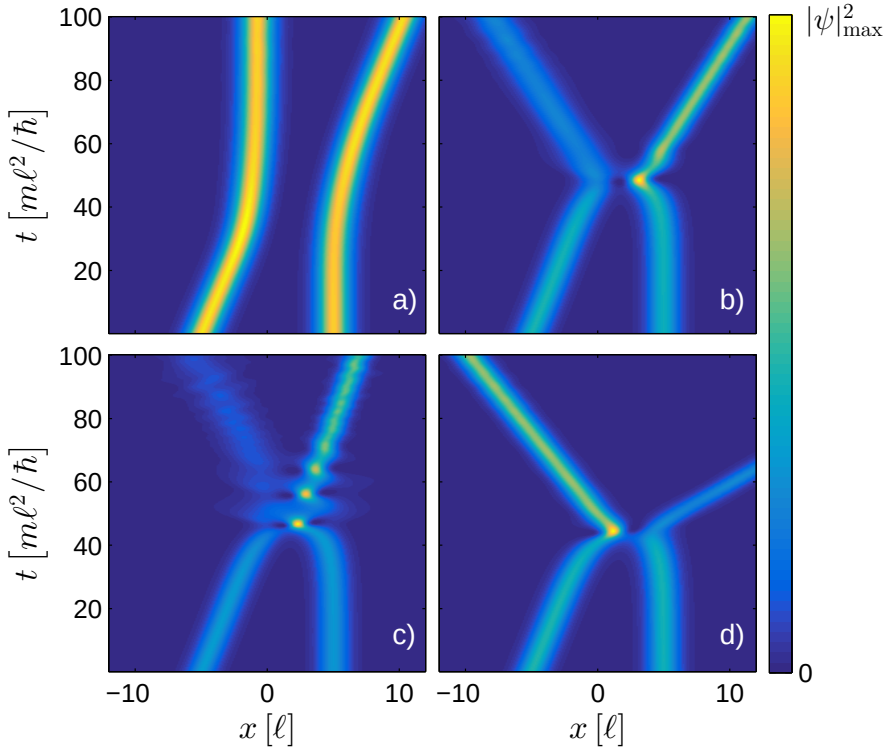

Figure 7.2: Examples of the collision dynamics between two chiral solitons in the weak-chiral regime, for various initial phase differences. The soliton parameters are taken as $g_{1D}m\ell/\hbar^2 = -4$, $v_1 m\ell/\hbar = 0.1$, $v_2 m\ell/\hbar = 0$, and $a_1/\hbar = 1.5$. The initial phase differences varies in each subplot as $\delta = 0$ (a), $\delta = 0.9\pi$ (b), $\delta = 0.98\pi$ (c), and $\delta = -0.9\pi$ (d).

solitons, and emitted radiation. This regime appears to be an example of in-phase or 'fully attractive' dynamics, which features the formation of a metastable (short-lived) bound state. The turning point of the population transfer is pictured in the data in Fig. 7.3, in which one sees there is a sudden change in the masses of the solitons as the transition point is crossed. Notably, this data also shows that outside the vicinity of the resonance peak, the solitons can exchange mass without significant losses to radiation, as the total soliton mass is approximately conserved for the majority of the parameter space.

A feature universal to the restitution data presented in Fig. 7.3 is that the location of each inelastic regime is cyclically shifted left-wards in δ for an increasing current strength. Comparing different gauge potential strengths, one can see that the elastic plateau shrinks for larger values, which can be explained by enhancement of the non-integrability effects. Although not shown here, the dip in the restitution data initially appears close to $\delta = 0$ for small values of the current strength, and cyclically displaces towards lower δ for increasing current strengths.

To complete the analysis for the weak-chiral regime, we perform a similar parameter scan as before, but now for the case when the relative phase difference is fixed to $\delta = 0$, with the initial velocity of the left-hand soliton allowed to vary. In this case,

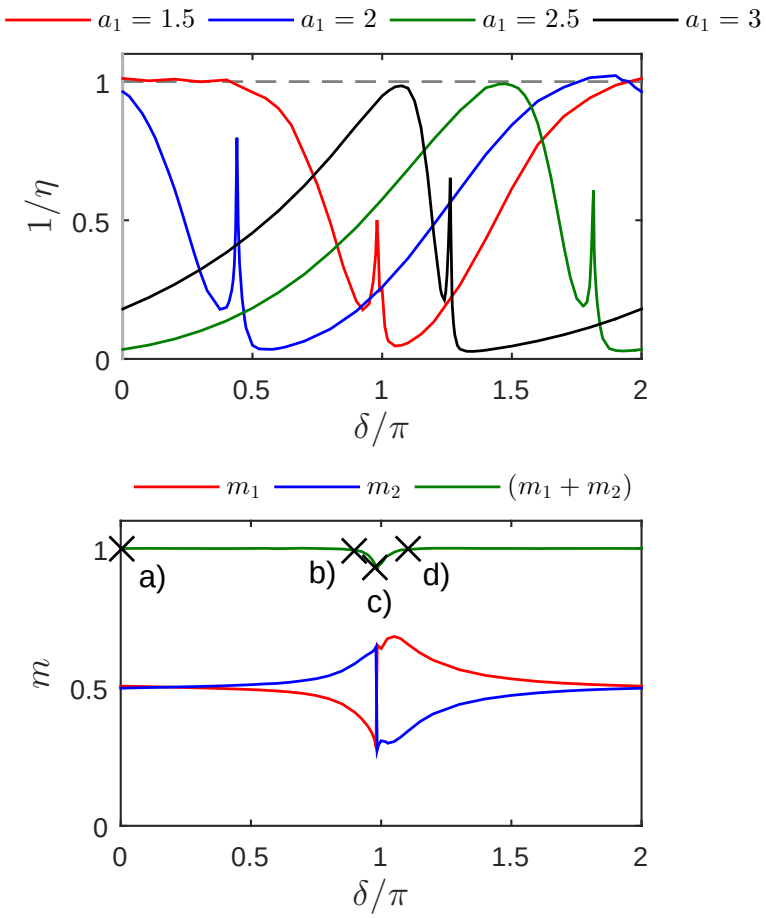

Figure 7.3: (Top) Inverse of the coefficient of restitution calculated from numerical simulations, with $g_{1D}m\ell/\hbar^2 = -4$, $v_1 m\ell/\hbar = 0.1$, and $v_2 m\ell/\hbar = 0$. The grey dashed line indicates the standard Gross-Pitaevskii results with perfectly elastic collisions. (Bottom) Population transfer for the soliton masses m_n with $a_1/\hbar = 1.5$. The black crosses correspond to the simulations labelled in Fig. 7.2.

the coefficient of restitution provides a poor illustration of the underlying dynamics, and we instead plot the outgoing velocity of the soliton travelling to the right for increasing values of the gauge-field strength, as shown in Fig. 7.4.

Depending on the choice of the initial velocity and gauge-field strength, the strength of the chiral interactions $|a_1(v_1 + v_2)|$ may be either small or comparable to the mean-field strength $|g_{1D}|$. Therefore, for extreme values of the parameters, it is expected that the dynamics will be generally inelastic in a similar manner to Fig. 7.1, whereas for smaller values the dynamics will be elastic. This reasoning is reflected in the pair of curves corresponding to $a_1/\hbar = 1$ and $a_1/\hbar = 1.25$ in Fig. 7.4(a), in which the incoming and outgoing velocity of the soliton is approximately equal. As the initial velocity increases, and by extension the interaction strength increases, this invariance begins to break and is particularly notable for $a_1/\hbar = 1.25$, which exhibits a sinusoidal behaviour above a critical value of $v_1 m\ell/\hbar = 0.5$.

As the gauge field strength is increased further, as in the case of $a_1/\hbar = 1.5$,

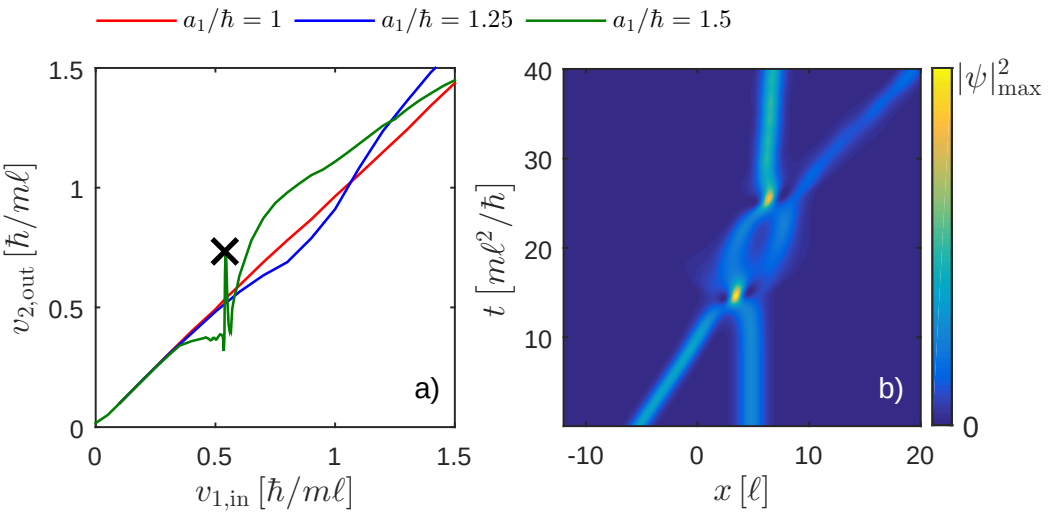

Figure 7.4: (a) Outgoing versus incoming velocities for asymmetric collisions between two chiral solitons for various gauge-field strength, with $g_{1\mathrm{D}}m\ell/\hbar^2 = -4$, $v_2 m\ell/\hbar = 0$, and $\delta = 0$ fixed in each instance. Black cross indicates the two-bounce resonance state shown in (b) for $v_1 m\ell/\hbar = 0.5425$ and $a_1/\hbar = 1.5$.

a 'resonance' feature appears in the restitution data where a two-bound resonance state is formed, as shown in Fig. 7.4(b). As mentioned previously, such states are a common occurrence in non-integrable models [183, 196–204], which arise due to energy exchange between the solitons and their internal modes. Therefore, in order to overcome the mutual potential influence, each soliton is required to collide several times in order to regain the energy temporarily stored in the internal mode. In performing this parameter scan, higher-order bound states, where the solitons collide more than twice, were not observed, as for stronger interaction strengths the appearance of a bound state tends to be suppressed in a similar manner to Fig. 7.2(c).

7.2.3 Bound States

To further investigate the inelastic dynamics of the density-dependent gauge theory, we also consider a set of symmetric collisions to see if two chiral solitons can form a molecule-like bound state [198, 215]. To achieve this, we consider the case where two stationary solitons are initially separated and observe whether the solitons oscillate around each other due to their mutual attraction.

In Fig. 7.5, we find in a similar manner to results obtained in the weakly perturbed cubic-quintic nonlinear Schrödinger [198, 203] and sine-Gordon equations [202], that a weak current nonlinearity is found to support a short-lived bound state, where the solitons collide several times before escaping. As before, the underlying mechanism here, is the presence of energy exchange which leads to a redistribution of the soliton

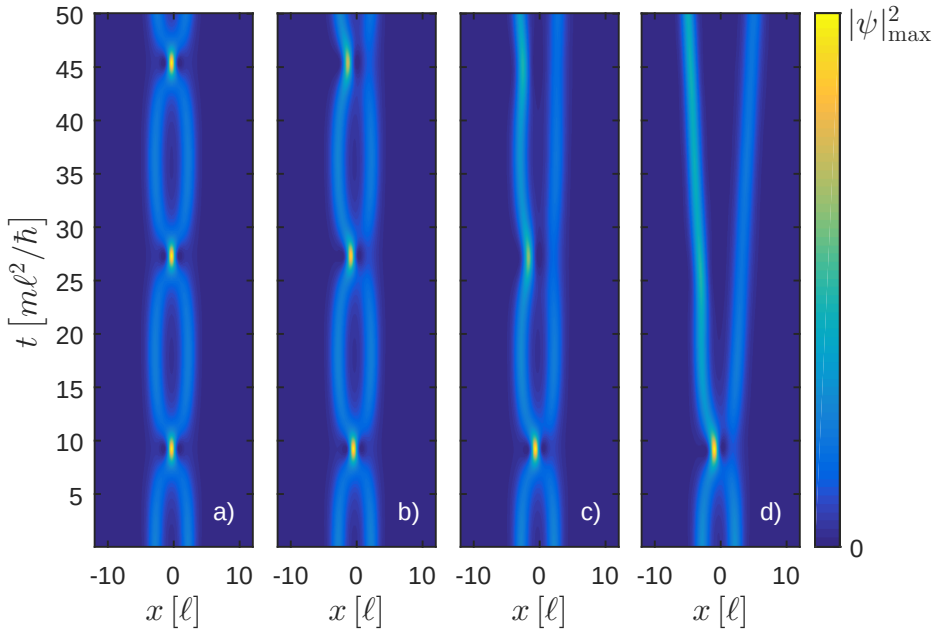

Figure 7.5: Breakdown of the soliton-soliton bound state due to the presence of the current nonlinearity. Two stationary solitons are initially placed at distance $x/\ell = 5$ units apart, with $g_{1D}m\ell/\hbar^2 = -4$ and $\delta = 0$. The gauge-field strength varies as $a_1/\hbar = 0$ (a), $a_1/\hbar = 0.125$ (b), $a_1/\hbar = 0.25$ (c), and $a_1/\hbar = 0.5$ (d).

masses and a shift of the absolute phases. However, as the magnitude of the interaction energy is now comparable to or larger than the kinetic energy, the solitons are required to collide several times in order to gain enough kinetic energy to escape the attractive interaction. Compared to the standard Gross-Pitaevskii dynamics shown in Fig. 7.5(a) with $a_1/\hbar = 0$, where the solitons are perpetually trapped with a fixed oscillation amplitude and frequency, a modest current strength can begin to destabilize the bound state, such as in Fig. 7.5(c) for $a_1/\hbar = 0.25$, where the solitons collide four times before escaping, and in Fig. 7.5(d) for $a_1/\hbar = 0.5$, where they collide only twice.

Interestingly, despite the interaction being initially symmetric, effects stemming from the current nonlinearity result in a left-handedness in the post-collision behaviour. For example, in Fig. 7.5(b) with $a_1/\hbar = 0.125$, the first collision at $(\hbar/m\ell^2)t = 10$ is noticeably attractive due to the presence of the anti-node at the interaction centre, but every subsequent collision becomes increasingly repulsive with the amplitude of the anti-node decreasing and its position shifting towards the left. In addition, a density node fills the vacancy left by the anti-node at each interaction centre, with some manifestation of the population transfer. This effect is seen to be most profound in Fig. 7.5(d) for $a_1/\hbar = 0.5$, where $\sim 60\%$ of the outgoing mass in captured in the left soliton. Returning to the two-bounce resonance state in Fig. 7.4, the existence of higher-order bound states appears unlikely due to the fact that each subsequent interaction becomes increasingly more repulsive. However, this effect can be mitigated provided the current strength is kept small.

These illustrations therefore conclude that the current nonlinearity can lead to the suppression, and ultimately, the breakdown of the soliton-soliton bound state.

7.3 Variational equations

To gain insight into how the current nonlinearity modifies the interactions between the solitons, we set out a pair of variational calculations in order to quantify the collision dynamics. This is achieved using two similar, but essentially different analytical techniques.

In the first instance, we approximate the two-soliton state as a linear superposition of two individual solitons, with the interactions treated as the spatial overlap of the soliton envelopes. This technique directly follows from the single-soliton variational calculation outlined in Sec. 5.4, and has been previously applied to interaction problems in the nonlinear Schrödinger and Gross-Pitaevskii equations [216–219], in addition to several others [220–224]. The advantage of this method, is the ability to derive an effective particle model for the soliton dynamics, in which two key results can be extracted. The first is an effective potential describing the interaction between the solitons, which will provide details into the phase dependence and range of the interactions. Secondly, by numerically solving the variational equations, we will be able to illustrate the dynamics of the particle model and directly compare it to the full numerical solutions presented previously.

For the second method, we follow the technique outlined in Refs. [225, 226], in which the soliton state is also approximated as a linear superposition, but restricted to the case of two stationary solitons which are well separated. In this case, the interaction is accounted for by the spatial overlap of one soliton with the 'weak tail' of the other, and may therefore be regarded as an asymptotic approximation to collision dynamics. From this, we will be able to derive asymptotic interaction potentials, for direct comparison to those obtained from the first method.

Based on the single-soliton ansatz described by Eq. (5.22), we define the corresponding two-soliton variational ansatz as

$$\psi_{\text{int}} \equiv \sum_{n=1,2} a \,\text{sech}\left(\left(x-\xi_j\right)/b\right) e^{i\left(k_n(x-\xi_n)+w(x-\xi_n)^2+\phi_n\right)}, \tag{7.5}$$

where once again, $a(t)$, $b(t)$, $\xi_n(t)$, $k_n(t)$, $w(t)$, and $\phi_n(t)$ are a set of time-dependent variational parameters. This ansatz models two bright solitons, in which the individual velocities and positions are allowed to evolve independently, with the interactions treated as the linear-overlap of the soliton envelopes. The constraint that the solitons have a common width, which in turn fixes both the amplitude and curvature

coordinates, is a necessary restriction in order to be able to explicitly calculate the interaction integrals in following analysis. Consequently, this restricts the variational analysis to the regime in which

$$\frac{b_1}{b_2} = \frac{g_{1\mathrm{D}} - 2a_1\hbar k_2/m}{g_{1\mathrm{D}} - 2a_1\hbar k_1/m} \approx 1, \tag{7.6}$$

which can be achieved by considering collisions with small velocities and by compensating the effects of the gauge field with a modest mean-field scattering strength. The above constraint therefore restricts our variational analysis to the weak-chiral regime, $|g_{1\mathrm{D}}| \gg |a_1\,(v_1 + v_2)\,|$.

Our choice of ansatz arises due to two reasons. First, our model is non-integrable, therefore a closed-formed expression for a two-soliton state via inverse scattering techniques is unavailable. Secondly, regardless of whether such a solution existed, Eq. (7.5) should work as a good approximation for the collision dynamics, as the solitons roughly retain their shape for the majority of parameter space $\delta \in [0, 2\pi]$. However, it must be stressed that this ansatz does not fully replicate all the features of the interaction and will generally fail at short length scales where the solitons begin to significantly overlap.

Substituting the two-soliton ansatz into Eq. (4.19) leads to the Lagrangian densities

$$\begin{aligned}\mathcal{L}_0' = \frac{a^4}{2}\sum_{n=1,2}\left(g_{1\mathrm{D}} - \frac{2a_1\hbar c_n}{m}\right)\operatorname{sech}^4\chi_n + \hbar a^2\sum_{n=1,2} d_n \operatorname{sech}^2\chi_n \\ + \frac{\hbar^2 a^2}{2m}\sum_{n=1,2}\left(c_n^2\operatorname{sech}^2\chi_n + \frac{1}{b^2}\tanh^2\chi_n\operatorname{sech}^2\chi_n\right),\end{aligned} \tag{7.7}$$

and

$$\begin{aligned}
\mathcal{L}'_{\text{int}} = a^4 \left(2g_{1\text{D}} - \frac{a_1\hbar\,(c_1+c_2)}{m}\right)\left[1+\frac{\cos(2\Delta S)}{2}\right]\prod_{n=1,2}\operatorname{sech}^2\chi_n \\
+ a^4\left(2g_{1\text{D}} - \frac{a_1\hbar\,(3c_1+c_2)}{m}\right)\cos(\Delta S)\operatorname{sech}^3\chi_1\operatorname{sech}\chi_2 \\
+ a^4\left(2g_{1\text{D}} - \frac{a_1\hbar\,(c_1+3c_2)}{m}\right)\cos(\Delta S)\operatorname{sech}\chi_1\operatorname{sech}^3\chi_2 \\
+ \hbar a^2\cos(\Delta S)\,(d_1+d_2)\prod_{n=1,2}\operatorname{sech}\chi_n \\
+ \frac{\hbar^2a^2}{mb}\sin(\Delta S)\,(c_1\tanh\chi_1 - c_2\tanh\chi_2)\prod_{n=1,2}\operatorname{sech}\chi_n \\
+ \frac{\hbar^2a^2}{2m}\cos(\Delta S)\left(c_1c_2+\frac{2}{b^2}\prod_{n=1,2}\tanh\chi_n\right)\prod_{n=1,2}\operatorname{sech}\chi_n,
\end{aligned} \tag{7.8}$$

which are identified by splitting the total Lagrangian density $\mathcal{L}' = \mathcal{L}'_0 + \mathcal{L}'_{\text{int}}$, into the sum of the free and interacting contributions to the action. In addition we have introduced the variables

$$c_n = k_n + 2bw\chi_n, \tag{7.9}$$

and

$$d_n = \dot{\phi}_n + \dot{w}b^2\chi_n^2 - k_n\dot{\xi}_n + b\dot{v}_n\chi_n - 2wb\dot{\xi}_n\chi_n, \tag{7.10}$$

for notational convenience. At this stage, one can see that the free Lagrangian for the interaction problem is simply the superposition of two copies of the single Lagrangian in Eq. (5.24), as expected.

To integrate the Lagrangian density, we redefine the arguments of the hyperbolic functions using the change of variables $\chi_1 = \tilde{\chi}$ and $\chi_2 = \tilde{\chi}+\epsilon$, where $\epsilon = (\xi_1 - \xi_2)/b$ is a new variational parameter corresponding to the relative positions of the solitons. Additionally, we assume that the magnitude of the velocity and curvature coordinates is small, such that the phase difference $\Delta S \approx \phi_1 - \phi_2 = \delta$ is an approximate function of solely the absolute phases. Although this approximation is not necessary in order to evaluate the interaction integrals [217], the resulting expressions are often too cumbersome for extracting meaningful results from. The corresponding

averaged Lagrangians are then given by

$$L_0 = \frac{4a^4 b}{3} g'_{1\mathrm{D}} + \frac{\hbar^2 a^2 b}{m}\left(\frac{2}{3b^2} + k_1^2 + k_2^2 + \frac{w^2 b^2 \pi^2}{3}\right) + 2\hbar a^2 b \sum_{n=1,2}\left(\dot{\phi}_n - k_n \dot{\xi}_n\right) \quad (7.11)$$

and

$$\begin{aligned} L_{\mathrm{int}} = {} & 8a^4 b g'_{1\mathrm{D}} \left(\left(1 + \frac{\cos(2\delta)}{2}\right)\left[\frac{\epsilon\cosh\epsilon}{\sinh^3\epsilon} - \frac{1}{\sinh^2\epsilon}\right] + \cos\delta\left[\frac{\cosh\epsilon}{\sinh^2\epsilon} - \frac{\epsilon}{\sinh^3\epsilon}\right]\right) \\ & + \hbar a^2 b\cos\delta\left(\frac{2bw\hbar}{m}\left(k_1 - k_2\right) - b\left(\dot{k}_1 - \dot{k}_2\right) + 2wb\left(\dot{\xi}_1 - \dot{\xi}_2\right)\right)\left[\frac{\epsilon^2}{\sinh\epsilon}\right] \\ & + 2\hbar a^2 b\cos\delta\left(\frac{\hbar k_1 k_2}{m} + \sum_{n=1,2}\left(\dot{\phi}_n - k_n\dot{\xi}_n\right)\right)\left[\frac{\epsilon}{\sinh\epsilon}\right] \\ & + \frac{4\hbar^2 a^2 b^3 w^2}{m}\cos\delta\left[\frac{\pi^2\epsilon}{6\sinh\epsilon} - \frac{\epsilon^3}{3\sinh\epsilon}\right] + 2\hbar a^2 b^3 \dot{w}\cos\delta\left[\frac{\pi^2\epsilon}{6\sinh\epsilon} + \frac{2\epsilon^3}{3\sinh\epsilon}\right] \\ & + \frac{4\hbar^2 a^2}{mb}\cos\delta\left[\frac{\cosh\epsilon}{\sinh^2\epsilon} + \frac{\epsilon}{2\sinh\epsilon} - \frac{\epsilon\cosh^2\epsilon}{\sinh^3\epsilon}\right] \\ & + \frac{2\hbar^2 a^2}{m}\left(k_1 + k_2\right)\sin\delta\left[\frac{\epsilon\cosh\epsilon}{\sinh^2\epsilon} - \frac{1}{\sinh\epsilon}\right], \end{aligned} \quad (7.12)$$

with $g'_{1\mathrm{D}} = g_{1\mathrm{D}} - a_1\hbar\left(k_1 + k_2\right)/m$. Additional details on how to perform the integration are provided in Appendix B, with each integral tabulated. At this stage, it is clear that the complexity of the above Lagrangian will be difficult to handle from an analytic perspective. Therefore, in order to proceed forward in a reasonable fashion, we have to simplify the model by setting the curvature coordinate as $w(t) = 0$.

Equations of motion for each variational parameter can now be derived from variations of the Lagrangian, and read as

$$\phi_n : \qquad \frac{\partial}{\partial t}\left(2\hbar a^2 b f\left(\epsilon, \delta\right)\right) = 0 \quad (7.13)$$

$$k_1 : \qquad k_1 = \frac{m}{\hbar}\dot{\xi}_1 l_1\left(\epsilon, \delta\right) + \frac{2a^2 a_1}{3\hbar} + d\left(\epsilon, \delta\right) - k_2\cos\delta\frac{\epsilon}{\sinh\epsilon} \quad (7.14)$$

$$k_2: \qquad k_2 = \frac{m}{\hbar}\dot{\xi}_2 l_2(\epsilon,\delta) + \frac{2a^2a_1}{3\hbar} + d(\epsilon,\delta) - k_1\cos\delta\frac{\epsilon}{\sinh\epsilon} \tag{7.15}$$

$$a: \qquad \frac{\partial\bar{L}}{\partial a} + 4\hbar ab\sum_{n=1,2}\left(\dot{\phi}_i - k_n\dot{\xi}_n\right) f(\epsilon,\delta) = 2\hbar ab^2\left(\dot{k}_1 - \dot{k}_2\right)\cos\delta\frac{\epsilon^2}{\sinh\epsilon} \tag{7.16}$$

$$\xi_1: \qquad \frac{\partial\bar{L}}{\partial\xi_1} + 2\hbar a^2 b\sum_{n=1,2}\left(\dot{\phi}_n - k_n\dot{\xi}_n\right)\frac{\partial}{\partial\xi_1}f(\epsilon,\delta) = -\frac{\hbar}{2}\dot{k_1}$$
$$+\hbar a^2b^2\cos\delta\left(\dot{k}_1 - \dot{k}_2\right)\frac{\partial}{\partial\xi_1}\frac{\epsilon^2}{\sinh\epsilon} \tag{7.17}$$

$$\xi_2: \qquad \frac{\partial\bar{L}}{\partial\xi_2} + 2\hbar a^2 b\sum_{n=1,2}\left(\dot{\phi}_n - k_n\dot{\xi}_n\right)\frac{\partial}{\partial\xi_2}f(\epsilon,\delta) = -\frac{\hbar}{2}\dot{k_2}$$
$$+\hbar a^2b^2\cos\delta\left(\dot{k}_1 - \dot{k}_2\right)\frac{\partial}{\partial\xi_2}\frac{\epsilon^2}{\sinh\epsilon} \tag{7.18}$$

where the functions

$$f(\epsilon,\delta) = 1 + \frac{\epsilon}{\sinh\epsilon}\cos\delta, \tag{7.19}$$

$$d(\epsilon,\delta) = \frac{4a^2a_1}{\hbar}\left(\left(1+\frac{\cos(2\delta)}{2}\right)\left[\frac{\epsilon\cosh\epsilon}{\sinh^3\epsilon} - \frac{1}{\sinh^2\epsilon}\right] + \cos\delta\left[\frac{\cosh\epsilon}{\sinh^2\epsilon} - \frac{\epsilon}{\sinh^3\epsilon}\right]\right)$$
$$-\frac{\sin(\delta)}{b}\left[\frac{\epsilon\cosh\epsilon}{\sinh^2\epsilon} - \frac{1}{\sinh\epsilon}\right] \tag{7.20}$$

and

$$l_{n=1(+),2(-)}(\epsilon,\delta) = 1 + \cos\delta\frac{\epsilon}{\sinh\epsilon} \mp \frac{1}{2a^2b}\frac{\partial}{\partial\xi_n}\left(a^2b^2\cos\delta\frac{\epsilon^2}{\sinh\epsilon}\right), \tag{7.21}$$

are also introduced for notational convenience. Additionally, the overbar Lagrangian

appearing in Eqs. (7.16) to (7.18) is given by

$$\bar{L} = 8a^4 b g'_{1\mathrm{D}} \left(\left(1 + \frac{\cos(2\delta)}{2} \right) \left[\frac{\epsilon \cosh\epsilon}{\sinh^3\epsilon} - \frac{1}{\sinh^2\epsilon} \right] + \cos\delta \left[\frac{\cosh\epsilon}{\sinh^2\epsilon} - \frac{\epsilon}{\sinh^3\epsilon} \right] \right)$$

$$+ \frac{2\hbar^2 a^2 b k_1 k_2}{m} \cos\delta \left[\frac{\epsilon}{\sinh\epsilon} \right] + \frac{4\hbar^2 a^2}{mb} \cos\delta \left[\frac{\cosh\epsilon}{\sinh^2\epsilon} + \frac{\epsilon}{2\sinh\epsilon} - \frac{\epsilon\cosh^2\epsilon}{\sinh^3\epsilon} \right]$$

$$+ \frac{2\hbar^2 a^2}{m} (k_1 + k_2) \sin\delta \left[\frac{\epsilon\cosh\epsilon}{\sinh^2\epsilon} - \frac{1}{\sinh\epsilon} \right], \tag{7.22}$$

and will be an important quantity in the calculations to follow. From these equations, we can now extract details of how the gauge field modifies the collision dynamics of the solitons.

Starting with the first variational equation, which can be obtained by varying either ϕ_1 or ϕ_2, one identifies Eq. (7.13) as the conservation law for the particle number of each individual soliton, in analogy with Eq. (5.13). One can then integrate the two-soliton ansatz as

$$\int_{-\infty}^{\infty} dx \, |\psi_{\mathrm{int}}|^2 = 4a^2 b f(\epsilon, \delta) = 1, \tag{7.23}$$

for $N = 1$, to obtain $a^2 = 1/(4bf(\epsilon, \delta))$. In the asymptotic limit where $\epsilon \to \infty$, this quantity reduces to $a^2 \sim 1/(4b)$, which is the correct amplitude for the two-soliton state. An important limitation of the particle model is highlighted by Eq. (7.23), as one finds that the two-soliton amplitude rapidly diverges in the $\lim_{\epsilon\to 0}$ for $\pi/2 < \delta < \pi$ and approaches a singularity at $\delta = \pi$. This effect is clearly not representative of the collision dynamics seen numerically, thereby requiring us to restrict our studies to the interval $\delta \in [0, \pi/2]$, for which the amplitude is non-divergent. For these values, the behaviour of the amplitude is more representative, such as for $\delta = 0$, which details that the soliton amplitude is increased by $1/\sqrt{2b}$ when they constructively interfere.

The equations for the velocities k_n highlight the main result of the variational analysis; that the velocities of the solitons are modified in the presence of the gauge field. The first and last terms of Eqs. (7.14) and (7.15), are the standard terms from the Gross-Pitaevskii equation, with the second and third terms appearing from the current nonlinearity. Together, they reduce in the asymptotic limit as $k_n \sim m\dot{\xi}_n/\hbar + a_1/(6\hbar b)$, highlighting that the individual solitons travel at a constant velocity when they are well separated. As we will demonstrate in the next subsection, these new terms arising from the current will be responsible for the interaction-

induced velocity shifts.

The equations for both $a(t)$ and ξ_n are not particularly transparent, but do highlight the coupling between all of the variational parameters. A variational equation for the soliton width b, is not required to proceed as the curvature coordinate has been excluded.

7.3.1 Numerics

In order to illustrate how the gauge field is the mechanism underlying the inelastic scattering in our system, we set out to first simplify and reduce the number of variational equations, in order to derive an effective particle model describing the collision dynamics. For this purpose, we begin by setting Eqs. (7.16) to (7.18) as a pair of simultaneous equations in order to eliminate the parameters $\dot{\phi}_n$ and $\dot{\xi}_n$. The pair of reduced equations then read as

$$a\frac{\partial \bar{L}}{\partial a}\frac{\partial f}{\partial \xi_1} - 2f\frac{\partial \bar{L}}{\partial \xi_1} = \hbar f\dot{k_1} - 2\hbar a^2 b^2 \cos\delta\left(\dot{k}_1 - \dot{k}_2\right)\left(\frac{\epsilon^2}{\sinh\epsilon}\frac{\partial f}{\partial \xi_1} - f\frac{\partial}{\partial \xi_1}\frac{\epsilon^2}{\sinh\epsilon}\right) \quad (7.24)$$

and

$$a\frac{\partial \bar{L}}{\partial a}\frac{\partial f}{\partial \xi_2} - 2f\frac{\partial \bar{L}}{\partial \xi_2} = \hbar f\dot{k_2} - 2\hbar a^2 b^2 \cos\delta\left(\dot{k}_1 - \dot{k}_2\right)\left(\frac{\epsilon^2}{\sinh\epsilon}\frac{\partial f}{\partial \xi_2} - f\frac{\partial}{\partial \xi_2}\frac{\epsilon^2}{\sinh\epsilon}\right) \quad (7.25)$$

with respect to the centre of masses of each soliton. Then, by using the chain rule to redefine the first term on the left-hand side of both equations, and similarly with the quotient rule for the last term of the right-hand side, then leads to the set of equations

$$\hbar\dot{k}_1 r(\epsilon,\delta) + \hbar\dot{k}_2\left(r(\epsilon,\delta) - 1\right) = -4\frac{\partial \bar{L}}{\partial \xi_1} \quad (7.26)$$

and

$$\hbar\dot{k}_1\left(r(\epsilon,\delta) - 1\right) + \hbar\dot{k}_2 r(\epsilon,\delta) = -4\frac{\partial \bar{L}}{\partial \xi_2}, \quad (7.27)$$

with the parameter

$$r(\epsilon,\delta) = 1 - \frac{b}{2}\frac{\partial}{\partial \xi_1}\frac{\epsilon\left(f(\epsilon,\delta) - 1\right)}{f(\epsilon,\delta)}. \quad (7.28)$$

Together with the velocity equations, the above set of coupled differential equations describe an effective particle model for the soliton dynamics, in which the details of the interaction are encoded in the expressions $r(\epsilon,\delta)$ and $\bar{L}(\epsilon,\delta)$. Once again, in

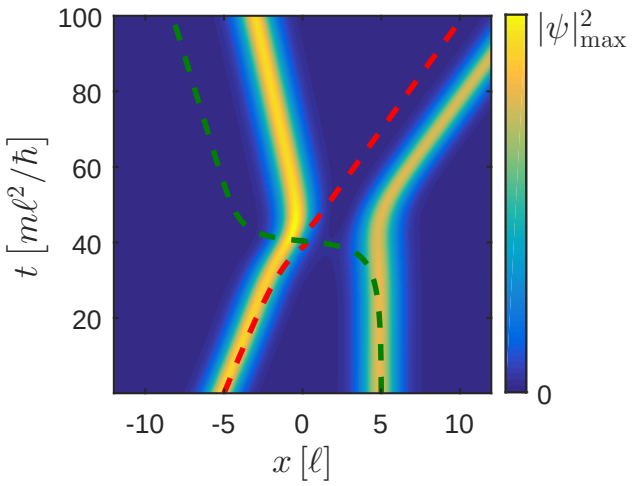

Figure 7.6: Comparison between the solutions of the variational equations (dashed-green/red) and full numerics (color) for the evolution of the solitons' centres of mass. The soliton parameters are taken as $g_{1D}m\ell/\hbar^2 = -4$, $v_1 m\ell/\hbar = 0.1$, $v_2 m\ell/\hbar = 0$, $a_1/\hbar = 3$, and $\delta = 0.4\pi$.

the asymptotic limit, both equations simplify to the single-soliton result $\dot{k}_i(t) \sim 0$, which details that the solitons travel at a constant velocity when they are well separated. A consequence stemming from the elimination of the parameters $\dot{\phi}_1(t)$ and $\dot{\phi}_2(t)$ in these equations, highlights that the phase in this particle model is *static*, and does not dynamically evolve over the course of the interaction. As this is a critical feature in our model, which is responsible for many of the phenomena present in the scattering dynamics, it is clear that our analysis is going to limited in applicability. However, we will still be able to obtain qualitative results which do not strongly depend on the phase δ, but will unfortunately not be able to address issues pertaining to the bound-states dynamics pictured in Fig. 7.5.

To proceed, we solve the set of differential equations numerically using a fourth-order Runge-Kutta method and compare our results to an example of the full numerics in Fig. 7.6. For the chosen set of parameters, the magnitude of the outgoing velocities are in good agreement, with the post-collision trajectories showing that the solitons pass through each other. However, the position shifts of the solitons are not captured well, with the left-outgoing soliton shifted too much, and the right-outgoing soliton shifted too little. This particular example represents the configuration that has the best agreement for the velocities. Although not shown here, for $\delta < 0.3\pi$ the particle model predicts that the solitons form a perpetual bound state with a centre of mass coordinate that increases linearly with time. Otherwise, for $\delta > \pi/2$, the dynamics feature a hard-core elastic interaction where the solitons collide, but rebound off each other. Although the dynamics in these two regimes are similar to what we have obtained numerically, in that we can identify regimes where the interaction is repulsive (and therefore elastic) and attractive (supporting bound states),

this correlation actually arises from *discrepancies* in our model. This is chiefly understood from the fact that the linear ansatz, described by Eq. (7.5), neglects the nonlinear deformation which takes place when the solitons overlap. This leads, in particular, to the absence of the dynamical phase $\delta(t)$, as well as the regularisation of the soliton amplitude when $\epsilon \to 0$.

From this, it is sensible to conclude that the variational analysis presented here is more suited to studying dynamics at the onset of the collision, but not for its entirety. These ideas will become clear in the study of interaction potentials in the following section.

7.4 Interaction potentials

So far in our analysis, we have detailed, albeit in a limited fashion, how the gauge-field modifies the interactions between the solitons in the context of the particle model. In order to gain a more qualitative understanding of this, we can also derive a set of interaction potentials which can illustrate both the range and phase dependence of the collisions. As mentioned previously, we will achieve this using two separate variational methods, as follows.

7.4.1 Linear potential

In the first case, we return to the particle model described by Eqs. (7.26) and (7.27). To derive an effective interaction potential, with reference to the dynamics pictured in Fig. 7.2, we begin by restricting our analysis at the onset of the collision, before the solitons begin to significantly overlap. In this regime, the second soliton remains approximately stationary such that the coordinates $\xi_2(t) \approx 0$ and $k_2(t) \approx 0$ can both be approximately set to zero. The set of coupled differential equations then simplify greatly, and we may readily integrate Eq. (7.26) to obtain

$$\hbar k_1 \dot{\xi}_1 = -4\bar{L} + C \tag{7.29}$$

where C is an arbitrary integration constant and $\bar{L}$ is defined in Eq. (7.22). Substituting Eq. (7.14) into the above expression, and then substituting the equation again to remove an additional factor of $\dot{\xi}_1(t)$, leads to the mechanical energy equation,

$$\frac{m}{2}\dot{\xi}_1^{\,2} + \frac{a_1}{6bf^2r}\dot{\xi}_1 + V_{\text{int}} = \frac{C}{2fr^2} \tag{7.30}$$

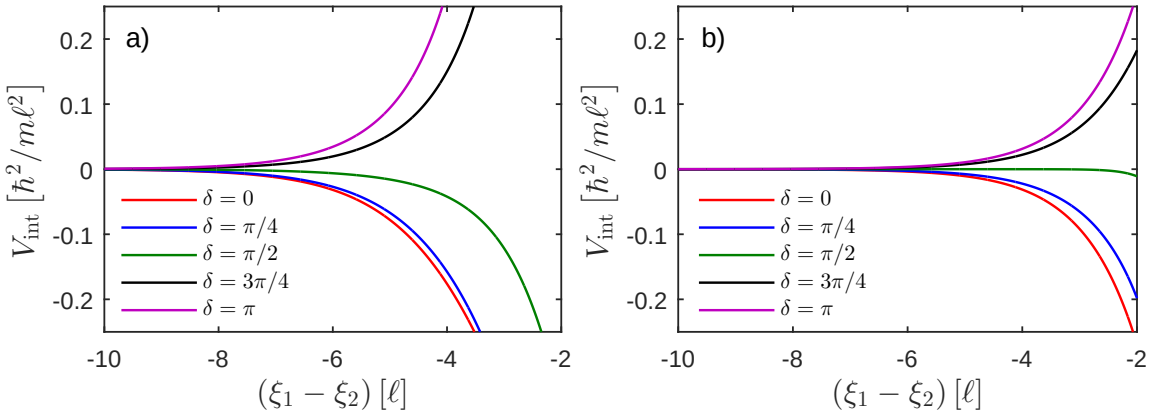

Figure 7.7: Set of interaction potentials from linear (a) and asymptotic (b) calculations, for various phase differences. In both cases, the soliton parameters are set as $g_{1D}m\ell/\hbar^2 = -4$, $v_1 m\ell/\hbar = 0.1$, and $a_1/\hbar^2 = 3$.

where we identify the soliton kinetic energy $m\dot{\xi}_1^2/2$, total energy $C/(2fr^2)$, and the effective interaction potential,

$$V_{\rm int} = -\frac{\hbar^2}{2mf^2r^2}\left[d\left(d + \frac{a_1}{6bfr} - k_1\right) - \frac{4mf}{\hbar^2}\bar{L}\right]. \tag{7.31}$$

The structure of the semi-classical equations described above, treats the motion of the first soliton as a classical particle moving through the potential landscape of the second.

In Fig. 7.7, we plot the interaction curves defined by Eq. (7.31) for the simulation parameters used in Fig. 7.2. Here, the potentials are plotted only for negative values of the separation, as the moving soliton approaches the stationary soliton from negative-x towards positive-x.

Surprisingly, these interaction curves do not differ drastically from the results known from the standard Gross-Pitaevskii equation, with an attractive potential for $\delta < \pi/2$ and a repulsive potential for $\delta > \pi/2$. The similarity of these potentials to that of the standard case, can be understood from studying the current-dependent terms in Eq. (7.31), as one finds that these contributions are generally shorter-ranged than the conventional Gross-Pitaevskii ones, and therefore they do not modify the collision dynamics significantly until the solitons are close to each other. The presence of an attractive potential in particular, therefore supports the existence of bound states in the context of the 'resonance' regime of the restitution data, and likewise for the repulsive potential detailing the elastic collisions in the model.

The limitations of the particle model detailed earlier are clearly visible in these interaction curves. In particular, as the attractive potentials do not turn repulsive close to $\epsilon = 0$ [215], the particle model therefore predicts that two in-phase solitons will be perpetually trapped in a bound state. Whereas as the hard-core elastic

interactions is hinted from the divergence of the soliton amplitude in the curves for $\delta = 3\pi/4$ and $\delta = \pi$, as the magnitude of the potentials increase rapidly for $\epsilon \to 0$, compared to the attractive curves.

7.4.2 Asymptotic potential

In addition to the linear interaction potentials, it is also useful to also consider the collision dynamics in the asymptotic regime, where the solitons are well separated. This can be achieved, as mentioned previously, using the techniques outlined in Refs. [225, 226], which treats the interaction of the solitons as the overlap of one soliton's envelope with the weak tail of the other.

To derive an effective interaction potential in the asymptotic regime, we again restrict our analysis to the weak-chiral regime, in which the second soliton can be taken as stationary with respect to the first. In addition, since $|g_{1\mathrm{D}}| \gg |a_1 (v_1 + v_2)|$, we note that the dominant contributions to the interaction potential will consist of terms not containing a factor of the velocities. Therefore we can further impose that the first soliton is also stationary, such that $k_1 = k_2 = 0$. The two-soliton state in the vicinity of the first soliton, can then be approximated as

$$\varphi \sim \varphi_1(\tilde{\chi}) + \varphi_2(\tilde{\chi} + \epsilon), \tag{7.32}$$

in which φ_1 represents the envelope of the first soliton and φ_2 is the exponential tail of the second, provided $\epsilon \gg b$. The reciprocal approximation is valid in the region around the second soliton. Inserting Eq. (7.32) into the transformed Lagrangian density and linearising to first order in $\varphi_2(\chi + \epsilon)$, leads to the interaction density

$$\begin{aligned}\mathcal{L}_{\mathrm{int}} \sim \frac{\hbar^2}{2m}\left(\frac{\partial\varphi_1}{\partial x}\frac{\partial\varphi_2^*}{\partial x} + c.c\right) + g_{1\mathrm{D}}|\varphi_1|^2\varphi_1\varphi_2 \\ - \frac{a_1\hbar}{2mi}\left(|\varphi_1|^2\varphi_1^*\frac{\partial\varphi_2}{\partial x} + \varphi_1^{*2}\varphi_2^*\frac{\partial\varphi_1}{\partial x} + 2|\varphi_1|^2\varphi_2^*\frac{\partial\varphi_1}{\partial x} + c.c\right),\end{aligned} \tag{7.33}$$

where we have identified terms containing at least one φ_1 and φ_2, and neglected those which otherwise do not. The non-interacting Lagrangian density will not be required to proceed.

Conveniently, one can also obtain Eq. (7.33) from variations of the Lagrangian density

$$\mathcal{L}_{\mathrm{int}} \sim \left[\varphi_2\frac{\partial\mathcal{L}}{\partial\varphi} + \frac{d\varphi_2}{dx}\frac{\partial\mathcal{L}}{\partial\varphi_x} + c.c\right]\Bigg|_{\varphi=\varphi_1}, \tag{7.34}$$

in which each derivative is evaluated at the point $\varphi = \varphi_1$. Then, as we only consider the case of stationary solutions for which $\delta\mathcal{L}/\delta\varphi = 0$, we may recast Eq. (7.34) using Eq. (4.9) and integration by parts, to obtain the simplified expression

$$L_{\rm int} \sim \left[\varphi_2 \frac{\partial \mathcal{L}}{\partial \varphi_x} + c.c\right]_{z_0}^{\infty}\Bigg|_{\varphi=\varphi_1} + \{1 \rightleftharpoons 2\}, \tag{7.35}$$

which, after substitution reads as

$$L_{\rm int} \sim \left[\left(\frac{\hbar^2}{2m}\frac{\partial \varphi_1^*}{\partial x} - \frac{a_1\hbar}{2mi}\varphi_1^*|\varphi_1|^2\right)\varphi_2 + \text{c.c.}\right]_{z_0}^{\infty} + \{1 \rightleftharpoons 2\}. \tag{7.36}$$

In writing Eq. (7.36), we have divided the integration domain at an arbitrary point z_0 located between the solitons and introduced the symmetric term $\{1 \rightleftharpoons 2\}$ to account for the contribution from the second soliton. Surprisingly, this expression highlights that in the asymptotic limit, the only contributions to the interaction potential arise from terms in the Lagrangian density which feature a spatial-derivative of $\varphi(x)$, with the mean-field interactions absent in the variational equation.

To proceed, we write the single-soliton states as

$$\varphi_n = \frac{1}{2\sqrt{b}} e^{i\phi_n} \times \begin{cases} \operatorname{sech}\tilde{\chi} & n = 1 \\ \operatorname{sech}(\tilde{\chi} + \epsilon) & n = 2 \end{cases} \tag{7.37}$$

where the two-soliton width $b = -4\hbar^2/m\tilde{g}_{1\rm D}$ is defined such that $\int_{-\infty}^{+\infty} dx|\varphi_n|^2 = 1/2$, with each soliton containing half the number of atoms. Furthermore, as we are interested in the weak interaction of the soliton tails, we can also simplify these expressions in the vicinity of z_0, with the asymptotic forms

$$\varphi_n \sim \frac{1}{\sqrt{b}} e^{i\phi_n} \times \begin{cases} e^{-\tilde{\chi}} & n = 1 \\ e^{\tilde{\chi}+\epsilon} & n = 2 \end{cases} \tag{7.38}$$

in keeping with the linearisation procedure used previously. Then, to evaluate the surface term defined in Eq. (7.36), we use the full expressions in Eq. (7.37) to evaluate the upper limit at $x = \infty$, together with the asymptotic forms in Eq. (7.38) to evaluate the lower limit at z_0. However, in order to obtain a contribution from the current to the effective potential, which is independent of the choice of arbitrary point z_0, we must go to the next order in the expression for φ_2 in the second term in Eq. (7.36), taking $\varphi_2 \sim e^{3(\tilde{\chi}+\epsilon)}e^{i\phi_2}/\sqrt{b}$. Substituting these expressions, we then obtain the asymptotic interaction potential

$$V_{\rm int} \sim -\frac{2\hbar^2}{mb^2}\left[e^{\epsilon}\cos\delta + \frac{a_1}{\hbar}e^{3\epsilon}\sin\delta\right], \tag{7.39}$$

which can be studied more directly. Appearing, are two contributions to the interaction potential. The first of these is the standard term describing the collision dynamics in the Gross-Pitaevskii equation, which is attractive or repulsive for the correct choice of the phase difference. Whereas the second is a new contribution which arises due to the presence of the gauge field, but critically, has a shorter interaction range compared to the former. This infers, that in the asymptotic limit, the gauge field does not contribute significantly to the collision dynamics far from the centre of interaction. These properties are illustrated in the Fig. 7.7, in comparison to those derived from the linear calculation. Here, one finds that both sets of potentials share the same qualitative features, with both attractive and repulsive interactions supported. Note, that the asymptotic and linear curves differ up to a universal scaling constant, which critically does not change the qualitative features of the potentials.

7.5 Summary and outlook

In this chapter, we have demonstrated how the non-integrability of the interacting gauge theory can lead to unconventional collision dynamics for bright matter-wave solitons; from inelastic collisions in the presence of population transfer and radiation losses, to short-lived bound states and soliton fission. Using variational techniques, we derived an effective particle model for the collision dynamics, which provided insight into both the inelastic scattering and phase dependence of the interactions. In particular, the presentation of interaction potentials, both in the linear and asymptotic approximations, was a key aid in the identification of attractive and repulsive collision dynamics, and qualitatively agreed with the results obtained from numerical simulations. Importantly, the success of the particle model, although limited, underlines that a variational description of the non-integrable dynamics is suitable provided the current nonlinearity is weak. Whereas as in the case of strong interactions, the particle model inevitably breaks down, due to the inability to describe the radiation emission and fracturing of the solitons.

These results therefore reinforce earlier comments, that understanding the role of non-integrability is crucial for the study of a dynamical model. In our case, it is evident that these non-integrable dynamics can be detrimental to the coherence of a chiral soliton. However, provided one is restricted to the weak-chiral regime in an experimental context, these effects will not have significant implications. As such, these dynamics support the studies in the previous chapter on the stability properties of the chiral solitons and their possible implementation in atomtronic systems [51, 195], where careful consideration of the collision dynamics is needed.

As a final note, we end with an open question on the 'resonance' regime of the restitution data pictured in Fig. 7.3. In other non-integrable models, it has been demonstrated that similar regimes are responsible for chaotic scattering, where the solitons collide several times. As this was briefly demonstrated in Fig. 7.4 for a two-bounce bound state, it is intriguing as to whether higher-order bound states exist, and whether the number of collisions depends fractally on the initial conditions. In this regard, the interacting gauge theory could represent a condensate model with both non-integrable and chaotic dynamics, offering a new platform to study nonlinear physics and mathematics.

Chapter 8

Conclusion

In this thesis, we have studied the nonlinear dynamics of one-dimensional chiral matter-wave solitons described by a density-dependent gauge theory. We began, by describing the origin of the physical model, in which a density-dependent gauge potential was engineered in an ultracold bosonic gas using light-matter interactions. We showed how the breakdown of both Galilean invariance and chiral symmetry in the resulting model, led to the emergence of chiral soliton solutions. By calculating the conservation laws and variational equations, we were able to quantify the particle nature of the solitons, and somewhat satisfyingly, show the classical correspondence of the gauge theory. The majority of the thesis was then devoted to the study of the stability and interactions of the bright solitons. In the first instance, we found the novel property that the chiral soliton was linearly stable in an almost exact manner to integrable systems, despite the interacting gauge theory being generally non-integrable. Whereas in the case of the collision dynamics, the system can be quite unmanageable, with the appearance of inelastic trajectories and population transfer, as well as metastable bound states and soliton fission. These studies concluded, that the role of non-integrability in a nonlinear model needs to be treated with care, not only for the purpose of theoretical studies, but also for a practical implementation in an experiment.

In the concluding sections of each chapter, we have already detailed several extensions to the work presented, from proposing the existence of grey and higher-dimensional solitons, to the stability of bright solitons in a perturbative model, and the prospect of fractal collision dynamics. The scope of possibilities is however much broader than this and covers topics relevant to both an experimental and theoretical viewpoint. For example, we have already hinted in Sec. 5.4 that the dynamics of a trapped chiral soliton is expected to be non-coherent, due to the presence of a perturbation-induced driving term in the variational equations. This has implications not only for the motion of the chiral soliton in the harmonic trap, but also for their elementary excitations [103, 173]. In a related note, it is also expected that the breakdown of Galilean invariance could be a major factor for the excitation spec-

trum of the condensate and possibly lead to the emergence of soliton trains as the interactions turn attractive under motion [72, 175, 176]. Additionally, we have for the most part, only focused on the dynamics of bright solitons and largely ignored the dark soliton case. Here, the interplay of chirality is expected to lead to density fluctuations in the background and the emission of sound [227].

A recurring topic in this thesis, has been ensuring that the chiral soliton retains its coherence in the presence of perturbations and collisions, in order for their possible applications in quantum dynamics such as interferometry and atomtronic based systems [49–51, 195, 213, 214]. The key idea in these systems, in a similar manner to the topic of quantum computing, is the engineering of purpose built systems to tackle problems where ultracold gases can provide a significant advantage over traditional methods. Typically, the idea here is to exploit the coherence and vast tunability of quantum gases for high precision interferometry [228], but also for quantum technologies which extend the scope of quantum simulation [195]. To achieve this, components analogue to those available in optics and electronics must be realised in order to construct a suitable basis, such as an atomic laser and beam splitters for an interferometer [136, 229]. In this regard, it is interesting as to whether the chiral dynamics of our solitons can be used for novel transport dynamics in these systems. In particular, since the chemical potential of a chiral soliton is defined in part by its velocity, it is speculative as to whether this chirality could be used to build a matter-wave diode; one of the fundamental components for atomtronic-based circuitry. Similar proposals have already appeared in discrete systems [51, 230], with the first steps in the experimental setting demonstrated recently [231].

Appendix A

The hypergeometric differential equation

In this appendix, we provide a brief overview of the hypergeometric differential equation and its solutions around each singular point. These details can be found in the majority of mathematical textbooks [232], particularly ones which centre on the topic of special functions [141]. As such, we present the following derivations solely for the sake of revision, in preparation for the analytical solution of the Bogoliubov-de Gennes equations presented in Chap. 6.

A.1 The hypergeometric function

Many of the special functions which appear in the solutions to problems in mathematical physics, such as the Legendre and Chebyshev polynomials, can be written in terms of or as a limiting case of the hypergeometric function [184].

Definition A.1: *For a complex argument z, the (Gauss) hypergeometric function is defined by the power series* [141, 232]

$$ {}_2F_1\left(\alpha,\beta;\gamma;z\right) = 1+\frac{\alpha\beta}{\gamma}z+\frac{\alpha(\alpha+1)\beta(\beta+1)}{2\gamma(\gamma+1)}z^2+\ldots=\sum_{n=0}^{\infty}\frac{(\alpha)_n(\beta)_n}{(\gamma)_n}\frac{z^n}{n!}, $$

where $\{(\alpha)_n,(\beta)_n,(\gamma)_n\}$ are a set of (rising) Pochhammer symbols

$$ (\alpha)_n = \begin{cases} (\alpha)_0 & = 1 \\ (\alpha)_k & = \alpha(\alpha+1)(\alpha+2)\ldots(\alpha+k-1)=\Gamma(\alpha+k)/\Gamma(\alpha) \end{cases}, $$

for $k\in\mathbb{Z}^+$.

The hypergeometric function is convergent inside the unit circle $|z|<1$ for $\gamma\neq\mathbb{Z}_0^-$ and at $|z|=1$ provided $\gamma>\alpha+\beta$. In addition, the function can be analytical continued outside $|z|=1$ provided the possible branch cut at $[1,\infty)$ is excluded. As

an example, for $\alpha = \beta = \gamma = 1$, the hypergeomtric function takes the form of the standard geometric series

$$ {}_2F_1\left(1,1;1;z\right) = 1 + z + z^2 + \ldots = \frac{1}{1-z}, \tag{A.1}$$

which contains a simple pole at $z = 1$.

The hypergeometric function is a solution to the hypergeometric differential equation

$$ z\left(1-z\right)\frac{d^2w}{dz^2} + \left[\gamma - \left(1+\alpha+\beta\right)z\right]\frac{dw}{dz} - \alpha\beta w = 0, \tag{A.2}$$

which contains three regular singular points at $z = 0$, $z = 1$, and $z = \infty$.

Definition A.2: *For a second-order differential equation of the form*

$$ \frac{d^2w}{dz^2} + p_1\frac{dw}{dz} + p_2 z = 0, $$

z_k is a regular singular point if $\left(z - z_k\right)p_1$ and $\left(z - z_k\right)^2 p_2$ are both finite in the limit $z \to z_k$. Otherwise z_k is an irregular singular point.

For example, at the point $z = 1$, both

$$ \lim_{z\to 1} \quad \left(z-1\right)\frac{\gamma - \left(1+\alpha+\beta\right)z}{z\left(1-z\right)} = -\gamma + \alpha + \beta + 1, \tag{A.3}$$

and

$$ \lim_{z\to 1} \quad -\left(z-1\right)^2\frac{\alpha\beta}{z\left(1-z\right)} = 0, \tag{A.4}$$

are finite, and likewise for the remaining singular points. Any second-order differential equation which contains three regular singular points can be converted into the hypergeometric differential equation.

A.2 Solutions to the hypergeometric differential equation

As Eq. (A.2) is algebraically bounded at each singular point, a general solution in the vicinity of any singularity can be constructed by the Frobenius method, with the series solution

$$ w = \sum_{m=0}^{\infty} c_m z^{q+m} \tag{A.5}$$

provided $c_0 \neq 0$. This is turn leads to a total of six special solutions (two around each singularity) denoted by w_n, which can be generalised into Kummer's 24 solutions if required [141].

A.2.1 Solution around $z = 0$

The first set of solutions to consider are the ones located in the vicinity of the singular point $z = 0$. Substituting Eq. (A.5) into Eq. (A.2) leads to the expression

$$\begin{aligned}\sum_{m=0}^{\infty} c_m \left(k+m\right)\left(k+m-1+\gamma\right) z^{k+m-1} \\ - \sum_{m=1}^{\infty} c_{m-1} \left(k+m-1+\alpha\right)\left(k+m-1+\beta\right) z^{k+m-1} = 0,\end{aligned} \tag{A.6}$$

where the lower limits of the summation indices are adjusted so that z^{k+m-1} is a common polynomial. Equating to zero the smallest power of z^{k+m-1} for $m = 0$, leads to the indicial equation

$$c_0\, q \left(q-1+\gamma\right) = 0, \tag{A.7}$$

with exponent pairs $q = 0$ and $q = -\gamma + 1$. Then, by equating the remaining terms of Eq. (A.6), one obtains the recurrence relation

$$c_m = c_{m-1} \frac{\left(k+m-1+\alpha\right)\left(k+m-1+\beta\right)}{\left(k+m\right)\left(k+m-1+\gamma\right)}. \tag{A.8}$$

For the exponent $k = 0$, the expansion coefficients can be determined iteratively

$$c_1 = c_0 \frac{\alpha\beta}{\gamma} \quad , \quad c_2 = c_1 \frac{\left(\alpha+1\right)\left(\beta+1\right)}{2\left(\gamma+1\right)} \quad , \quad c_3 = c_2 \frac{\left(\alpha+2\right)\left(\beta+2\right)}{3\left(\gamma+2\right)}, \tag{A.9}$$

and so forth. Substituting the coefficients into Eq. (A.5) then leads to first fundamental solution

$$w_1 = \sum_{m=0}^{\infty} c_m z^m = c_0 + c_1 z + c_2 z^2 + c_3 z^3 + \ldots = \ {}_2F_1\left(\alpha, \beta; \gamma; z\right) \tag{A.10}$$

which as expected, is simply the hypergeometric function with $c_0 = 1$. The same procedure follows for the second exponent $k = 1 - \gamma$, leading to the second fundamental solution

$$w_2 = z^{1-\gamma}\ {}_2F_1\left(\alpha - \gamma + 1, \beta - \gamma + 1; 2 - \gamma; z\right). \tag{A.11}$$

The general solution is then given by

$$w = A\ {}_2F_1\left(\alpha, \beta; \gamma; z\right) + Bz^{1-\gamma}\ {}_2F_1\left(\alpha - \gamma + 1, \beta - \gamma + 1; 2 - \gamma; z\right), \tag{A.12}$$

where A and B are arbitrary constants.

A.2.2 Solution around $z = 1$

For the solutions around the singularity at $z = 1$, we begin by introducing the change of variables $y = 1 - z$. The hypergeometric differential equation becomes

$$y\left(1 - y\right)\frac{d^2w}{dy^2} + \left[\alpha + \beta - \gamma + 1 - \left(1 + \alpha + \beta\right)y\right]\frac{dw}{dy} - \alpha\beta w = 0, \tag{A.13}$$

which is identical to Eq. (A.2) except for the transformation of the γ variable as $\gamma \to \alpha + \beta - \gamma + 1$. The general solution at $z = 1$ is then given by transforming the solution at $z = 0$ by setting $\gamma \to \alpha + \beta - \gamma + 1$ for $y = 1 - z$, and reads as

$$\begin{aligned} w = A\ {}_2F_1\left(\alpha, \beta; \alpha + \beta - \gamma + 1; 1 - z\right) \\ + B(1 - z)^{\gamma - \alpha - \beta}\ {}_2F_1\left(\gamma - \beta, \gamma - \alpha; \gamma - \alpha - \beta + 1; 1 - z\right), \end{aligned} \tag{A.14}$$

with the set of fundamental solutions notated by w_3 and w_4 respectively.

A.2.3 Solution around $z = \infty$

The final set of solutions at $z = \infty$ requires applying the Möbius transformation $z = 1/s$, such that the hypergeometric differential equation is rewritten as

$$s^2\left(s - 1\right)\frac{d^2w}{ds^2} + \left[s^2\left(\gamma - 2\right) - s\left(\alpha + \beta - 1\right)\right]\frac{dw}{ds} - \alpha\beta w = 0. \tag{A.15}$$

Obtaining the general solution of Eq. (A.15) follows the same procedure as outlined for $z = 0$, by identifying the indicial and recurrence equations for the exponent pairs $k = \alpha$ and $k = \beta$. The general solution is given by

$$\begin{aligned} w = Az^{-\alpha}\ {}_2F_1\left(\alpha, \alpha - \gamma + 1; \alpha - \beta + 1; 1/z\right) \\ + Bz^{-\beta}\ {}_2F_1\left(\beta, \beta - \gamma + 1; \beta - \alpha + 1; 1/z\right), \end{aligned} \tag{A.16}$$

with w_5 and w_6 corresponding to the fundamental solutions. This completes the solutions of the hypergeometric differential equation.

Appendix B

Contour integrals

In this appendix, we show how to evaluate the interaction integrals which appear in the two-soliton variational analysis using the method of residues. Although these calculations can be found in the literature [217, 220], we recapitulate and expand on the details here, in order to provide a basis for evaluating the more complicated contour integrals which arise specifically in the case of the interacting gauge theory.

B.1 Integral example I

The simplest interaction integral to evaluate is

$$I_1 = \int_{-\infty}^{+\infty} \frac{dx}{\cosh(x)\cosh(x+a)}. \tag{B.1}$$

To proceed, we consider the following contour integral

$$\oint_{\mathcal{C}} dz\ f(z) = \oint_{\mathcal{C}} \frac{dz\ z}{\cosh(z)\cosh(z+a)}, \tag{B.2}$$

in which the contour path $\mathcal{C}$ forms a rectangular region in the complex plane, $z = x + iy$, with dimensions $-R < x < R$ and $0 < y < \pi$, such that

$$\oint_{\mathcal{C}} dz\ f(z) = \int_{-R}^{R} \frac{dx\ x}{\cosh(x)\cosh(x+a)} + \int_{0}^{i\pi} \frac{dy\ \ (R+iy)}{\cosh(R+iy)\cosh(R+iy+a)}$$

$$+ \int_{R}^{-R} \frac{dx\ \ (x+i\pi)}{\cosh(x+i\pi)\cosh(x+i\pi+a)} + \int_{i\pi}^{0} \frac{dy\ \ (-R+iy)}{\cosh(-R+iy)\cosh(-R+iy+a)}. \tag{B.3}$$

The complex function $f(z)$ is analytic in the region except for a pair of (simple) poles at $z_1 = i\pi/2$ and $z_2 = i\pi/2 - a$. These properties are illustrated in Fig. (B.1).

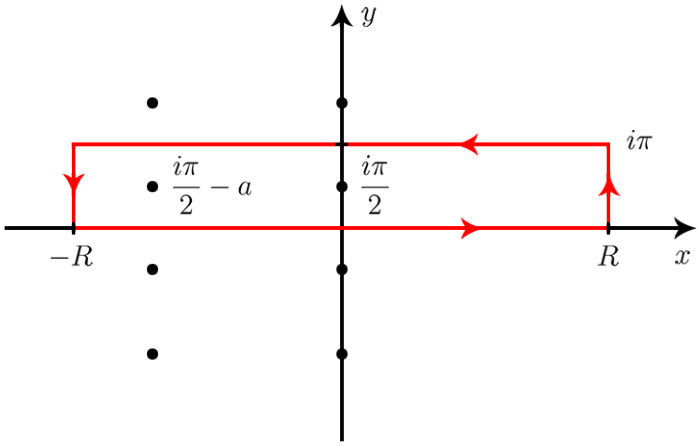

Figure B.1: Map of the complex plane $z = x + iy$, highlighting the location of the poles (black dots) and contour path $\mathcal{C}$ (red line) for all interaction integrals. The integration path is taken counter-clockwise.

In the limit of $R \to \infty$, the line integrals along the vertical paths vanish

$$\lim_{R\to\infty} \int_0^{i\pi} \frac{dy\ (R+iy)}{\cosh(R+iy)\cosh(R+iy+a)} \sim \int_0^{i\pi} dy\ Re^{-2R} \to 0, \tag{B.4}$$

as $f(z)$ exponentially converges to zero. The horizontal paths also vanish due to the periodicity of $f(z)$, except for a contribution from the top path which is proportional to the desired integral

$$\begin{aligned} &\int_{-\infty}^{\infty} \frac{dx\ x}{\cosh(x)\cosh(x+a)} + \int_{\infty}^{-\infty} \frac{dx\ (x+i\pi)}{\cosh(x+i\pi)\cosh(x+i\pi+a)} \\ &\qquad = -i\pi \int_{-\infty}^{\infty} \frac{dx}{\cosh(x)\cosh(x+a)} = -i\pi I_1. \end{aligned} \tag{B.5}$$

Therefore, from the residue theorem we can write

$$\oint_{\mathcal{C}} dz\ f(z) = -i\pi I_1 = 2\pi i \sum_{k=1,2} \mathrm{Res}\left(f(z), z_k\right). \tag{B.6}$$

The task of evaluating I_1 reduces to simply, albeit tediously, computing the residues of $f(z)$.

Definition C.1: *The residue of a m-th order pole at the singular point z_k, is given by*

$$\mathrm{Res}\left(f(z), z_k\right) = \frac{1}{(m-1)!} \lim_{z\to z_k} \frac{d^{(m-1)}}{dz^{(m-1)}} \left\{ (z - z_k)\, f(z)^m \right\}.$$

Using Definition C.1, the residues are calculated as

$$\mathrm{Res}\left(f(z), z_1\right) = \lim_{z \to z_1} \left(z - z_1\right) f\left(z\right) = \frac{\pi}{2i \sinh(a)}, \tag{B.7}$$

and

$$\mathrm{Res}\left(f(z), z_2\right) = \lim_{z \to z_2} \left(z - z_2\right) f\left(z\right) = -\frac{\pi}{2i \sinh(a)} - \frac{a}{\sinh(a)}, \tag{B.8}$$

where the first-order Laurent expansions

$$\lim_{z \to i\pi/2} \cosh(z) = \left\{ i \left(z - \frac{i\pi}{2} \right) \right\} + \mathcal{O}(x)^3, \tag{B.9}$$

and

$$\lim_{z \to i\pi/2 - a} \cosh(z + a) = \left\{ i \left(z - \frac{i\pi}{2} + a \right) \right\} + \mathcal{O}(x)^3. \tag{B.10}$$

have been used. Collating the results, we find

$$I_1 = \frac{2a}{\sinh(a)}. \tag{B.11}$$

Lemma C.1: *The interaction integral I_1 reduces to the non-interacting result*

$$\int_{-\infty}^{\infty} dx \ \mathrm{sech}^2(x) = 2, \tag{B.12}$$

for $a = 0$.

Definition C.2: *For a pair of functions, $f(x)$ and $g(x)$, which are differentiable in a given interval, L'Hôpital's rule states:*

$$\lim_{x \to a} \frac{f(x)}{g(x)} = \lim_{x \to a} \frac{df(x)/dx}{dg(x)/dx}.$$

Proof: Using Definition C.2, one can easily determine that

$$\lim_{a \to 0} \frac{2a}{\sinh(a)} = \lim_{a \to 0} \frac{2}{\cosh(a)} = 2. \tag{B.13}$$

B.2 Integral example II

A more involved example is

$$I_2 = \int_{-\infty}^{\infty} \frac{dx\ x \tanh(x+a)}{\cosh(x)\cosh(x+a)}. \tag{B.14}$$

In this case, we consider the following contour integral

$$\oint_{\mathcal{C}} g(z)dz = \oint_{\mathcal{C}} \frac{dz\ z^2 \sinh(z+a)}{\cosh(z)\cosh^2(z+a)}, \tag{B.15}$$

in which the contour path $\mathcal{C}$ is identical to the one used in the previous example. In contrast, the integrand now contains a simple pole and a second-order one. Equating the horizontal paths of the contour integral leads to the expression

$$\begin{aligned}\int_{-\infty}^{\infty} \frac{dx\ x^2 \sinh(x)}{\cosh(x)\cosh^2(x+a)} + \int_{\infty}^{-\infty} \frac{dx\ \ (x+i\pi)^2 \sinh(x)}{\cosh(x+i\pi)\cosh^2(x+i\pi+a)} \\ = \left(\pi^2 - 2\pi i x\right) \int_{-\infty}^{\infty} \frac{dx \sinh(x)}{\cosh(x)\cosh^2(x+a)},\end{aligned} \tag{B.16}$$

such that

$$\oint_{\mathcal{C}} g(z)dz = -2\pi i I_2 + \pi^2 I_3 = 2\pi i \sum_{k=1,2} \mathrm{Res}\left(g(z), z_k\right). \tag{B.17}$$

The task of evaluating I_2 now depends on computing the residues of $g(z)$ and knowledge of the integral

$$I_3 = \int_{-\infty}^{\infty} \frac{dx\ \tanh(x+a)}{\cosh(x)\cosh(x+a)} = -\frac{2}{\sinh(a)} + \frac{2a\cosh(a)}{\sinh^2(a)}, \tag{B.18}$$

which can determined using the same techniques. The residues in this instance are given by

$$\mathrm{Res}\left(g(z), z_1\right) = \lim_{z\to z_1} \left(z - z_1\right) g\left(z\right) = \frac{\pi^2 \cosh(a)}{4\sinh^2(a)}, \tag{B.19}$$

and

$$\begin{aligned}\mathrm{Res}\left(g(z), z_2\right) = \lim_{z\to z_2} \frac{d}{dz}\left[\left(z - z_2\right)^2 g\left(z\right)\right] \\ = (i\pi - 2a)\frac{1}{\sinh(a)} + \left(a - \frac{i\pi}{2}\right)^2 \frac{\cosh(a)}{\sinh^2(a)},\end{aligned} \tag{B.20}$$

with

$$\lim_{z\to i\pi/2-a}\cosh^2(z+a)=\left\{i\left(z-\frac{i\pi}{2}+a\right)\right\}^2+\mathcal{O}(x)^4. \tag{B.21}$$

Collating the results, we find

$$I_2=-\frac{a^2\cosh(a)}{\sinh^2(a)}+\frac{2a}{\sinh(a)}. \tag{B.22}$$

Lemma C.2: *The interaction integral I_2 reduces to the non-interacting result*

$$\int_{-\infty}^{\infty}dx\;x\tanh(x)\operatorname{sech}^2(x)=1, \tag{B.23}$$

for $a=0$.

Proof: Applying L'Hôpital's rule leads to the expression

$$\lim_{a\to 0}\left\{-\frac{a}{\sinh a}+\frac{a^2}{2\cosh a}+\frac{2}{\cosh a}\right\}=1, \tag{B.24}$$

as required.

$$\int_{-\infty}^{\infty} \frac{dx}{\cosh(x)\cosh(x+a)} = \frac{2a}{\sinh(a)} \tag{B.25}$$

$$\int_{-\infty}^{\infty} \frac{dx\ x}{\cosh(x)\cosh(x+a)} = -\frac{a^2}{\sinh(a)} \tag{B.26}$$

$$\int_{-\infty}^{\infty} \frac{dx\ (x+a)}{\cosh(x)\cosh(x+a)} = \frac{a^2}{\sinh(a)} \tag{B.27}$$

$$\int_{-\infty}^{\infty} \frac{dx\ x(x+a)}{\cosh(x)\cosh(x+a)} = \frac{\pi^2 a}{6\sinh(a)} - \frac{a^3}{3\sinh(a)} \tag{B.28}$$

$$\int_{-\infty}^{\infty} \frac{dx\ x^2}{\cosh(x)\cosh(x+a)} = \frac{\pi^2 a}{6\sinh(a)} + \frac{2a^3}{3\sinh(a)} \tag{B.29}$$

$$\int_{-\infty}^{\infty} \frac{dx\ (x+a)^2}{\cosh(x)\cosh(x+a)} = \frac{\pi^2 a}{6\sinh(a)} + \frac{2a^3}{3\sinh(a)} \tag{B.30}$$

$$\int_{-\infty}^{\infty} \frac{dx}{\cosh^2(x)\cosh^2(x+a)} = \frac{4a\cosh(a)}{\sinh^3(a)} - \frac{4}{\sinh^2(a)} \tag{B.31}$$

$$\int_{-\infty}^{\infty} \frac{dx\ x}{\cosh^2(x)\cosh^2(x+a)} = \frac{2a}{\sinh^2(a)} - \frac{2a\cosh(a)}{\sinh^3(a)} \tag{B.32}$$

$$\int_{-\infty}^{\infty} \frac{dx\ (x+a)}{\cosh^2(x)\cosh^2(x+a)} = -\frac{2a}{\sinh^2(a)} + \frac{2a\cosh(a)}{\sinh^3(a)} \tag{B.33}$$

$$\int_{-\infty}^{\infty} \frac{dx}{\cosh^3(x)\cosh(x+a)} = \frac{2\cosh(a)}{\sinh^2(a)} - \frac{2a}{\sinh^3(a)} \tag{B.34}$$

$$\int_{-\infty}^{\infty} \frac{dx}{\cosh(x)\cosh^3(x+a)} = \frac{2\cosh(a)}{\sinh^2(a)} - \frac{2a}{\sinh^3(a)} \tag{B.35}$$

$$\int_{-\infty}^{\infty} \frac{dx\ x}{\cosh^3(x)\cosh(x+a)} = \frac{a^2}{\sinh^3(a)} - \frac{1}{\sinh(a)} \tag{B.36}$$

$$\int_{-\infty}^{\infty} \frac{dx\ (x+a)}{\cosh^3(x)\cosh(x+a)} = -\frac{a^2}{\sinh^3(a)} - \frac{1}{\sinh(a)} + \frac{2a\cosh(a)}{\sinh(a)^2} \tag{B.37}$$

$$\int_{-\infty}^{\infty} \frac{dx\ x}{\cosh(x)\cosh^3(x+a)} = \frac{a^2}{\sinh^3(a)} + \frac{1}{\sinh(a)} - \frac{2a\cosh(a)}{\sinh(a)^2} \tag{B.38}$$

$$\int_{-\infty}^{\infty} \frac{dx\ (x+a)}{\cosh(x)\cosh^3(x+a)} = -\frac{a^2}{\sinh^3(a)} + \frac{1}{\sinh(a)} \tag{B.39}$$

$$\int_{-\infty}^{\infty} \frac{dx\ \tanh(x)}{\cosh(x)\cosh(x+a)} = \frac{2}{\sinh(a)} - \frac{2a\cosh(a)}{\sinh^2(a)} \tag{B.40}$$

$$\int_{-\infty}^{\infty} \frac{dx\ \tanh(x+a)}{\cosh(x)\cosh(x+a)} = -\frac{2}{\sinh(a)} + \frac{2a\cosh(a)}{\sinh^2(a)} \tag{B.41}$$

$$\int_{-\infty}^{\infty} \frac{dx\ x\tanh(x+a)}{\cosh(x)\cosh(x+a)} = -\frac{a^2\cosh(a)}{\sinh^2(a)} + \frac{2a}{\sinh(a)} \tag{B.42}$$

$$\int_{-\infty}^{\infty} \frac{dx\ (x+a)\tanh(x)}{\cosh(x)\cosh(x+a)} = -\frac{a^2\cosh(a)}{\sinh^2(a)} + \frac{2a}{\sinh(a)} \tag{B.43}$$

$$\int_{-\infty}^{\infty} \frac{dx\ \tanh(x)\tanh(x+a)}{\cosh(x)\cosh(x+a)} = \frac{4\cosh(a)}{\sinh^2(a)} + \frac{2a}{\sinh(a)} - \frac{4a\cosh^2(a)}{\sinh^3(a)} \tag{B.44}$$

Contour shifts

$$\int_{-\infty}^{\infty} dx\ f\,(x,a)\,x^{n-1} \to \int_{\mathcal{C}} dz\ f\,(z,a)\,z^n \tag{B.45}$$

$$\int_{-\infty}^{\infty} dx\ f\,(x,a)\,(x+a)^{n-1} \to \int_{\mathcal{C}} dz\ f\,(z,a)\,(z+a)^n \tag{B.46}$$

where $n \in \mathbb{Z}^+$ and $f(x,a)$ is a product of hyperbolic functions.

Laurent expansions

$$\lim_{z\to i\pi/2} \cosh^n(z) = \left\{ i\left(z - \frac{i\pi}{2}\right)\right\}^n + \mathcal{O}(x)^{n+2} \tag{B.47}$$

$$\lim_{z\to i\pi/2-a} \cosh^n(z+a) = \left\{ i\left(z - \frac{i\pi}{2} - a\right)\right\}^n + \mathcal{O}(x)^{n+2} \tag{B.48}$$

where $n \in \mathbb{Z}^+$.

Bibliography

[1] Aktosun, T. *Inverse Scattering Transform and the Theory of Solitons.* Springer, (2009).

[2] Yang, J. *Nonlinear Waves in Integrable and Nonintegrable Systems.* SIAM, (2010).

[3] Gardner, C. S., Greene, J. M., Kruskal, M. D., and Miura, R. M. *Phys. Rev. Lett.* **19**, 1095 (1967).

[4] Zakharov, V. F. and Shabat, A. B. *Jetp* **34**, 118 (1972).

[5] Ablowitz, M. J., Kaup, D. J., Newell, A. C., and Segur, H. *Phys. Rev. Lett* **31**, 125 (1973).

[6] Drazin, P. G. and Johnson, R. S. *Solitons: an introduction.* Cambirdge University Press, (1989).

[7] Scott, A. *Phys. Rep.* **217**, 1 (1992).

[8] Dauxois, T. and Peyrard, M. *Physics of Solitons.* Cambridge University Press, (2006).

[9] Agrawal, G. P. *Nonlinear Fiber Optics.* Academic Press, (2001).

[10] Trillo, S. and Torruellas, W. *Spatial Solitons.* Springer-Verlag Berlin Heidelberg, (2001).

[11] Ichikawa, Y. H. and Watanabe, S. *J. Phys. Colloques* **38**, C6–15 (1977).

[12] Kosevich, A. M., Ivanov, B. A., and Kovalev, A. S. *Phys. Rep.* **194**, 117 (1990).

[13] Scott, A. *Encyclopedia of Nonlinear Science.* Routledge, (2005).

[14] Pethick, C. J. and Smith, H. *Bose-Einstein Condensation in Dilute Gases.* Cambridge University Press, (2008).

[15] Pitaevskii, L. and Stringari, S. *Bose-Einstein Condensation and Superfluidity.* Oxford University Press, (2016).

[16] Hasegawa, A. and Tappert, F. *Appl. Phys. Lett.* **23**, 142 (1973).

[17] Haus, H. A. and Wong, W. S. *Rev. Mod. Phys.* **68**, 423 (1996).

[18] Ablowitz, M. J., Biondini, G., and Ostrovsky, L. A. *Chaos* **10**, 471 (2000).

[19] Dalfovo, F., Giorgini, S., Pitaevskii, L. P., and Stringari, S. *Rev. Mod. Phys.* **71**, 463 (1999).

[20] Anderson, M. H., Ensher, J. R., Matthews, M. R., Wieman, C. E., and Cornell, E. A. *Science* **269**, 198 (1995).

[21] Davis, K. B., Mewes, M., Andrews, M. R., van Druten, N. J., Durfee, D. S., Kurn, D. M., and Ketterle, W. *Phys. Rev. Lett.* **75**, 3969 (1995).

[22] Bradley, C. C., Sackett, C. A., and Hulet, R. G. *Phys. Rev. Lett.* **78**, 985 (1997).

[23] Modugno, G., Ferrari, G., Roati, G., Brecha, R. J., Simoni, A., and Inguscio, M. *Science* **294**, 1320 (2001).

[24] Stellmer, S., Tey, M. K., Huang, B., Grimm, R., and Schreck, F. *Phys. Rev. Lett.* **103**, 200401 (2009).

[25] Takasu, Y., Maki, K., Komori, K., Takano, T., Honda, K., Kumakura, M., Yabuzaki, T., and Takahashi, Y. *AIP Conf. Pro.* **770**, 254 (2005).

[26] Lu, M., Burdick, N. Q., Youn, S. H., and Lev, B. L. *Phys. Rev. Lett.* **107**, 190401 (2011).

[27] Morsch, O. and Oberthaler, M. *Rev. Mod. Phys.* **78**, 179 (2006).

[28] Henderson, K., Ryu, C., MacCormick, C., and Boshier, M. G. *New. J. Phys.* **11**, 043030 (2009).

[29] Boyer, V., Godun, R. M., Smirne, G., Cassettari, D., Chandrashekar, C. M., Deb, A. B., Laczik, Z. J., and Foot, C. J. *Phys. Rev. A* **73**, 031402 (2006).

[30] Görlitz, A., Vogels, J. M., Leanhardt, A. E., Raman, C., Gustavson, T. L., Abo-Shaeer, J. R., Chikkatur, A. P., Gupta, S., Inouye, S., Rosenband, T., and Ketterle, W. *Phys. Rev. Lett.* **87**, 130402 (2001).

[31] Harrison, P. and Valavanis, A. *Quantum Wells, Wires and Dots.* Wiley-Blackwell, (2016).

[32] Chin, C., Grimm, R., Julienne, P., and Tiesinga, E. *Rev. Mod. Phys.* **82**, 1225 (2010).

[33] Bourdel, T., Khaykovich, L., Cubizolles, J., Zhang, J., Chevy, F., Teichmann, M., Tarruell, L., Kokkelmans, S., and Salomon, C. *Phys. Rev. Lett.* **93**, 050401 (2004).

[34] Feynman, R. P. *Int. J. Theor. Phys.* **21**, 467 (1982).

[35] Bloch, I., Dalibard, J., and Nascimbéne, S. *Nat. Phys.* **8**, 267 (2012).

[36] Unruh, W. G. *Phys. Rev. Lett.* **46**, 1351 (1981).

[37] Wiese, U. *Nucl. Phys. A* **931**, 246 (2014).

[38] Greiner, M., Mandel, O., Esslinger, T., Hänsch, T. W., and Bloch, I. *Nature* **415**, 39 (2002).

[39] Simon, J., Bakr, W. S., Ma, R., Tai, M., Preiss, P. M., and Greiner, M. *Nature* **472**, 307 (2011).

[40] LeBlanc, L. J., Beeler, M. C., Jiménez-Garcia, K., Perry, A. R., Sugawa, S., Williams, R. A., and Spielman, I. B. *New. J. Phys.* **15**, 073011 (2013).

[41] Qu, C., Hamner, C., Gong, M., Zhang, C., and Engels, P. *Phys. Rev. A* **88**, 021604 (2013).

[42] Aidelsburger, M., Atala, M., Lohse, M., Barreiro, J. T., Paredes, B., and Bloch, I. *Phys. Rev. Lett.* **111**, 185301 (2013).

[43] Blatt, R. and Roos, C. F. *Nat. Phys.* **8**, 277 (2012).

[44] Aspuru-Guzik, A. and Walther, P. *Nat. Phys.* **8**, 285 (2012).

[45] Houck, A. A., Türeci, H. E., and Koch, J. *Nat. Phys.* **8**, 292 (2012).

[46] Goldman, N., Juzeliūnas, G., Öhberg, P., and Spielman, I. B. *Rep. Prog. Phys,* **77**, 126401 (2014).

[47] Dalibard, J., Gerbier, F., Juzeliūnas, G., and Öhberg, P. *Rev. Mod. Phys* **83**, 1523 (2011).

[48] Edmonds, M. J., Valiente, M., Juzeliūnas, G., Santos, L., and Öhberg, P. *Phys. Rev. Lett.* **110**, 085301 (2013).

[49] Helm, J. L., Cornish, S. L., and Gardiner, S. A. *Phys. Rev. Lett.* **114**, 134101 (2015).

[50] Mcdonald, G. D., Kuhn, C. C. N., Hardman, K. S., Bennetts, S., Everitt, P. J., Altin, P. A., Debs, J. E., Close, J. D., and Robbins, N. P. *Phys. Rev. Lett.* **113**, 013002 (2017).

[51] Seaman, B. T., Krämer, M., Anderson, D. Z., and Holland, M. J. *Phys. Rev. A* **75**, 023615 (2007).

[52] Dingwall, R. J. and Öhberg, P. *Phys. Rev. A* **99**, 023609 (2019).

[53] Dingwall, R. J., Edmonds, M. J., Helm, J. L., Malomed, B., and Öhberg, P. *New. J. Phys* **20**, 043004 (2018).

[54] Steck, D. A. *Rubidium 87 D Line Data* , https://steck.us/alkalidata/ (2003).

[55] Madison, K. W., Chevy, F., Wohlleben, W., and Dalibard, J. *Phys. Rev. Lett.* **84**, 806 (2000).

[56] Abo-Shaeer, J. R., Raman, C., Vogels, J. M., and Ketterle, W. *Science* **20**, 476 (2001).

[57] Engels, P., Coddington, I., Haljan, P. C., Schweikhard, V., and Cornell, E. A. *Phys. Rev. Lett.* **90**, 170405 (2003).

[58] Schweikhard, V., Coddington, I., Engels, P., Mogendorff, V. P., and Cornell, E. A. *Phys. Rev. Lett.* **92**, 040404 (2004).

[59] Juzeliūnas, G. and Öhberg, P. *Phys. Rev. Lett.* **93**, 033602 (2004).

[60] Ruseckas, J., Juzeliūnas, G., Öhberg, P., and Fleischhauer, M. *Phys. Rev. Lett.* **95**, 010404 (2005).

[61] Struck, J., Ölschläger, C., Weinberg, M., Hauke, P., Simonent, J., Eckardt, A., Lewenstein, M., Sengstock, K., and Windpassinger, P. *Phys. Rev. Lett.* **108**, 225304 (2012).

[62] Meinert, F., Mark, M. J., Lauber, K., Daley, A. J., and Nägerl, H. C. *Phys. Rev. Lett.* **116**, 205301 (2016).

[63] Lin, Y.-J., Compton, R. L., Jiménez-García, K., Porto, J. V., and Spielman, I. B. *Nature* **462**, 628 (2009).

[64] Lin, Y.-J., Jiménez-García, K., and Spielman, I. B. *Nature* **471**, 83 (2011).

[65] Gross, E. P. *Il Nuovo Cimento* **20**, 454 (1961).

[66] Pitaevskii, L. P. *JETP* **40**, 451 (1961).

[67] Stringari, S. *Phys. Rev. Lett.* **77**, 2360 (1996).

[68] Edwards, M., Ruprecht, P. A., Burnett, K., Dodd, R. J., and Clark, C. W. *Phys. Rev. Lett.* **77**, 1671 (1996).

[69] Ruprecht, P. A., Edwards, M., , Burnett, K., and Clark, C. W. *Phys. Rev. A* **54**, 4178 (1996).

[70] Jin, D. S., Ensher, J. R., Matthews, M. R., Wieman, C. E., and Cornell, E. A. *Phys. Rev. Lett.* **77**, 420 (1996).

[71] Öhberg, P., Surkov, E. L., Tittonen, I., Stenholm, S., Wilkens, M., and Shlyapnikov, G. V. *Phys. Rev. A* **56**, R3346 (1997).

[72] Strecker, K. E., Partridge, G. B., Truscott, A. G., and Hulet, R. G. *Nature* **417**, 150 (2002).

[73] Khaykovich, L., Schreck, F., Ferrari, G., Bourdel, T., Cubizolles, J., Carr, L. D., Castin, Y., and Salomon, C. *Science* **296**, 1290 (2002).

[74] Burger, S., Bongs, K., Dettmer, S., Ertmer, W., Sengstock, K., Sanpera, A., Shlyapnikov, G. V., and Lewenstein, M. *Phys. Rev. Lett.* **83**, 5198 (1999).

[75] Denschlag, J., Simsarian, J. E., Feder, D. L., Clark, C. W., Collins, L. A., Cubizolles, J., Deng, L., Hagley, E. W., Helmerson, K., Reinhardt, W. P., Rolston, S. L., Schneider, B. I., and Phillips, W. D. *Science* **287**, 97 (2000).

[76] Deng, L., Hagley, E. W., Wen, J., Trippenbach, M., Band, Y., Julienne, P. S., Simsarian, J. E., Helmerson, K., Rolston, S. L., and Phillips, W. D. *Nature* **398**, 218 (1999).

[77] Berry, M. V. *Pro. Royal Society of London. A. Math. Phys. Sciences* **4**, 45 (1984).

[78] Cohen-Tannoudji, C., Diu, B., and Laloe, F. *Quantum Mechanics.* Wiley, (2006).

[79] Cirac, J. I., Maraner, P., and Pachos, J. K. *Phys. Rev. Lett.* **105**, 190403 (2010).

[80] Banerjee, D., Dalmonte, M., Müller, M., Rico, E., Stebler, P., Wiese, U. J., and Zoller, P. *Phys. Rev. Lett.* **109**, 175302 (2012).

[81] Banerjee, D., Bögli, M., Dalmonte, M., Rico, E., Stebler, P., Wiese, U. J., and Zoller, P. *Phys. Rev. Lett.* **110**, 125303 (2013).

[82] Tagliacozzo, L., Celi, A., Orland, P., Mitchell, M. W., and Lewenstein, M. *Nat. Comm.* **4**, 2615 (2013).

[83] Zheng, J.-H., Xiong, B., Juzeliūnas, G., and Wang, D.-W. *Phys. Rev. A* **92**, 013604 (2015).

[84] Greschner, S., Sun, G., Poletti, D., and Santos, L. *Phys. Rev. Lett.* **113**, 215303 (2014).

[85] Martinez, E. A., Muschik, C. A., Schindler, P., Nigg, D., Erhard, A., Heyl, M., Hauke, P., Dalmonte, M., Monz, T., Zoller, P., and Blattl, R. *Nat. Phys.* **534**, 516 (2016).

[86] Clark, L. W., Anderson, B. M., Feng, L., Gaj, A., Levin, K., and Chin, C. *Phys. Rev. Lett.* **121**, 030402 (2018).

[87] Butera, S., Valiente, M., and Öhberg, P. *J. Phys. B: At. Mol. Opt. Phys* **49**, 015304 (2016).

[88] Butera, S., Valiente, M., and Öhberg, P. *New. J. Phys.* **18**, 085001 (2016).

[89] Pérez-García, V. M., Michinel, H., and Herrero, H. *Phys. Rev. A* **57**, 3837 (1998).

[90] Kivshar, Y. S., Alexander, T. J., and Turitsyn, S. K. *Phys. Lett. A* **278**, 225 (2001).

[91] Aglietti, U., Griguolo, L., Jackiw, R., Pi, S. Y., and Seminara, D. *Phys. Rev. Lett.* **77**, 4406 (1996).

[92] Kaup, D. J. and Newell, A. C. *J. Math. Phys.* **9**, 798 (1978).

[93] Calogero, F. and Lillo, S. D. *Inverse Problems* **3**, 663 (1987).

[94] Chen, H. H., Lee, Y. C., and Liu, C. S. *Phys. Scr.* **20**, 490 (1979).

[95] Clarkson, P. A. and Cosgrove, C. M. *J. Phys. A: Math. Gen.* **20**, 2003 (1987).

[96] Nishino, A., Umeno, Y., and Wadati, M. *Chs. Sol. Frac.* **9**, 1063 (1998).

[97] Jackiw, R. *Non. Math. Phys.* **4**, 261 (1997).

[98] Harikumar, E., Kumar, C. N., and Sivakumar, M. *Phys. Rev. D* **58**, 107703 (1998).

[99] Edmonds, M. J., Valiente, M., and Öhberg, P. *Europhys. Lett.* **110**, 36004 (2015).

[100] Lee, J. H., Lin, C. K., and Pashaev, O. K. *Chaos Sol. Frac.* **19**, 109 (2003).

[101] Sackett, C. A., Gerton, J. M., Welling, M., and Hulet, R. G. *AIP Conf. Pro.* **477**, 58 (1999).

[102] Khaykovich, L. and Malomed, B. A. *Phys. Rev. A* **74**, 023607 (2006).

[103] Frantzeskakis, D. J. *Jour. Phys. A: Math. Theo.* **43**, 213001 (2010).

[104] Nguyen, J. H. V., Dyke, P., Luo, D., Malomed, B. A., and Hulet, R. G. *Nat. Phys.* **10**, 918 (2014).

[105] Zhu, Q., Zhang, C., and Wu, B. *EPL* **100**, 50003 (2012).

[106] Zheng, W., Yu, Z., Cui, X., and Zhai, H. *J. Phys. B: At. Mol. Opt. Phys* **46**, 134007 (2013).

[107] Fermi, E., Pasta, J., and Ulam, S. *Studies of non Linear Problems* **LA-1940**, 978 (1955).

[108] Hayashi, N. and Ozawa, T. *Physica D: Nonlear Phenomena* **55**, 14 (1992).

[109] Hayashi, N. *Nonlinear Anaylsis: Theory, Methods and Applications* **20**, 823 (1993).

[110] Galitski, V. and Spielman, I. B. *Nature* **494**, 49 (2013).

[111] Ashhab, S. and Leggett, A. J. *Phys. Rev. A* **68**, 063612 (2003).

[112] Galitski, V., Juzeliūnas, G., and Spielman, I. B. *Physics Today* **494**, 38 (2019).

[113] Greiner, W. and Reinhardt, J. *Field Quantization*. Springer, (1996).

[114] Peskin, M. E. and Schroeder, D. V. *An Introduction to Quantum Field Theory*. Perseus, (1995).

[115] Altland, A. and Simons, B. D. *Condensed Matter Field Theory*. Cambridge University Press, (2010).

[116] Chaikin, P. M. and Lubensky, T. C. *Principles of condensed matter physics*. Cambridge University Press, (2010).

[117] Goldstein, H., Poole, C., and Safko, J. *Classical Mechanics*. Addison Wesley, (2000).

[118] Sykes, A. G. *J. Phys. A: Math. Theor.* **44**, 135206 (2011).

[119] Russell, J. S. *Report on Waves, in Report of the 14th Meeting of the British Association for the Advancement of Science* , 311 (1844).

[120] González, J. A., Bellorín, A., and Guerrero, L. E. *Phys. Rev. E* **60**, R37 (1999).

[121] Lee, C. and Brand, J. *Europhys. Lett.* **73**, 321 (2006).

[122] Wang, C., Hong, T., Lee, R., and Wang, D. *Opt. Exp.* **20**, 22675 (2012).

[123] Gertjerenken, B., Billiam, T. P., Khaykovich, L., and Weiss, C. *Phys. Rev. A* **86**, 033608 (2012).

[124] Pelinovsky, D. E., Kivshar, Y. S., and Afanasjev, V. V. *Phys. D* **116**, 121 (1998).

[125] Toda, M. *J. Phys. Soc. Jpn.* **22**, 431 (1967).

[126] Dobrek, L., Gajda, M., Lewenstein, M., Sengstock, K., Birkl, G., and Ertmer, W. *Phys. Rev. A* **60**, R3381 (1999).

[127] Marchant, A. L., Billam, T. P., Yu, M. M. H., Rakonjac, A., Helm, J. L., Polo, J., Weiss, C., Gardiner, S. A., and Cornish, S. L. *Phys. Rev. A.* **93**, 021604 (2016).

[128] Weller, A., Ronzheimer, J. P., Gross, C., Esteve, J., Oberthaler, M. K., Frantzeskakis, D. J., Theocharis, G., and Kevrekidis, P. G. *Phys. Rev. Lett.* **101**, 130401 (2008).

[129] Becker, C., Stellmer, S., Soltan-Panahi, P., Dörscher, S., Baumert, M., Richter, E., Kronjaäger, J., Bongs, K., and Sengstock, K. *Nat. Phys.* **4**, 496 (2008).

[130] Busch, T. and Anglin, J. R. *Phys. Rev. Lett.* **87**, 010401 (2001).

[131] Kevrekidis, P. G. and Frantzeskakis, D. J. *Rev. in Phys.* **1**, 140 (2016).

[132] Bland, T., Edmonds, M. J., Proukakis, N. P., Martin, A. M., O'Dell, D. H. J., and Parker, N. G. *Phys. Rev. A* **92**, 063601 (2015).

[133] Edmonds, M. J., Bland, T., O'Dell, D. H. J., and Parker, N. G. *Phys. Rev. A* **93**, 063617 (2016).

[134] Edmonds, M. J., Bland, T., Doran, R., and Parker, N. G. *New J. Phys.* **19**, 023019 (2017).

[135] Achilleos, V., Frantzeskakis, D. J., Kevrekidis, P. G., and Pelinovsky, D. E. *Phys. Rev. Lett.* **110**, 264101 (2013).

[136] Sakaguchi, H., Li, B., and Malomed, B. A. *Phys. Rev. E* **89**, 032920 (2014).

[137] Li, Y., Liu, Y., Fan, Z., Pang, W., Fu, S., and Malomed, B. A. *Phys. Rev. A* **95**, 063613 (2017).

[138] Malomed, B. A. *Europhys Lett.* **122**, 36001 (2018).

[139] Wu, H. Y. *J. Math. Anlys. App.* **192**, 151 (1995).

[140] Hirota, R. *Phys. Rev. Lett.* **27**, 1192 (1971).

[141] Olver, F. W. J., Lozier, D. W., Boisvert, R. F., and Clark, C. W. *NIST Handbook of Mathematical Functions*. Cambridge Univeristy Press, http://dlmf.nist.gov, (2010).

[142] Carretero-González, R., Frantzeskakis, D. J., and Kevrekidis, P. G. *Nonlinearity* **21**, R139 (2008).

[143] Kivshar, Y. S. and Yang, X. *Phys. Rev. E.* **49**, 1657 (1994).

[144] Pérez-García, V. M., Michinel, H., Cirac, J. I., Lewenstein, M., and Zoller, P. *Phys. Rev. Lett.* **77**, 5320 (1996).

[145] Pérez-García, V. M., Michinel, H., Cirac, J. I., Lewenstein, M., and Zoller, P. *Phys. Rev. A* **56**, 1424 (1997).

[146] Abdullaev, F. K., Gammal, A., and Tomio, L. *J. Phys. B: At. Mol. Opt. Phys* **37**, 635 (2004).

[147] Umarov, B. A., Messikh, A., Regaa, N., and Baizakov, B. B. *J. Phys. Conf. Ser.* **435**, 012024 (2013).

[148] Saleh, M. and Öhberg, P. *J. Phys. B: At. Mol. Opt. Phys* **51**, 045303 (2018).

[149] Kivshar, Y. S. and Królikowski, W. *Opt. Comm.* **114**, 353 (1995).

[150] Grillakis, M., Shatah, J., and Strauss, W. *J. Func. Anly* **74**, 160 (1987).

[151] Weinstein, M. I. *Comm. Pure Appl. Math* **39**, 51 (1986).

[152] Kuznetsov, E. A., Rubenchik, A. M., and Zakharov, V. E. *Phys. Rep.* **142**, 103 (1986).

[153] Zakharov, V. E. and Kuznetsov, E. A. *Phys.-Usp* **55**, 535 (2012).

[154] Carr, L. D. and Brand, J. *Multidimensional Solitons: Theory.* Springer, (2008).

[155] Zhang, Y., Zhou, Z., Malomed, B. A., and Pu, H. *Phys. Rev. Lett.* **115**, 253902 (2015).

[156] Buggy, Y. and Öhberg, P. *arXiv:1708.07712* (2017).

[157] Fogel, M. B., Trullinger, S. E., Bishop, A. R., and Krumhansl, J. A. *Phys. Rev. B* **15**, 1578 (1977).

[158] Kaup, D. J. *Phys. Rev. A* **42**, 5689 (1990).

[159] Bonderson, A., Lisak, M., and Anderson, D. *Phys. Scr.* **20**, 479 (1978).

[160] Kivshar, Y. S. and Malomed, B. A. *Rev. Mod. Phys.* **61**, 763 (1989).

[161] Elgin, J. N. *Phys. Rev. A* **47**, 4331 (1993).

[162] Anderson, D. *Phys. Rev. A* **27**, 3135 (1983).

[163] Merterns, F. G., Qunitero, N. R., and Bishop, A. R. *Phys. Rev. E* **81**, 016608 (2010).

[164] Vakhitov, N. G. and Kolokolov, A. A. *Radiophys. Quantum Electron* **16**, 783 (1973).

[165] Kivshar, Y. S., Pelinovsky, D. E., Cretegny, T., and Peyrard, M. *Phys. Rev. Lett.* **80**, 5032 (1998).

[166] Pelinovsky, D. E., Afanasjev, V. V., and Kivshar, Y. S. *Phys. Rev. E.* **53**, 1940 (1996).

[167] Anderson, D. and Lisak, M. *Phys. Rev. A* **27**, 1393 (1973).

[168] Chen, Y. and Yan, Z. *Sci. Rep.* **6**, 23478 (2016).

[169] Chen, Y. and Yan, Z. *Phys. Rev. E* **95**, 012205 (2017).

[170] Yan, Z., Wen, Z., and Konotop, V. V. *Phys. Rev. A* **92**, 023821 (2015).

[171] Musslimani, Z. H., Makris, K. G., El-Ganainy, R., and Christodoulides, D. *Phys. Rev. Lett.* **100**, 030402 (2008).

[172] Bogoliubov, N. *J. Phys.(USSR)* **11**, 23 (1947).

[173] Muryshev, A. E., van Linden van den Huevell, H. B., and Shlyapnikov, G. V. *Phys. Rev. A* **60**, R2665 (1999).

[174] Martin, A. D., Adams, C. S., and Gardiner, S. A. *Phys. Rev. Lett.* **98**, 020402 (2007).

[175] Carr, L. D. and Brand, J. *Phys. Rev. Lett.* **92**, 040401 (2004).

[176] Nhuyen, J. H. V., Lou, D., and Hulet, R. G. *Science* **28**, 422 (2017).

[177] Sinha, S., Cherny, A. Y., Kovrizhin, D., and Brand, J. *Phys. Rev. Lett.* **96**, 030406 (2006).

[178] Brand, J. and Reinhardt, W. P. *Phys. Rev. A* **65**, 043612 (2002).

[179] Ma, M., Carretero-González, R., Kevrekidis, P. G., Frantzeskakis, D. J., and Malomed, B. A. *Phys. Rev. A* **82**, 023621 (2002).

[180] Mostafazadeh, A. *J. Math. Phys.* **43**, 205 (2002).

[181] Lekner, J. *Amer. J. Phys.* **75**, 1151 (2007).

[182] Sachs, R. L. *SIAM J. Math. Anal.* **14**, 674 (1983).

[183] Yang, J. and Tan, Y. *Phys. Rev. Lett.* **85**, 3624 (2000).

[184] Flügge, S. *Practical Quantum Mechanics*. Springer, (1971).

[185] Lamb, G. L. *Elements of Soliton Theory*. John Wiley and Sons, (1980).

[186] Landau, L. D. and Lifshitz, E. M. *Quantum Mechanics*. Pergamon Press, (1965).

[187] Cooper, F., Khare, A., and Sukhatme, U. *Phys. Rep.* **251**, 5320 (1995).

[188] Díaz, J. I., Negro, J., Nieto, L. M., and Rosas-Ortiz, O. *J. Phys. A: Math. Gen.* **32**, 8447 (1999).

[189] Kaup, D. J. *J. Math. Anal. Appl.* **54**, 849 (1976).

[190] Kovrizhin, D. L. *Phys. Lett. A* **287**, 392 (2001).

[191] Yan, J. and Tangr, Y. *Phys. Rev. E* **54**, 6816 (1996).

[192] Biswas, A. *Nuc. Phys. B* **806**, 457 (2009).

[193] Dziarmaga, J. and Sacha, K. *Phys. Rev. A* **68**, 043607 (2003).

[194] Altin, P. A., Dennis, G. R., McDonald, G. D., Döring, D., Debs, J. E., Close, J. D., Savage, C. M., and Robins, N. P. *Phys. Rev. A* **84**, 033632 (2011).

[195] Amico, L., Nirki, G., Boshier, M., and Kwek, L. *New. J. Phys* **19**, 020201 (2017).

[196] Goodman, R. H. and Haberman, R. *SIAM J. Appl. Dyn. Syst.* **4**, 1195 (2005).

[197] Anninos, P., Oliveira, S., and Matzner, R. A. *Phys. Rev. D* **44**, 1147 (1991).

[198] Dmitriev, S. V. and Shingenari, T. *Chaos* **12**, 324 (2002).

[199] Campbell, D. K., Peyrard, M., and Sodano, P. *Physica D* **19**, 165 (1986).

[200] Frauenkron, H., Kivshar, Y. S., and Malomed, B. A. *Phys. Rev. E* **54**, R2244 (1996).

[201] Dmitriev, S. V., Kevrekidis, P. G., and Kivshar, Y. S. *Phys. Rev. E* **78**, 046604 (2008).

[202] Dmitriev, S. V., Kivshar, Y. S., and Shingenari, T. *Phys. Rev. E.* **64**, 056613 (2001).

[203] Dmitriev, S. V., Semagin, D. A., Sukhorukov, A. A., and Shingenari, T. *Phys. Rev. E* **66**, 046609 (2002).

[204] Zhu, Y., Haberman, R., and Yang, J. *Phys. Rev. Lett.* **100**, 143901 (2008).

[205] Pigier, C., Uzdin, R., Carmon, T., Segev, M., Nepomnyaschchy, A., and Musslimani, Z. H. *Opt. Lett.* **26**, 1577 (2001).

[206] Musslimani, Z. H., SoljaČiĆ, M., Segev, M., and Christodoulides, D. N. *Phys. Rev. E* **63**, 066608 (2001).

[207] Scharf, R. and Bishop, A. R. *Phys. Rev. A* **46**, R2973 (1992).

[208] Martin, A. D., Adams, C. S., and Gardiner, S. A. *Phys. Rev. A* **77**, 013620 (2008).

[209] Martin, A. D. *Phys. Rev. A* **93**, 023631 (2016).

[210] Parker, N. G., Martin, A. M., Cornish, S. L., and Adams, C. S. *J. Phys. B: At. Mol. Opt. Phys* **41**, 045303 (2008).

[211] Yan, D., Chang, J. J., Hamner, C., Hoefer, M., Kevrekidis, P. G., Engles, P., Achilleos, V., Frantzeskakis, D. J., and Cuevas, J. *J. Phys. B: At. Mol. Opt. Phys.* **45**, 115301 (2012).

[212] Baizakov, B. B., Al-Marzoug, S., and Bahlouli, H. *Phys. Rev. A* **92**, 033605 (2015).

[213] Sakaguchi, H. and Malomed, B. A. *New. J. Phys.* **18**, 025020 (2016).

[214] Gertjerenken, B., Billam, T. P., Blackley, C. L., Sueur, C. R. L., Khaykovich, L., Cornish, S. L., and Weiss, C. *Phys. Rev. Lett.* **111**, 100406 (2013).

[215] Khawaja, U. A. and Stoff, H. T. C. *New J. Phys* **13**, 085003 (2011).

[216] Fengwu, Z. and Jiaren, Y. *Chin. Phys. Lett.* **5**, 265 (1993).

[217] Baron, H. E., Luchini, G., and Zakrzewski, W. J. *J. Phys. A: Math. Theor.* **47**, 265201 (2014).

[218] Yu, H., Pan, L., Yan, J., and Tang, J. *J. Phys. B: At. Mol. Opt. Phys.* **42**, 025301 (2009).

[219] Khawaja, U. A., Stoof, H. T. C., Hulet, R. G., Strecker, K. E., and Partridge, G. B. *Phys. Rev. Lett.* **89**, 200404 (2002).

[220] Yan, J. R., Yan, X. H., You, J. Q., and Zhong, J. X. *Phys. Fluids A.* **5**, 1651 (1993).

[221] Yan, J. R. and Mei, Y. P. *Europhys. Lett.* **23**, 335 (1993).

[222] Chen, W., Shen, M., Kong, Q., Shi, J., Wang, Q., and Krolikowski, W. *Opt. Lett.* **39**, 1764 (2014).

[223] Nishida, M., Furukawa, Y., Fujii, T., and Hatakenaka, N. *Phys. Rev. E* **80**, 036603 (2009).

[224] Anderson, D. and Lisak, M. *Phys. Scr.* **33**, 193 (1986).

[225] Malomed, B. A. and Nepomnyashchy, A. A. *Europhys. Lett.* **27**, 649 (1994).

[226] Malomed, B. A. *Phys. Rev. E* **58**, 7928 (1998).

[227] Parker, N. G., Proukakis, N. P., Leadbeater, M., and Adams, C. S. *Phys. Rev. Lett.* **90**, 220401 (2003).

[228] Arnold, A. S., Garvie, C. S., and Riis, E. *Phys. Rev. A* **73**, 041606 (2006).

[229] Mewes, M. O., Andrews, M. R., Kurn, D. M., Durfee, D. S., Townsend, C. G., and Ketterle, W. *Phys. Rev. Lett.* **78**, 582 (1997).

[230] Pepino, R. A., Cooper, J., Anderson, D. Z., and Holland, M. J. *Phys. Rev. Lett.* **103**, 140405 (2009).

[231] Labouvie, R., Santra, B., Heun, S., Wimberger, S., and Ott, H. *Phys. Rev. Lett.* **115**, 050601 (2015).

[232] Arfken, G. B. and Weber, H. J. *Mathematical Methods for Physicists*. Elsevier, (2005).